

# **SANDIA REPORT**

SAND2015-10496

Unlimited Release

November 2015

## **NSRD-6: Computational Capability to Substantiate DOE-HDBK-3010 Data**

Louie, David L.Y., and Brown, Alexander L.

Prepared by  
Sandia National Laboratories  
Albuquerque, New Mexico 87185 and Livermore, California 94550

Sandia National Laboratories is a multi-program laboratory managed and operated by Sandia Corporation, a wholly owned subsidiary of Lockheed Martin Corporation, for the U.S. Department of Energy's National Nuclear Security Administration under contract DE-AC04-94AL85000.

Approved for public release; further dissemination unlimited.



**Sandia National Laboratories**

Issued by Sandia National Laboratories, operated for the United States Department of Energy by Sandia Corporation.

**NOTICE:** This report was prepared as an account of work sponsored by an agency of the United States Government. Neither the United States Government, nor any agency thereof, nor any of their employees, nor any of their contractors, subcontractors, or their employees, make any warranty, express or implied, or assume any legal liability or responsibility for the accuracy, completeness, or usefulness of any information, apparatus, product, or process disclosed, or represent that its use would not infringe privately owned rights. Reference herein to any specific commercial product, process, or service by trade name, trademark, manufacturer, or otherwise, does not necessarily constitute or imply its endorsement, recommendation, or favoring by the United States Government, any agency thereof, or any of their contractors or subcontractors. The views and opinions expressed herein do not necessarily state or reflect those of the United States Government, any agency thereof, or any of their contractors.

Printed in the United States of America. This report has been reproduced directly from the best available copy.

Available to DOE and DOE contractors from

U.S. Department of Energy  
Office of Scientific and Technical Information  
P.O. Box 62  
Oak Ridge, TN 37831

Telephone: (865) 576-8401  
Facsimile: (865) 576-5728  
E-Mail: [reports@osti.gov](mailto:reports@osti.gov)  
Online ordering: <http://www.osti.gov/scitech>

Available to the public from

U.S. Department of Commerce  
National Technical Information Service  
5301 Shawnee Rd  
Alexandria, VA 22312

Telephone: (800) 553-6847  
Facsimile: (703) 605-6900  
E-Mail: [orders@ntis.gov](mailto:orders@ntis.gov)  
Online order: <http://www.ntis.gov/search>



## **NSRD-06: Computational Capability to Substantiate DOE-HDBK-3010 Data**

Louie, David L.Y.<sup>1</sup> and Brown, Alexander L.<sup>2</sup>

<sup>1</sup>Severe Accident Analysis Department (MS0748)

<sup>2</sup>Fire Science and Technology Department (MS1135)

Sandia National Laboratories

P.O. Box 5800

Albuquerque, New Mexico 87185

### **Abstract**

Safety basis analysts throughout the U.S. Department of Energy (DOE) complex rely heavily on the information provided in the DOE Handbook, DOE-HDBK-3010, *Airborne Release Fractions/Rates and Respirable Fractions for Nonreactor Nuclear Facilities*, to determine source terms. In calculating source terms, analysts tend to use the DOE Handbook's bounding values on airborne release fractions (ARFs) and respirable fractions (RFs) for various categories of insults (representing potential accident release categories). This is typically due to both time constraints and the avoidance of regulatory critique. Unfortunately, these bounding ARFs/RFs represent extremely conservative values. Moreover, they were derived from very limited small-scale table-top and bench/laboratory experiments and/or from engineered judgment. Thus the basis for the data may not be representative to the actual unique accident conditions and configurations being evaluated.

The goal of this research is to develop a more accurate method to identify bounding values for the DOE Handbook using the state-of-art multi-physics-based high performance computer codes. This enables us to better understand the fundamental physics and phenomena associated with the types of accidents for the data described in it. This research has examined two of the DOE Handbook's liquid fire experiments to substantiate the airborne release fraction data. We found that additional physical phenomena (i.e., resuspension) need to be included to derive bounding values. For the specific cases of solid powder under pressurized condition and mechanical insult conditions the codes demonstrated that we can simulate the phenomena. This work thus provides a low-cost method to establish physics-justified safety bounds by taking into account specific geometries and conditions that may not have been previously measured and/or are too costly to do so.

## **ACKNOWLEDGMENTS**

Dr. Louis F. Restrepo of Atkins NS has provided guidance and review for this project. He is one of the original contributors and reviewers to DOE-HDBK-3010, and both his expertise with DOE-HDBK-3010 and his extensive experience in the U.S. Department of Energy (DOE) facility nuclear safety have helped this project significantly. We also thank the summer intern, Ethan T. Zepper, for providing support in the simulations of the pool fire scenario, Dr. John Bignell for assisting the use of Presto code for the impact powder can simulation early in the project, and many of the SIERRA's solid mechanics team for their support, especially Dr. Nathan K. Crane and San Le. We also appreciate Dr. John Bignell, San Le, and Dr. Fred Gelbard for providing the review of this document. Finally, the authors would like to express their appreciation to Dr. Alan Levin, Program Manager of DOE's Nuclear Safety Research and Development Program for overseeing this research. This work is supported by the DOE's Nuclear Safety Research and Development Program under WAS Project No. 2014-AU-2014033. This program is managed by the Office of Nuclear Safety (AU-30) in the Office of Environment, Health, Safety and Security at DOE.

# CONTENTS

Acknowledgments.....	4
Contents .....	5
Figures.....	6
Tables.....	8
Nomenclature.....	9
1 Introduction.....	13
2 DOE-HDBK-3010 Data.....	15
2.1 Five-Factor Formula .....	16
2.2 Organization of Handbook Data .....	16
2.3 Handbook Data Derivation and Reviews.....	17
3 Modeling Approach .....	19
3.1 SIERRA Code Suite.....	20
3.1.1 Adagio.....	21
3.1.2 Fuego.....	22
4 Liquid Fire Simulations .....	23
4.1 Beaker Fire.....	23
4.1.1 Methods.....	26
4.1.2 Results.....	28
4.1.3 Discussion.....	34
4.1.4 Conclusions.....	36
4.2 Pool Fire .....	36
4.2.1 Evaporation Induced Entrainment (EIE) .....	38
4.2.2 Surface Agitation by Wind .....	39
4.2.3 Surface Agitation by Boiling .....	39
4.2.4 Residue Entrainment.....	40
4.2.5 Methods.....	41
4.2.6 Simulation Scenarios .....	46
4.2.7 Results.....	47
4.2.8 Discussions .....	53
4.2.9 Conclusions.....	54
4.3 Improvement Needs in Fuego.....	54
4.3.1 SIERRA/Fuego Improvements .....	54
4.3.2 Dataset improvements.....	56
5 Exporatory Simulations .....	59
5.1 Impacts to Powder Can .....	59
5.1.1 Mie-Grunesien EOS Model .....	62
5.1.2 Soil-Crushable Foam Material Model .....	64
5.1.3 Discussions and Results.....	64
5.2 Pressurized Powder Release .....	77
5.2.1 MELCOR Simulations.....	79

5.2.2 Fuego Simulations .....	85
6 Summary and Conclusion .....	89
7 Recommendations for Future WORK .....	93
8 References.....	95
Appendix A: Summary Table for Handbook Data .....	99

## FIGURES

Figure 4-1. Boiling Entrainment (left) and Surface Wave Entrainment (right) for Liquid in Air.24	
Figure 4-2. An Extraction of the Number Frequency Data from [Borkowski 1986]. .....	27
Figure 4-3. Predicted Liquid Entrainment from [Mishima 1973] Tests, with Particle Parcel Sizes Exaggerated for Visibility. ....	29
Figure 4-4. Predicted Mass Deposited for the First 600 Seconds (20 mm Height Pool).....	30
Figure 4-5. Predicted Mass Deposited for the Final 600 Seconds (0 mm Height Pool).....	30
Figure 4-6. Predicted Particle Number Deposited for the First 600 Seconds (20 mm Height Pool). .....	31
Figure 4-7. Predicted Particle Number Deposited for the Final 600 Seconds (0 mm Height Pool). .....	31
Figure 4-8. Summary % ARF Plot for the Baseline Turbulence Assumption for Various Particle Input Files and Initial Liquid Heights.....	33
Figure 4-9. Percentage of ARF for a 20 mm Initial Height for a Variety of Particle Input Files (the simulation number) and Turbulence Assumptions (the simulation letter) Compared to the Data. ....	34
Figure 4-10. Selected Entrainment Mechanisms. ....	42
Figure 4-11. Wind Tunnel Mesh Geometry and Surfaces (# represents a surface number).....	44
Figure 4-12. Evaporation-Induced Entrainment: Predicted Mass Deposition vs Time for Case 1E. ....	48
Figure 4-13. Boiling: Predicted Mass Deposition vs. Time for Case 1B. ....	48
Figure 4-14. Boiling: Predicted Number Deposition vs. Time for Case1B.....	49
Figure 4-15. Predicted End of Simulation Mass Fate: Evaporation Case 1E. ....	50
Figure 4-16. Predicted End of Simulation Mass Fate: Boiling Case 1B. ....	50
Figure 4-17. Predicted Evaporation-Induced Entrainment Scenario: Mass Deposition. ....	51
Figure 4-18. Predicted Boiling Atomization Entrainment Scenario: Mass Deposition.....	52
Figure 4-19. Predicted and Reported Airborne Release Fraction.....	52
Figure 5-1. Geometry of a Projectile Impact to a Powder Can.....	61
Figure 5-2. Simulations of Case 1 at Time Zero.....	66
Figure 5-3. Simulations of Case 1 at 0.01 s. (coarse mesh, Mie-Gruneisen EOS material model, water properties and UO2 density at the impact speed of 20 meters per second.) .....	66
Figure 5-4. Simulations of Case 1 at 0.02 s. (coarse mesh, Mie-Gruneisen EOS material model, water properties and UO2 density at the impact speed of 20 meters per second) .....	67
Figure 5-5. Simulations of Case 1 at 0.03 s. (Coarse mesh, Mie-Gruneisen EOS material model, water properties and UO2 density at the impact speed of 20 meters per second) .....	67

Figure 5-6. Initial Configuration of Case 2 (same as Case 1, except the impact speed is at 175 meters per second).	68
Figure 5-7. Simulation of Case 2 at Time Zero (same as Case 1, except the impact speed is at 174 meters per second).	68
Figure 5-8. Simulation of Case 2 at 0.005 s (same as Case 1, except the impact speed is at 175 meters per second).	69
Figure 5-9. Simulation of Case 2 at 0.03 s (same as Case 1, except the impact speed is at 175 meters per second).	69
Figure 5-10. Simulation of Case 2 at 0.05 s (same as Case 1, except the impact speed is at 175 meters per second).	70
Figure 5-11. Simulation of Case 2 at 0.1 s (same as Case 1, except the impact speed is at 175 meters per second).	70
Figure 5-12. Simulation of Case 2 at 0.12 s (same as Case 1, except the impact speed is at 175 meters per second).	71
Figure 5-13. Simulation of Case 2 at ~0.15 s (same as Case 1, except the impact speed is at 175 meters per second).	71
Figure 5-14. Simulations for Case 3 at 0.01 s (coarse mesh, Mie-Gruneisen EOS material model, sand/air properties and UO <sub>2</sub> density at the impact speed of 20 meters per second).	72
Figure 5-15. Simulations for Case 3 (coarse mesh, Mie-Gruneisen EOS material model, sand/air properties and UO <sub>2</sub> density at the impact speed of 20 meters per second).	72
Figure 5-16. Simulations for Case 3 at 0.04 s (coarse mesh, Mie-Gruneisen EOS material model, sand/air properties and UO <sub>2</sub> density at the impact speed of 20 meters per second).	73
Figure 5-17. Simulations for Case 3 at 0.1 s (coarse mesh, Mie-Gruneisen EOS material model, sand/air properties and UO <sub>2</sub> density at the impact speed of 20 meters per second).	73
Figure 5-18. Simulations for Case 4 at 0.01 s (same as Case 3, except using soil and crushable foam material model).	74
Figure 5-19. Simulations for Case 4 at 0.03 s (same as Case 3, except using soil and crushable foam material model).	74
Figure 5-20. Simulations for Case 4 at 0.04 s (same as Case 3, except using soil and crushable foam material model).	75
Figure 5-21. Simulations for Case 4 at 0.1 s (same as Case 3, except using soil and crushable foam material model).	75
Figure 5-22. Simulations for Case 5 (same as Case 4, except using fine mesh).	76
Figure 5-23. Simulations for Case 5 (same as Case 4, except using fine mesh).	76
Figure 5-24. Layout of PARE [Sutter, 1983].	78
Figure 5-25. Schematic of PART [Sutter, 1983].	78
Figure 5-26. Aerosol Histogram Results in PARE Volume for a Single PART Volume at 50 psig Case at 30 Minutes.	80
Figure 5-27. Aerosol Histogram Results in PART Volume for a Single PART Volume at 50 psig Case at 30 Minutes.	81
Figure 5-28. Aerosol Histogram Results in PARE Volume for a 2 PART-Volume at 50 psig Case at 30 Minutes.	82
Figure 5-29. Aerosol Histogram Results in Bottom PART Volume for a 2-PART Volumes at 50 psig Case at 30 Minutes.	82
Figure 5-30. Aerosol Histogram Results in PARE Volume for a Single PART Volume at 250 psig Case at 30 Minutes.	83

Figure 5-31. Aerosol Histogram Results in PART Volume for a Single PART Volume at 250 psig Case at 30 Minutes. ....	84
Figure 5-32. Aerosol Histogram Results in PARE Volume for a 2 PART-Volume at 250 psig Case at 30 Minutes. ....	84
Figure 5-33. Aerosol Histogram Results in the Bottom PART Volume for a 2 PART-Volume at 250 psig Case at 30 Minutes. ....	85
Figure 5-34. Fuego Mesh Used. ....	87
Figure 5-35. Fuego Simulation Results for the 50 psig Pressurized Powder Release Test. ....	88

## TABLES

Table 2-1. Effects and Descriptions of Major Accident Types .....	15
Table 3-1. Selected Simulation Codes at SNL* .....	19
Table 3-2. Summary of SIERRA Code Suite* .....	20
Table 4-1. Turbulence parameters for the sensitivity study .....	33
Table 4-2. Entrainment Mechanisms Believed Potentially Active in Pool Fire .....	38
Table 4-3. Plutonium Release Rate Data [Mishima 1968] .....	43
Table 4-4. Turbulence parameters* .....	45
Table 4-5. Entrainment Scenarios* .....	46
Table 4-6. Evaporation Induced Entrainment Simulation Variations .....	47
Table 4-7. Boiling Entrainment Simulation Variations .....	47
Table 4-8. Baseline ARF for Evaporation and Boiling .....	49
Table 4-9. Existing models capabilities not deployed for these calculations .....	55
Table 4-10. Models not existing but needed .....	55
Table 4-11. Correlations that Need Better Justification .....	56
Table 4-12. Recommended Dataset Improvements to the Beaker Fire Test of [Mishima 1973].	57
Table 4-13. Recommended Dataset Improvements to the Pool Fire Test of [Mishima 1973a] ...	57
Table 5-1. Mesh Size for Fine and Coarse Cases .....	61
Table 5-2. Mie-Gruneisen Model Parameters Used in Simulations .....	63
Table 5-3. Simulation Cases for Impacts to Powder Can .....	65
Table 5-4. Input Parameters for the MELCOR 2.1 Models [Sutter 1983] .....	79
Table 7-1. Fuego Improvement Proposed for Next Year .....	93
Table 7-2. Recommendation for Modeling Mechanical Insult Accident Using SIERRA SM Code .....	93
Table 7-3. Recommendations on Modeling Pressurized Powder release Simulations for Next Year .....	94

## NOMENCLATURE

AED	Aerodynamic equivalent diameter
ARF	Airborne release fraction
ASC	Advanced Simulation and Computing
CFD	Computational Fluid Dynamics
DOE	Department of Energy
DR	Damage ratio
DSA	Document Safety Analysis
DUO	Depleted uranium oxide
EDC	Eddy dissipation concept
EOS	Equation of state
FD	Fluid dynamics
FFF	Five-Factor Formula
HEPA	High efficiency particulate air
hr	Hour
IC	Integrated Code
ITAR	International Traffic in Arms Regulations
LES	Large-eddy simulation
LPF	Leak path factor
MAR	Material-at-risk
mph	Miles per hour
NRC	Nuclear Regulatory Commission
NSRD	Nuclear Safety Research and Development
PARE	Pressurized airborne release equipment
PART	Pressurized airborne release tank
PNL	Pacific Northwest Laboratory
RANS	Reynolds averaging of the Navier Stokes equations
RF	Repairable fraction
SD	Structural dynamics
SM	Solid mechanics
SNL	Sandia National Laboratories
SPH	Spherical particle hydrodynamics
ST	Source term
TBP	Tributyl phosphine

### **Symbol – Applicable only for Chapter 4**

$D_H$	Vessel diameter
$D_H^*$	Dimensionless vessel diameter
$E_{fg}$	Entrainment factor
$A_p$	Area of the pan
$A$	Fit parameter in Equation (4-9)
$E$	Erosion rate in Equation (4-9)
$j$	Velocity
$t$	Total time of the fire while the fluid is boiling
$V_f$	Volume of the remaining fluid in Equation (4-10)

$j_g$	Superficial gas velocity
$j_{fg}$	Superficial drop velocity
$j_g^*$	Dimensionless velocity
$H$	Height above liquid
$h^*$	Dimensionless height above liquid
$N_{\mu g}$	Dimensionless gas viscosity
$D_H$	Vessel diameter
$D_H^*$	Dimensionless vessel diameter
$\mu$	Viscosity
$d$	Characteristic length (size of the particle)
$g$	Gravity
$m$	Fit parameter in Equation (4-9)
$n$	Fit parameter in Equation (4-9)

#### Subscript

$g$	Gas
$fe$	Liquid (droplet)
$f,w$	Fluid
$s$	Solid layer

#### **Symbol – Applicable only for Chapter 5**

$E$	Specific internal energy
$F_{drag}$	Draft force
$P$	Mean pressure
$Re_p$	Reynolds number for particle
$S$	The slope of the equation between $u_s$ and $u$ (see Equation 5-2)
$c$	sound speed
$f_1$	Constant in Equation 5.1-4
$f_2$	Constant in Equation 5.1-4
$f_D$	Drag coefficient
$k$	Bulk modulus
$p$	Pressure
$s_{ij}$	Stress deviators
$u$	Particle velocity
$u_s$	Shock velocity
$v_f$	Velocity of fluid
$y_0$	Yield strength
$\epsilon$	Strain
$\eta$	Density change
$\rho$	Density
$\Gamma$	Gruneisen parameter
$\mu$	Shear modulus

$\mu_f$     Viscosity  
 $\nu$       Poisson's ratio

Subscript

0      Ambient value or input value  
H      Along the principal Hugoniot  
b      bulk

Intentionally Left Blank

# 1 INTRODUCTION

Safety analysts throughout the U.S. Department of Energy (DOE) complex rely heavily on the data provided in the DOE Handbook (referred to herein as the Handbook), DOE-HDBK-3010 [DOE 1994], to determine source terms in support of safety and risk analyses documented in documented safety analysis (DSA) or risk analysis documents. In calculating source terms, analysts tend to use the Handbook's bounding values on airborne release fractions (ARF) and respirable fractions (RF) for various categories of insults (representing potential accident release categories). This is typically due to both time constraints and the avoidance of regulatory critique. Unfortunately, these bounding ARF/RFs represent extremely conservative values. Moreover, they were derived from very limited small-scale table-top and bench/laboratory experiments, as well from engineered judgment which may not be substantiated and that may not be representative to the actual unique accident conditions and configurations being evaluated. In response, we have proposed the inclusion of high-fidelity modeling to provide a more accurate method to identify not only bounding values, but also more representative ones for the Handbook and for analysts tasked with risk assessments.

Advances in computing capability at national laboratories have enabled us to use computer simulation to better model hydrodynamic, structural dynamic, and thermal/fluid dynamic phenomena and to better understand and seek insights of the fundamental physics related to potential accident scenarios that could occur or could be postulated. Today, the availability of the high-fidelity computer resources (both hardware and software) that incorporate state-of-the-art models at national laboratories allows safety and risk analysts to utilize these methods for non-weapon-related safety activities.

If our research determines that the data are too conservative, the DSA source term may overspecify the implementation of design and operating controls, which may lead to substantial design/construction and/or implementation costs to DOE. On the other hand, if our research determines the data that are non-conservative, this means that the DSA underestimates the source term, which could translate to a potentially significant safety concern to the workers and to the public. In either case, the results of our investigation could enhance how safety analysts across the DOE complex approach the selection of adequate bounding ARFs/RFs. This could improve both the defensibility of the safety analyses and the confidence level of these data.

This report describes the initial progress of this research, which was funded by DOE Nuclear Safety Research and Development (NSRD) Program for Fiscal Year (FY) 2015. In this initial research, we are addressing the impact of fires (or thermal insults) on the liquid material form as presented in Chapter 3 of the Handbook. The most probable accident scenarios encountered across the DOE complex are fires and deflagration phenomena. Fires can be caused by combustible solids, flammable liquid or reactive solutions. Deflagration is usually due to the presence of hydrogen, which can be generated by chemical reactions and other flammable gases (such as natural gas) for either process use or operation-induced processes, such as radiolysis of hydrocarbon material or water to produce hydrogen. The recent study performed on spent fuel processing source terms for the Nuclear Regulatory Commission (NRC) indicates that both solid mechanics and fluid dynamics codes can be used to provide ARF/RF for a red oil explosion accident [Gelbard 2013]. We are presently examining the use of a fluid dynamics code to address

the source term from a contaminated pool fire. If this work is successful, we believe that we have additional capabilities to address releases from explosion/criticality and liquid fire, also detailed in the Handbook. In addition, we are providing the computer simulation capability to address the Handbook data solids, powders, and contaminated surfaces.

This report is divided into seven chapters. A brief description of the DOE-HDBK-3010 is provided in Chapter 2, which also provides the source term equation derived from the Five-Factor Formula. Chapter 3 provides a brief description of the available high-fidelity computer codes available at Sandia National Laboratories (SNL), including the identification of the computer codes that supported this research. Chapter 4 describes and discusses the simulations of the two liquid fire experiments from the Handbook. Chapter 5 describes the exploratory simulations of powder release due to mechanical insult condition and a pressurized condition. Chapter 6 provides a summary and conclusion, and Chapter 7 outlines the future planned work for this research.

## 2 DOE-HDBK-3010 DATA

DOE-HDBK-3010 is a widely used reference document for the majority of the safety analysts across the DOE complex, particularly for determining source terms. The content and usefulness of this Handbook is described briefly in this chapter. For detailed descriptions and applicability of the Handbook, readers are encouraged to consult the text firsthand.

In the Handbook, data are organized by the physical form of the material affected (e.g., gas, liquid, solid, surface contamination) and by suspension stresses (e.g., spill, thermal stress, shock wave, and blast stress). In general, the Handbook focuses on five major accident types encountered in most DOE facilities: spill, nuclear criticality, fire, explosion, and earthquake. Table 2-1 lists the accident types and their descriptions, including severity to the health of workers and the public.

**Table 2-1. Effects and Descriptions of Major Accident Types**

Accident Type	Description	Typical Source Term Severity*	
		Worker	Public
Earthquake	Earthquakes often include with induced explosion and fire	significant	significant
Explosion <sup>A</sup>	Explosions usually occur within 10 <sup>-4</sup> s or longer time ranges with a large energy surge. Detonation creates shock waves, and deflagration creates blast effect. Explosions can be chemical and physical induced. Chemical tends to yield a more energetic event than a physical explosion, because of accompanying product gases. Physical explosion is due to pressure build-up.	significant	significant
Fire <sup>A,B</sup>	Duration of fire, ranging from minutes to hours, depends on the amount of combustible (flammable liquid or solids) available and other reactants that yield fires.	significant	significant
Nuclear Criticality <sup>C</sup>	An event that depends on the available fissile/fissionable material presence, geometry, reflection, moderation and other conditions allows nuclear excursion to occur.	significant	Minor <sup>D</sup>
Spill	This event includes drops (free-fall), which usually yield the least release in comparison to other accident types.	significant	extremely small

\*This measures the dose consequence to both workers and public – significant means that the dose associated to this accident type generally would result large source term, minor means that because of distance and magnitude of the accident a small source term would result, and extremely small means that the airborne release fraction for this accident type is generally very small, and the resulting source term may not have an effect. PuO<sub>2</sub> is a hazardous material that could contribute most of the dose consequence.

<sup>A</sup> In some accidents, explosion can lead to secondary fire or vice versa.

<sup>B</sup> Although the amount of energy release per unit time for fire is much smaller than that of the explosion, the long duration could yield a total energy that could exceed the total energy release from an explosion.

<sup>C</sup> Unlike a chemical explosion, where the explosion may be a point, areal or segment source, nuclear criticality usually associates with a volume, because criticality requires some homogeneity in the solution and solid to permit nuclear excursion to occur which may last in few seconds to minutes; the nuclear excursion will not involve large product gases. Only a small portion of gases and vapors may result from fission.

<sup>D</sup> Nuclear excursion accompanies gamma and neutron radiation, which may not have a direct exposure to the public, because of the distance rule, assuming that the facility structure and ventilation could contain most of the fission-induced airborne radionuclides.

The remainder of this chapter includes a definition of the source term, which is often referred to as the Five-Factor formula (FFF). It also includes a brief description of the organization for the Handbook data.

## 2.1 Five-Factor Formula

The source term is defined as the airborne respirable radioactive materials that are released into the environment during an accident. Such releases could be high and low-energy induced, as shown in Table 2-1. Thus, an FFF can be used to express this source term (ST), defined as:

$$ST = MAR \cdot DR \cdot ARF \cdot RF \cdot LPF \quad (2-1)$$

where

MAR =the material-at-risk, which represents the amount of radionuclides (in mass or radioactivity) available to be acted by a given physical insult (chemical or mechanical, such as described in Table 2-1).

DR =the damage ratio, which is defined as the fraction of MAR actually impacted by the physical insult. For a breached container, the amount of MAR that gets out can be determined by DR.

ARF =the airborne release fraction, which defines the amount of radioactive material that can be suspended in air and made available for airborne transport under a specific set of induced physical stresses (e.g., accident conditions).

RF =the respirable fraction, which defines the fraction of ARF that contains aerosol sizes below 10  $\mu\text{m}$  aerodynamic equivalent diameter (AED).

LPF =the leak path factor, which quantifies the fraction of airborne aerosols, including those that are subjected to particle interactions (such as agglomeration or settlement) that may subsequently be released out of the facility (to the environment) when the accident occurs inside. This factor often is assumed to be in unity when the accident occurs outdoors or when estimating the source terms in unmitigated situations. The value of the LPF highly depends on the release pathways within a facility, which can be an open door, building penetrations, or those penetrations created by postulated accidents or insults, the ventilation designed pathway, and evacuation paths. Thus, it often cannot be pre-defined, and is unique per facility design and accident condition.

Note that when the MAR is in a gaseous form during an accident and is subjected to release, any non-unity DR will result in 100% release of gases to the environment, since all ARF, RF, and LPF are usually unity for gases. Thus, the full set of terms in Equation (2-1) is more important when dealing with aerosols than radioactive gases. Median and bounding values of ARF and RF can be found throughout the Handbook for various material forms and accident conditions; in some cases, aerosol-size distributions can be provided. However, safety analysts have to assume the conservative aerosol size distributions in most cases because the distributions are not readily available for all accident conditions.

## 2.2 Organization of Handbook Data

DOE Handbook 3010 provides useful source term information for safety analysts. Thus, understanding the organization of the data is important. The Handbook is organized by physical form of the material affected, including gas (Chapter 2), liquid (Chapter 3), solid (Chapter 4, which includes powders) and surface contamination (Chapter 5). In addition, suspension stresses,

such as spill, thermal stress, and shock wave and blast stresses are also given for the material affected. Chapter 6 describes the inadvertent nuclear excursion (criticality), which can occur in most of the material affected above. In terms of criticality, liquids and solids are of greatest interest. Chapter 7 shows examples of the application of the data. Further discussion of Chapter 7 is not given, since this research is dealing with substantiating the Handbook data, which is contained in previous chapters. The above contents are included in Volume I of the Handbook. Volume II provides the detailed information for the experiments and derived data provided in the Handbook.

A tabulated summary of the Handbook data in terms of the materials affected is presented in Appendix A. This summary represents the authors' current understanding of the Handbook data.

Most chapters of the Handbook provide a summary of the data analysis, including the bounding values of ARF and RF. For criticality, a summary of the bounding release estimates is provided.

In general, the Handbook data, particularly for ARF and RF values, are derived from limited experimental data. The Handbook outlines the basis for the guidelines, which predominantly consists of data and correlations gathered from experiments between the 1960s and 1980s. Much of the experimental data are in the form of integrated results rather than in details of the events. As shown in Appendix A, some of the Handbook data have been extrapolated by engineering judgment. Such application may have little basis and can be difficult to assess for accuracy due to a lack of existing data.

## **2.3 Handbook Data Derivation and Reviews**

The acknowledgement section of the Handbook identifies the processes and reviews performed in assembling the Handbook's data. Panel experts reviewed and refined the data before publishing in 1994. Although the Handbook was reaffirmed in 2013, many of the individuals who contributed to it are no longer available for reviews (due to either professional inactivity or death). However, Dr. Louis Restrepo, one of the original formal reviewers and contributors, is providing guidance and review to this project.

The introduction of the Handbook states that its purpose is to "provide a compendium and analysis of experimental data from which ARFs and RFs may be derived. The information provided in this handbook aids in making such estimates." It later states, "...However, these data and the analyses of the data contained herein need to be critically evaluated for applicability in each situation in which they are used, and represent one source of information in a complete safety analysis or design process." The authors and reviewers of this Handbook had indicated reasons for the derived data as described in the introduction:

- Experiments discussed evaluate release phenomena holistically.
- No attempt is made to precisely characterize total airborne material in terms of individual mechanisms acting within an overall given release.

- The release is kept in short distance from the point of generation to avoid any immediate physical chaos of the stress-induced event itself, which is why the experiments were performed on a small scale.
- The bounding values are often conservative because of the uncertainty associated with the experiments and other parameters identified in the FFF, such as ARFs and RFs combined.
- The goal of the Handbook is to provide a better understanding of the potential bounding hazards presented at the DOE facilities and to provide information to support “general bases” of decision making.
- The Handbook supports unmitigated release and verifies the effectiveness of mitigative measures.

Based on the above comments and concerns, regulators and safety analysts should apply the data with a corresponding level of care and confidence. Consequently, regulators may impose safety factors in the analyses performed by safety analysts by using the data provided in the Handbook, or they may require the use of the Handbook’s bounding values. Because of the need to extrapolate results from small-scale experiments and the simple variety of potential tests required to assess a large spectrum of accident conditions, there should be a significant confidence issue associated with the Handbook’s data.

### 3 MODELING APPROACH

Both the advancement in computing power and the relaxation of the availability of state-of-the-art DOE-weapon three-dimensional computational tools allow analysts to address many safety-related issues for non-defense areas. This work proposes to utilize these capabilities to substantiate the DOE-HDBK-3010 data on ARF, specifically by performing computational calculations to benchmark some of the small-scale experiments in the Handbook and derive values for specific releases or accident conditions. As a part of the ongoing research project with the NRC to develop a spent fuel reprocessing source term tool, we have demonstrated that these tools can be used to address chemical (organic solution) detonation phenomena by modeling a previous accident. This effort can be extended to model liquid criticality (wherein both the modeling of criticality and the explosion can be similar [see Table 2-1]). The computational capability for this research relies on the most advanced tools available at SNL to perform and assess the airborne release parameters and initial aerosol distribution, which are given in Table 3-1. These tools were developed to support the abnormal environment safety predictions for both the weapons component of DOE and for shock physics applications.

**Table 3-1. Selected Simulation Codes at SNL\***

Code Name	Capability	Application	Possible Applications to Section #(Heading) of the Handbook
CTH	A multi-material, Eulerian, large deformation, strong shock physics and solid mechanics code	Shock physics, penetration, fragmentation and impact	Section 4 (solid, includes powder)
SIERRA/Fuego**	A low-Mach number Lagrangian/Eulerian fluid mechanics computational fluid dynamic fire code	Fuel fire, droplet dynamic, and gas/particle transport	Section 3 (liquid), 4(solid), 5(surface contamination)
SIERRA/Presto**	A finite element Lagranigan structural dynamics code	Impacts and explosion for solid and liquid	Section 3 (liquid), 4(solid)

\*Not all SNL codes are provided in this table. More details are provided below.

\*\*These codes are part of the SIERRA Thermal Fluid and Solid Mechanics tools and are developed and maintained at SNL. They codes have been used to simulate a denitrator accident due to the red oil explosion. See [Gelbard 2013]

The Advanced Simulation and Computing (ASC) Integrated Code (IC) program, named SIERRA at SNL, provides state-of-the-art computer simulation tools as part of DOE National Nuclear Security Administration's (NNSA's) core mission. A number of integrated codes are multi-physics simulation codes that incorporate physics and engineering models:

- SIERRA Code Suite – permits coupled simulation capabilities for thermal, fluid (TF), aerodynamics, solid mechanics (SM), and structural dynamics (SD). Predict the performance of a weapon system in normal and abnormal environments, such as a crash or fire. This code suite will be further discussed in Section 3.1.
- RAMSES – provides simulation capabilities for radiation, electrical, and electromagnetic effects. This code is not further described, since it is not applicable to the current research.
- ALEGRA – simulates large deformations and strong shock physics, including solid dynamics as well as magnetics, magneto-hydrodynamics, electro-mechanics, and high-

energy physics applications. No further discussion for this code is given, since it is outside of the scope of the current research.

- CTH – simulates a multi-material, multi-dimensional, large deformation, strong shock wave and solid mechanics. It also models multi-phase, elastic, viscoplastic, porous, and explosive materials. No further discussion of this code is given, since it is outside of the scope of the current research.

### 3.1 SIERRA Code Suite

The description of the SIERRA code suite is based on the documentation from SIERRA 4.36 [SNL 2015]. It is important to note that this is the latest documentation currently available at the time of this report, even though the simulations may use a later code version.

**Table 3-2. Summary of SIERRA Code Suite\***

Module/Code Name	Description	Potential Application
Solid mechanics (SM) [SNL 2015a]	<p>A three-dimensional solid mechanics code with a number of features: versatile element library, nonlinear material models, large deformation capabilities, and contact.</p> <ul style="list-style-type: none"> <li>• Adagio –The standard SM code that currently provides the full suite of both explicit and implicit capabilities. In the past, the SM code for solving problems in explicit and implicit capabilities was separated into Presto and Adagio, respectively. Thus, Presto executable becomes obsolete.</li> <li>• Presto_itar – This SM code version provides capabilities to material models with an energy-dependent pressure response, such as for very large deformations and strain rates and for blast modeling [SNL 2015b]. The use of this code version falls under the U.S. Department of State’s International Traffic in Arms Regulations (ITAR) export-control rules. Many of the material models in this version are similar to those models in CTH.</li> <li>• Peridynamics – an extension of the SM code for modeling classical solid mechanics problems, such as modeling of bodies in which discontinuities occur spontaneously.</li> </ul>	May be used to model impacts, large deformation of solids, powders, and liquid dispersals using an SPH model.
Structural dynamics (SD)	Used to perform most traditional structural dynamics simulations in time and frequency domains, including stress and fatigue calculations. These calculations could include energy dissipation at discrete joints. Since this SD module has a massively parallel capability, it can efficiently perform simulations to millions of degrees of freedom. Its variety of equations solvers enables solving problems with a large number of constraints. This module also includes a structural-acoustics capability for simulating-noise induced structural vibration or response due to a given noise source [SNL 2015c].	May be used to determine the failure of the structural-related components in the problem. No apparent applications for this research at this time.
Thermal Analysis**	<p>Aria, Calore, and Chaparral modules comprise the state-of-the-art thermal analysis tools using massive parallel capability:</p> <ul style="list-style-type: none"> <li>• Aria is a Galerkin finite element-based program for targeting applications that involve incompressible flow and primarily focus on energy transport;</li> </ul>	May be used to determine situations requiring detailed thermal analysis. No apparent applications for this research at this time.

	<p>species transport with reactions; electrostatics; and the general transport of scalar, vector, and tensor quantities in two and three dimensions for both transient and direct-to-steady state.</p> <ul style="list-style-type: none"> <li>• Calores approximates linear and nonlinear continuum models of heat transfer.</li> <li>• Chaparral is a library package to address three-dimensional enclosure radiation heat transfer problems.</li> </ul>	
Fluid dynamics (FD) with low Mach**	<p>Fuego is an FD module for the SIERRA code suite. Fuego is designed to predict low-Mach number (<math>M &lt; 0.3</math>) reacting flows, and has a capability to model particle and drop transport using a dilute spray approximation Lagrangian/Eulerian coupling. The liquid phase can be modeled as individual Lagrangian drops that interact through momentum source terms with the Eulerian gas phase. It couples with Syrinx, a media radiation heat transfer module, to simulate a more complete heat transfer and FD problems, such as fires. Fuego models particles in terms of user input or code generated as soot from a fire. With the particle capability, it can model particle dispersal; however, Fuego does not currently model particle interaction, which is important for the particulate release out of a pathway.</p>	Useful to model fire with particulates and droplet/powder release due to an elevated pressure effect.
Fluid dynamics (FD) with high Mach**	<p>Aero module that can model flow problems at Mach numbers higher than Mach 8. It can model gas flow in two and three-dimensional problems, which can approximate the compressible Navier-Stokes equations on unstructured meshes.</p>	Useful to model deflagration types of accidents, particularly their flow conditions. Aero currently does not have a particle model, and thus has no apparent applications for this research at this time.

\*see [SNL 2015] for more details on the specific module description and usage. This suite is compliant to DOE Order 414.1D [Minana 2012].

\*\*These codes and modules make up the SIERRA Thermal Fluid (TF).

The SIERRA SM code, particularly Adagio and Presto\_itar, will be used in the simulations as described in Chapter 5 of this report (e.g., powder release simulations). The primary focus of Chapter 5 is to identify if Adagio and/or Presto\_itar can be used for simulating powder release due to a mechanical insult. On the other hand, SIERRA FD code, particularly Fuego, which is known to address fire scenarios, will be used in simulating two liquid fire experiments from the Handbook. In addition, we will determine if Fuego can model pressurized powder release.

### 3.1.1 Adagio

Adagio is the current code name to execute the SIERRA SM code, replacing the obsolete Presto as shown in Table 3-2. However, for explosion simulations where shock physics may be required, Presto is still used, although it is referred to as “Presto\_itar,” (see Table 3-2). For the remainder of this report, Presto refers herein to Presto\_itar. In general, Adagio and Presto require nearly identical inputs, except that Presto includes extra materials that are applicable only for shock physics and explosion conditions. Section 5.1 describes the use of these codes for a projectile hitting a can filled with powder. Other inputs required include:

- Material specifications
- Element specifications
- Boundary and initial conditions

- Contact information when two elements are in contact, particularly when an element is failed or dead and reassignment or deletion may be required
- Output and interface information, including output specifications for Fuego simulations

### 3.1.2 *Fuego*

Fuego is the code name to execute the SIERRA FD code in the low Mach regime. As indicated in Section 3.1, Fuego will be used to simulate two liquid fire experiments from Chapter 3 of the Handbook: beaker fire and gasoline pool fire (see Chapter 4 of this report). In Fuego, a particle region and a fluid region can be modeled for both fire and other types of the particulate release simulation, such as pressurized release. Although Fuego is primarily used for simulating fires, another application is also being investigated. The description of the Fuego capability will be described more details in Chapter 4 and Section 5.2 of this report.

## 4 LIQUID FIRE SIMULATIONS

This chapter describes the SIERRA FD code, Fuego simulations of the liquid fire data from the Handbook as described in the NSRD effort. Section 4.1 details the results of an effort to compare Fuego predictions to laboratory-scale experiments, namely a beaker fire, as described in [Brown 2015]. Section 4.2 details the results of an effort to compare Fuego predictions to a larger-scale pool fire test, as described originally in [Brown 2015a]. Section 4.3.1 highlights discussion points and conclusions from the previous two sections, suggesting productive follow-on work.

### 4.1 Beaker Fire

The evolution of airborne contaminants from a burning liquid is a well-established phenomenon, but mechanistic models are still being developed. While literature exists on the basic phenomenology, it has yet to be consolidated and verified in a way that provides confident predictions of fuel fire ARF and RF for a variety of scenarios (see comparatively recent reviews by [Kogan 2008] and [Bagul 2013]).

This section describes an effort to model the entrainment of contaminated liquid fuel using a computational fluid dynamics (CFD) reacting flow code (such as Fuego). The long-term goal is to demonstrate and subsequently build confidence in predictive tools to aid in the assessment of risks and hazards associated with the entrainment of contaminated liquids. In this project, experiments of [Mishima 1973] are simulated to assess the ability of modern simulation tools to make quantitative predictions of reported experiments. The work in [Mishima 1973] constitutes some of the primary data that are relied upon for facility safety in the Handbook. Additionally, it highlights some important physical phenomena that need to be simulated to have confidence in model predictions. The increased fidelity of information from the model underscores a need to better understand the phenomenological nature of these events.

The physical mechanism for the entrainment of particles is assumed to be primarily due to the drop formation from boiling bubbles or surface wave entrainment bubbles that rupture at the surface of the liquid/gas interface. Two basic regimes exist for initial boiling. In the first regime, which is commonly referred to as the film breakup regime, the drops are formed as the bubble dome collapses. For commonly studied fluids such as water and salt water, this would result in 1-100  $\mu\text{m}$  diameter range drops. The second rupture entrainment mechanism is called the jet regime, and results from the rise and pinch-off of liquid tendrils as the liquid collapses around the bubble void after the film ruptures. This results in much larger drops, usually in the range of 100-300  $\mu\text{m}$  of diameter [Borkowski 1986].

According to the Handbook, for airborne release of particles in nuclear facilities, the film breakup regime is active for bubbles greater than 0.2 mm in diameter. The bubble mechanism is illustrated on the left side of Figure 4-1. The right side demonstrates the potential for wave action to create bubbles and entrainment from stretching and collapsing waves. This alternate entrainment mechanism is understood to be highly dependent on the wind speed or liquid/air interface surface velocities. Entrainment is also possible in either the residual layer after the fuel has burned off or deposits on the surrounding surfaces.

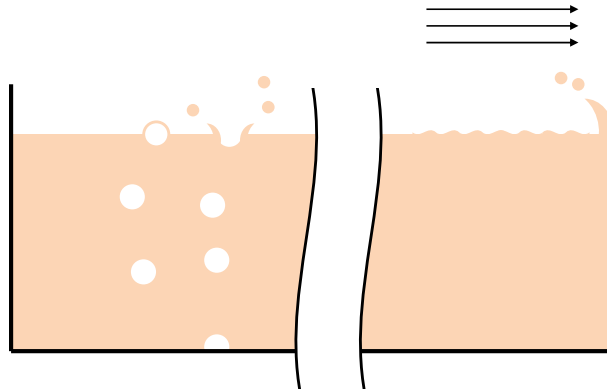


**Figure 4-1. Boiling Entrainment (left) and Surface Wave Entrainment (right) for Liquid in Air.**

The Handbook recommends the literature model from [Kataoka 1983], who reviewed an extensive quantity of literature and developed an analytical model for entrainment using an entrainment factor that is defined as the upward liquid mass flux divided by the upward gas mass flux. Additionally, [Kataoka 1983] provides separate models for the entrainment in three distinct regions that are separated by a characteristic height. The near surface region entrains the most liquid mass, but the drops are mostly expected to fall back to the surface. For this regime, the entrainment factor ( $E_{fg}$ ) is defined by the following:

$$E_{fg} = 4.84 \times 10^{-3} \left( \frac{\rho_g}{\Delta\rho} \right)^{-1.0} \quad (4-1)$$

This relation is described as valid in the range:

$$0 \leq h^* \leq 1.038 \times 10^3 j_g^* N_{\mu g}^{0.5} D_H^{*0.42} \left( \frac{\rho_g}{\Delta\rho} \right)^{0.23} \quad (4-2)$$

The entrainment factor is defined as the upward liquid mass flux divided by the upward gas mass flux:

$$E_{fg} = \frac{\rho_f j_{fe}}{\rho_g j_g} \quad (4-3)$$

where  $\rho_f$  is the fluid density,  $\rho_g$  is the gas density,  $j_{fe}$  is the superficial liquid velocity (droplets), and  $j_g$  is the superficial gas velocity. Dimensionless parameters used in the formulation include:

$$j_g^* = \frac{j_g}{(\sigma g \Delta\rho / \rho_g^2)^{1/4}} \quad (4-4)$$

$$h^* = \frac{h}{(\sigma/g\Delta\rho)^{1/2}} \quad (4-5)$$

$$N_{\mu g} = \frac{\mu_g}{[\rho_g \sigma (\sigma/g\Delta\rho)^{1/2}]^{1/2}} \quad (4-6)$$

$$D_H^* = \frac{D_H}{(\sigma/g\Delta\rho)^{1/2}} \quad (4-7)$$

Here,  $\sigma$  is the surface tension,  $g$  is the acceleration of gravity, and  $\rho$  is density, with the 'g' subscript implying gas.  $\Delta\rho$  is the density difference between the gas and liquid,  $D_H$  is the vessel diameter,  $\mu_g$  is the gas viscosity, and  $h$  is the height above the pool surface.

Equation (4-1) provides the correlation for boiling entrainment the first of three regions. The credibility of these relations is based on comparison to historical data and self-similarity arguments, which are described in more detail in [Kataoka 1983]. The other relations are for higher dimensionless heights, but the one presented here is the most generally applicable because it pertains to all pools in the near surface region. Curiously, the entrainment parameter does not involve any of the dimensionless parameters; it is only a function of the gas density and the difference in density between the gas and liquid. There are two fit parameters: the exponential factor and the pre-exponential factor. For most air and water systems, the exponential term will simplify to around 1000, which means that the mass of liquid entrained will be about five times the gas entrainment. However, this value appears to be too large, because the gas is unlikely to drive more liquid than it weighs. The resolution to this issue is to note that the entrainment at the near surface level is superficial. In other words, the drops formed are simply formed, not necessarily ejected and entrained. In fact, much of the mass will fall back to the surface. Thus, it is possible that the mass entrained through this mechanism will have frequently undergone near-surface entrainment before it actually entrains and departs. This means that the liquid, on average, becomes airborne several times before it is finally evaporated or entrained and transported away from the pool.

Since the Handbook was published in 1994, there has been a moderate amount of follow-on work for estimating entrainment phenomena in recent years. Cosandy et al. ([Cosandy 2003], [Cosandy 2001]) measured entrainment of soluble and non-soluble contaminants in water. Spiel ([Spiel 1997], [Spiel 1997a]) measured saltwater entrainment from bubbles bursting at a surface. New analysis and simulation methods have also been reported. [Duchemin 2002] performed a numerical study of jet-formed drops. Koch et al. [Koch 2000] uses a surface marker particle method for predicting the dynamics analysis. A modified formula for determining the critical drop diameter for jet formation is also a multiphase solution to the Navier Stokes equations. [Zhang 2012] presents a new formula for predicting the number of jet drops emerging from a drop based on dimensionless. [Zhang 2012] includes data from water as well as molten metal bubbles in the formulation, and provides a correlation for highly varying conditions. Correlations for the height of the rising jet and the height of drop ejection can be found in [Bagul 2013]. While models exist for some phenomena, none of the separate capabilities have been consolidated in a generalized model, as was done in [Kataoka 1983]. Accurately modeling the entrainment of drops from a boiling surface remains a difficult problem.

After a liquid fire is extinguished (or burned out), there may be a residual layer. A non-volatile contaminant may be found in high concentration in the residual layer. Deposition may also occur on surrounding surfaces, resulting in subsequent entrainment. These phenomena have been reviewed recently by [Henry 2014]. They are complex and further complicated for conditions that do not involve idealized single-component round particles. Wind, surface thermal stress, and morphology may also be complicating factors. A residual layer may entrain mass well after fuel has been completely consumed, as in the case of a contaminated liquid fuel fire. Resuspension is also an important phenomenon for contaminant entrainment; however, this study will only focus on physics that occur earlier in the problem of interest: the release of particles from a burning liquid during the generation of bubbles due to boiling. It is assumed that the generation of particles due to surface wave entrainment is relatively small when compared to release through boiling bubble formation entrainment.

#### *4.1.1 Methods*

As described above, there are models and correlations for predicting mass flux from a boiling surface. We are motivated to use the methods of [Kataoka 1983], primarily because the relations are suggested in the Handbook. Another component of this problem is particle size distribution. This is a complex issue, as models for it are not as prominent or well-characterized. Specifically, the flow dynamics near the boiling surface are complex due to the jetting of gases following the rupture of bubbles; the problem of drop evolution from a boiling surface is not well resolved. While numerous studies examine the size of drops formed from boiling systems, none combine all of the components needed to apply the models at the boundary of a CFD code.

With a relationship for the entrainment mass defined in Equation (4-1), the injection velocity spatial location and size distribution are the remaining factors needed to fully describe the system input. Boiling data from [Borkowski 1986] comprise a component of the drop size data presented and recommended by the Handbook. Different size data exist for different bubble sizes. Size distribution plots in terms of drop number frequency are presented, and the distribution is bimodal. The smallest drops form in the film region and result from the rupture of the surface bubble. The largest drops come from the jet region and result from the collapse of the bubble and the rebound of the bubble cavity mass. Figure 4-2 shows a plot of the size distribution for a 1.4 mm bubble of a 0.1% NaCl-Water solution. This plot is an extraction from the presented distribution and reflects the model that is to be subsequently used. The extraction points are treated as interpolation points, and the model for the distribution is generated by sampling drop sizes probabilistically, generating drops that reflect the mean mass and diameter with respectable accuracy. A computational script was written to sample the data and generate a tabulated list of input particles that would be distributed in space and time such that the mass and number mean from [Borkowski 1986] data are well-represented. The mass mean particle diameter was approximately 130  $\mu\text{m}$ , and the number mean was around 3-4  $\mu\text{m}$ .

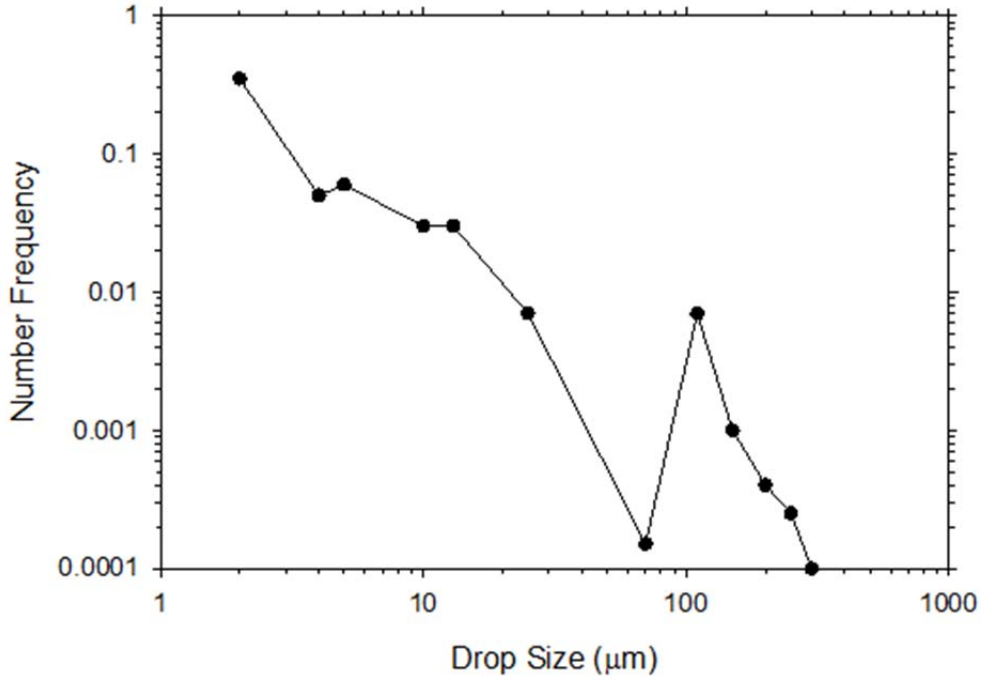


**Figure 4-2. An Extraction of the Number Frequency Data from [Borkowski 1986].**

The experiments of [Mishima 1973] involve the burning of a beaker filled with kerosene and 30% tributyl phosphate (TBP) contaminated with various materials. Iodine, one of the contaminants, was found to volatilize and was therefore more prone to become airborne. The other contaminants (including TBP) were not volatile and yielded similar results to each other, suggesting that the primary method of evolution was by drop transport. Researchers pre-heated the liquid to its boiling point and then ignited the fuel in a 50 mL beaker. We assume a standard dimension (from current commercial product data) of 56 mm height and 42 mm outer diameter for the beaker.

Additional assumptions are required to perform the simulation. Boiling was assumed uniform over the surface of the liquid, resulting in a uniform spatial release of particles. The tests typically lasted 50 minutes, during which time the liquid level receded from about 20 mm above the bottom of the beaker to near the bottom (4-9 mL of residue remained according to the test report). Since receding liquid (i.e., modeling with a moving computational mesh) is not a current capability of Fuego, simulations were performed for a short time with the liquid layer near maximum and minimum points to assess the trends. The behavior of the system between the two steady-state conditions can be estimated by interpolation between the two modeled conditions. Because the evaporation model did not allow for differing evaporation potential for multiple constituencies, the particles were assumed to be non-evaporating drops. The baseline turbulence parameters at the inlet are presumed to be negligibly low (described in more detail in Table 4-1), and the inlet velocity of the drops is assumed to be random between 0-1 m/s. Simulations are initialized with the beaker initially full of air at ambient condition. The fuel evaporation is modeled as a constant flow rate of fuel from the liquid surface ( $7 \times 10^6$  kg/sec).

As shown in Section 3.1, the SIERRA architecture enables calculations that take advantage of the massively parallel architecture computers at SNL. Fuego is designed to predict low-Mach

number ( $M < 0.3$ ) reacting flows, and has a capability to model particle and drop transport using a dilute spray approximation Lagrangian/Eulerian coupling. The liquid phase can be modeled as individual Lagrangian drops that interact through momentum source terms with the Eulerian gas phase.

Particles in Fuego are modeled with a parcel concept. Instead of modeling the transport of every unique drop, the parcel concept assumes that the general behavior can be appropriately modeled by statistically grouping like-sized particles and transporting the mass together. The parcels greatly facilitate modeling the system, as many of the fine drops have little individual effect on the flow and can be transported in bulk. Thus, the particles are transported in a more efficient way that statistically represents the bulk behavior, as particles that impact a surface are assumed to stick. No collisional effects are presently modeled. A drop vaporization model exists, but is not used in this case under the assumption that the burn rate is completely described by the gas evolution at the surface of the fuel. This facilitates quantitative comparison. Mass entrained and exiting the system is assumed to have a proportional amount of contaminant to the initial mixture. The liquid evolution from the surface is assumed to contain a proportional amount of contaminant to the initial mixture. Reactions are modeled with the eddy dissipation concept (EDC) model [Magnussen 1981].

The models for drop size and mass presented above are used to generate drops that emerge at the surface of the burning fuel. The last factor necessary to model the behavior of these drops is the turbulence source terms at the inlet boundary. Turbulence is treated as a free parameter, and is described more in detail below in the context of the results. It is important to note that all simulations were conducted using SIERRA version 4.34.

#### 4.1.2 Results

Figure 4-11 shows predicted flame temperatures and particles (exaggerated for visibility) based on modeling performed with Fuego. As shown this figure, temperatures are plotted on the left, and particle parcels are exaggerated in size and colored according to their size with the hemispheric-cut semi-transparent surface sides of the beaker colored by number deposition density. As speculated in the data report, significant deposition is predicted on the sides of the beaker. The initiation of the fire results in significant entrainment, which decreases as the fire matures. Smaller particles are more likely to be entrained, while larger particles are more likely to fall back to the surface of origin due to gravitational settling. The larger particles tend not to rise as high because gravity is a more significant force relative to the other forces on the particle with increasing size.

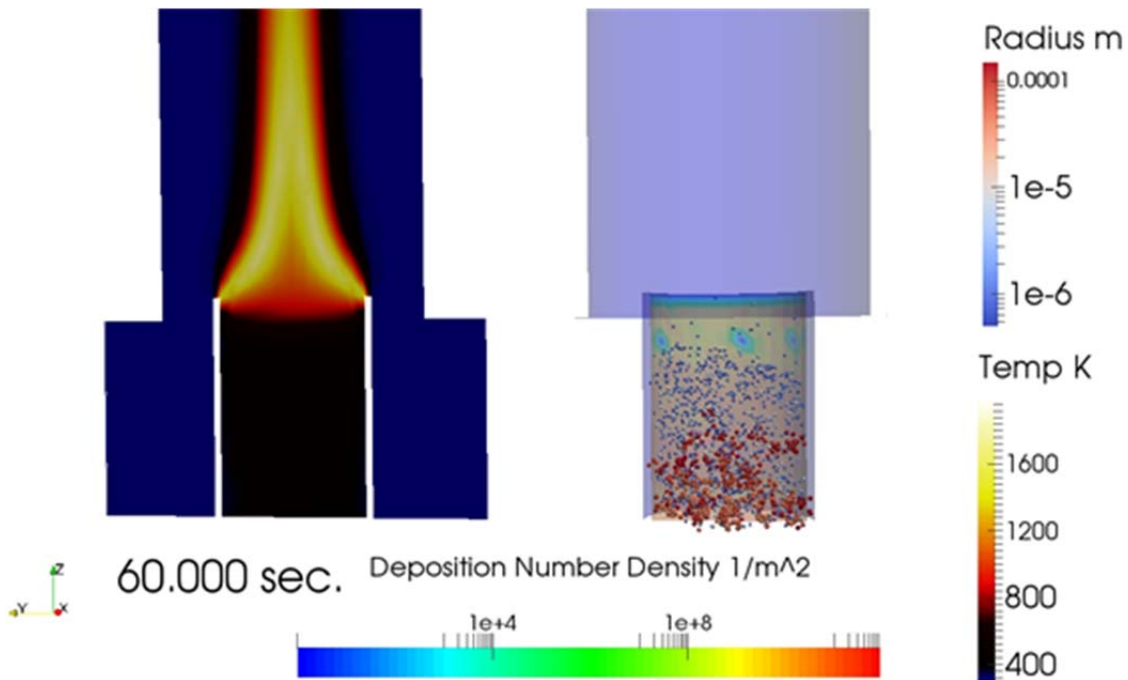


**Figure 4-3. Predicted Liquid Entrainment from [Mishima 1973] Tests, with Particle Parcel Sizes Exaggerated for Visibility.**

The first set of simulated results helped define subsequent analyses. The ultimate destination for the particle mass is initially calculated for two ten-minute intervals for a baseline scenario. The first interval is the starting 10 minutes, and predicts the behavior of the system during start-up conditions. After about one minute, a steady-state fire condition is attained, where the fire is burning regularly and the deposition of drops becomes steady. The mass of drops from the boiling fuel surface to deposit on three key surfaces is shown in Figure 4-4 for the early time interval. The significant portion of this plot, relative to the data from [Mishima 1973], is the “escaped” mass, which is essentially released in the first few seconds after ignition. This is due to the transient nature of the start-up, allowing more particles to escape as the flame dynamics occur nearer the fuel surface. The mass deposition for the last ten minutes simulated with the pool depth near the bottom of the beaker is shown in Figure 4-5. In this simulation, the end time was simulated by tracking the constant particle rate as it interacts with a constant fire at increased depth. The intent of the simulation was to explore the steady-state deposition towards burn-out to provide a basis for estimating the long-term trend (by interpolation). It was thought that the initial transient information from this simulation would not be used. Researchers observed that the magnitude of the initial pulse was approximately the same as for the scenario at the first 10 minutes. Because of this and the fact that the initial pulse involved most of the entrained mass, further evaluation of this finding is warranted. Visualization (like Figure 4-3, but not herein reproduced) of the results suggests that the very small particles continue to escape after the initial transient. Figure 4-6 and Figure 4-7 show the deposition based on number of particles. Unlike the mass deposition in Figure 4-4 and Figure 4-5, the particle count suggests that there is still escape of some particles following the initial transient. The escaping particles are quite small; their masses are not significant enough to contribute to the mass deposition. These plots also suggest that the deposition rate of particles becomes relatively steady after the initial transient.

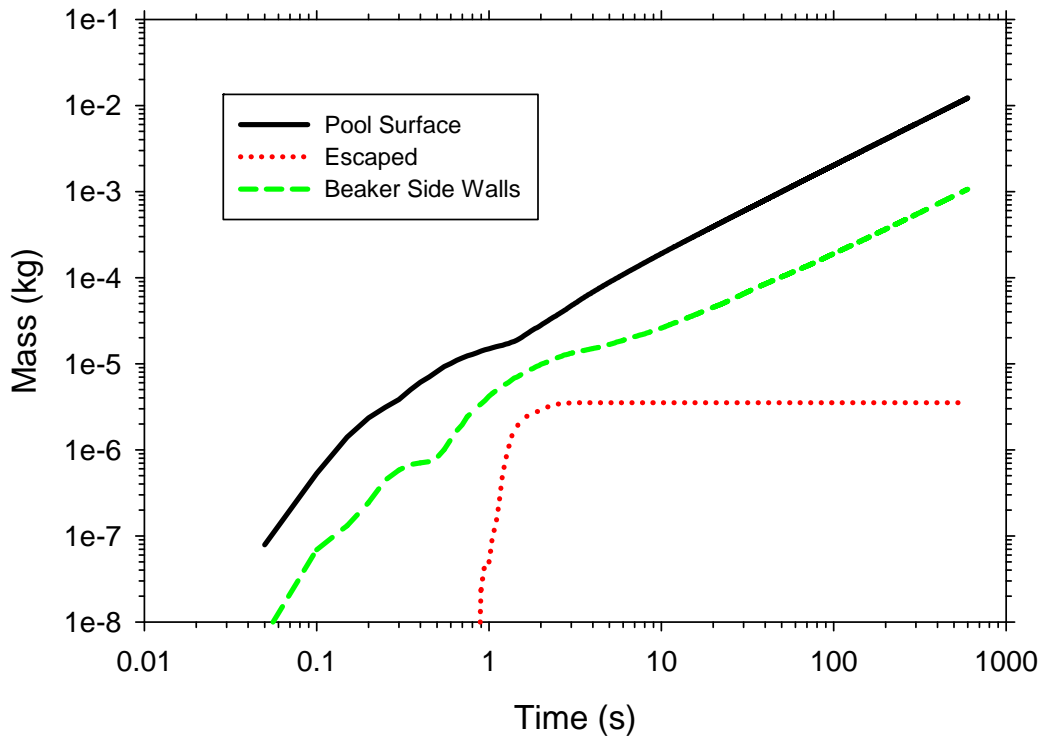


Figure 4-4. Predicted Mass Deposited for the First 600 Seconds (20 mm Height Pool).

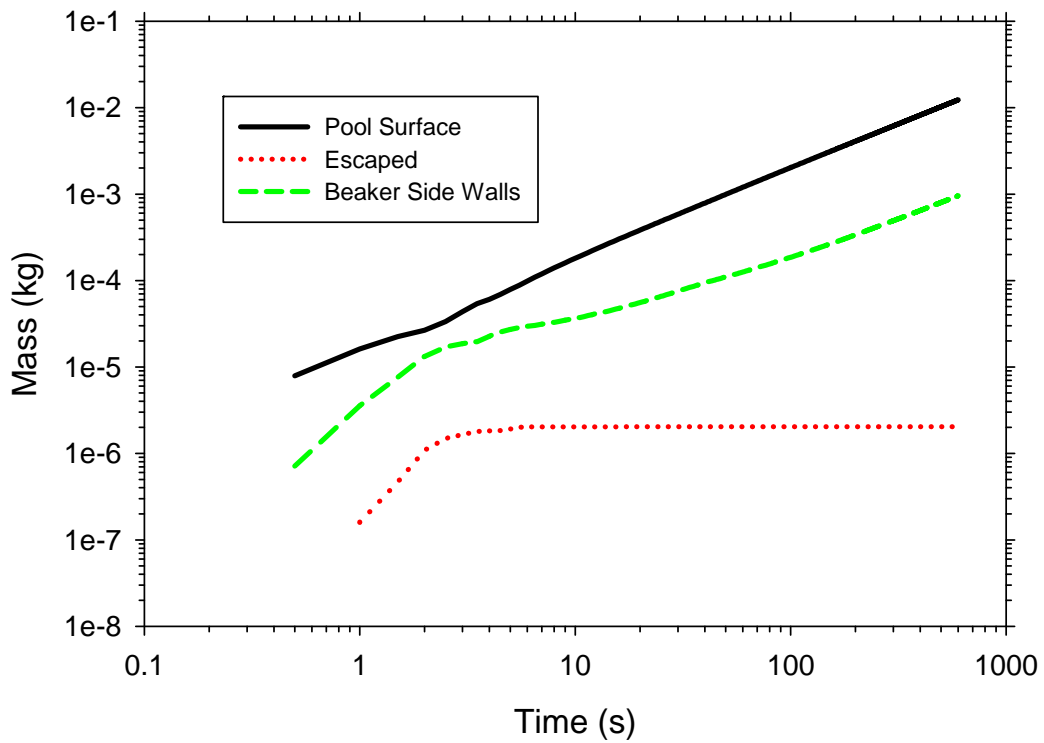
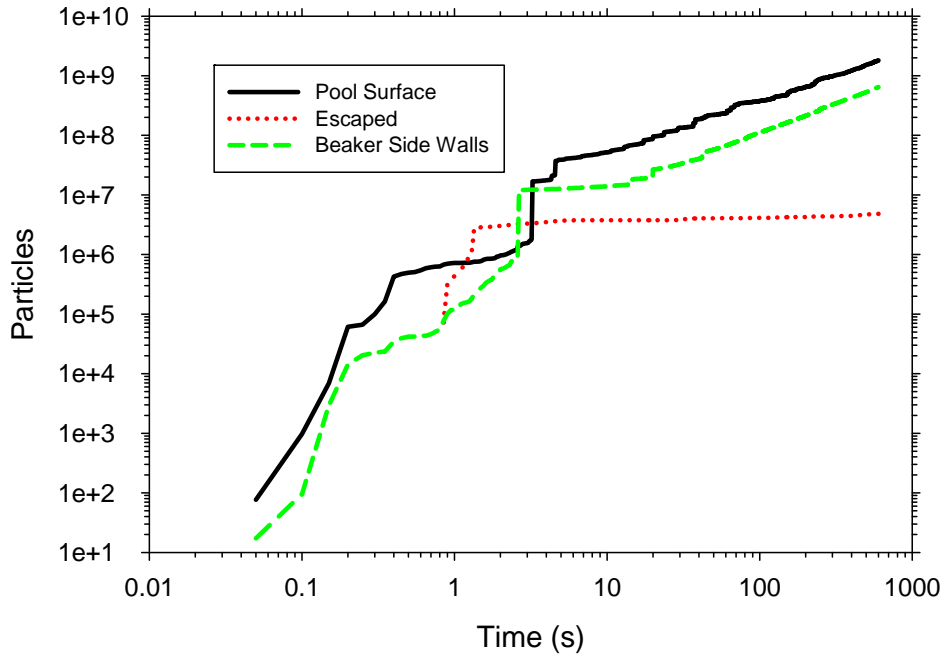
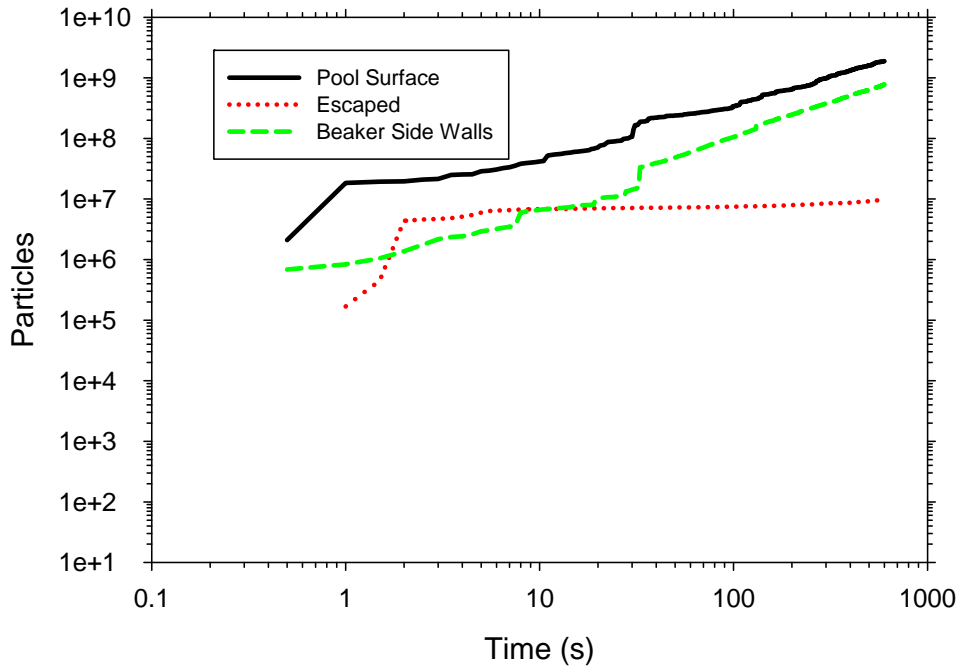


Figure 4-5. Predicted Mass Deposited for the Final 600 Seconds (0 mm Height Pool).



**Figure 4-6. Predicted Particle Number Deposited for the First 600 Seconds (20 mm Height Pool).**



**Figure 4-7. Predicted Particle Number Deposited for the Final 600 Seconds (0 mm Height Pool).**

A large amount of the particle mass is found deposited on the beaker side walls, which occurs as the drops formed from the boiling liquid impact them. The deposited mass in the actual tests might subsequently react to evaporate off the walls, but might also descend back to the pool

surface through gravitational forces. Entrainment from deposition on the beaker walls was postulated as being a potentially significant source of entrainment of contaminant particles [Mishima 1973]. This computational work in the magnitude of the predicted deposition indicates agreement that this entrainment mechanism is potentially significant.

This first set of simulations helped determine the subsequent models that were run. During the first six seconds, almost all of the particle masses exited the beaker to the collection point, and almost no mass was subsequently collected. This suggests that the initial transient was the driving factor in the total release. This finding was not anticipated, as the experimental report did not suggest this to be the case, and it was instead thought that the longer transient would result in a more significant emission. The main purpose for initially running the two liquid heights was to extract the effect of the liquid height on the steady emission of particles over the duration of the flaming. Comparing Figure 4-4 and Figure 4-5 indicates that the simulation for the final 10 minutes (which has a lower liquid layer in the beaker) resulted in a comparable initial emission of particle mass. This is presumably due to the buoyant effect of flames initiated deeper in the container. The increased motion of the flames is better able to lift particles, even though the particles have farther to go to exit the beaker. This raises the question of whether the experiment was indeed a conservative test, because there was no effort to vary the initial liquid height. Several different particle input files were used, and the magnitude of the initial six-second mass escaping the beaker depended on the particulars of the input file. This is likely due to the precise spatial distribution of particles relative to the flame during the initial ignition. The main difference in the particle input files was in the location of individual particles as a function of time, and could be viewed as a good model for the actual physical uncertainty in this regard. There was negligible difference in the particle size distribution. The sensitivity to different particle input files and to the initial liquid height were therefore selected as parameters of variation for further investigation.

For the baseline turbulence scenario, the initial liquid height above the bottom of the beaker and the particle input file were varied. The results are plotted in Figure 4-8 (in terms of ARF for consistency with the data). The data were for a single initial liquid height, and indicate a general increase in ARF with a decrease in the liquid height for baseline pulse simulations. The simulations with 40 mm initial height had the lowest ARF from the pulse, but particles were increasingly able to entrain in the plume at that height. Simulations were run to 160 seconds, and the trend for 60 seconds from 80-140 seconds was projected out to the full 50-minute duration by linearly interpolating the entrainment trend from the 40 mm height value during the first minute out to the zero value obtained for the steady-state emission case, where ignition occurred with the liquid height 20 mm above the bottom of the beaker. The green squares indicate the ARF that is projected using this method, and represent the sum of the baseline pulse data and an estimate of the ARF due to the steady entrainment over the course of the burn. The baseline pulse data for the 20 mm initial height case exhibits a greater spread than the data, but generally agrees with the mean.

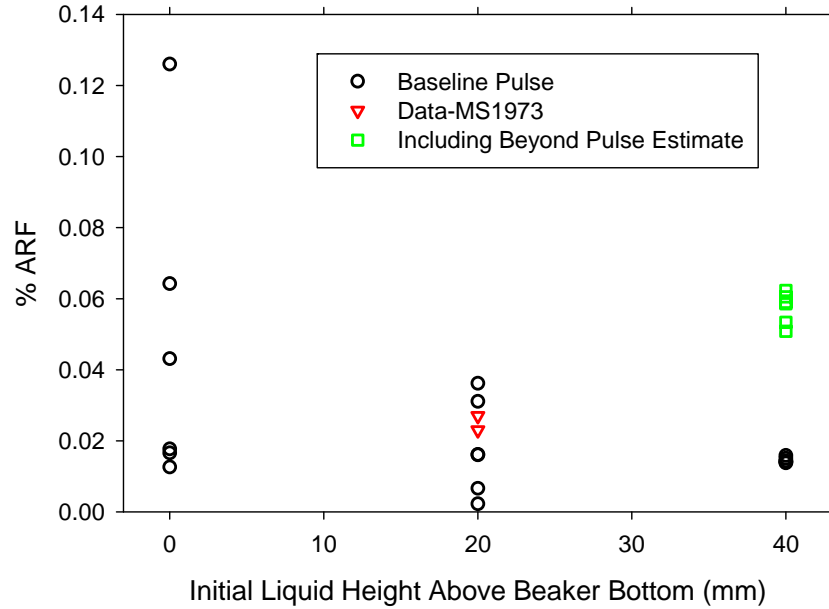


**Figure 4-8. Summary % ARF Plot for the Baseline Turbulence Assumption for Various Particle Input Files and Initial Liquid Heights.**

The particle transport model uses a stochastic function that is scaled by local turbulence parameters to model the effect of sub-grid turbulence on the transport of the particles. Turbulence was modeled in these cases with the temporal of the Navier Stokes (TFNS) model in [Tieszen 2005]. This Navier Stokes model belongs to the class of turbulence models that are a hybridization of large-eddy simulation (LES) and Reynolds and that average the Navier Stokes equations (RANS) methods. Sub-grid turbulence that is presumably due to the agitation of the boiling liquid/gas interface is believed to contribute to particle motion. Characteristic length-scales of turbulence might vary from the smallest postulated boiling drop size (around 0.5 mm) up to the internal diameter of the beaker (40 mm). Turbulence intensity (fluctuating velocity over the mean) is difficult to assess, but may be significantly higher than unity because it is augmented by the rupture of bubbles at the surface of the liquid and the motion in the cylinder. The local contributing velocities may be much higher than the bulk mean flow of fuel vapor. The initial tests used the low baseline values in Table 4-1 as boundary conditions at the fuel surface. Subsequent analysis included four variations, labeled from A to D as indicated in Table 4-1. This was to ascertain whether the finding that the main particle emissions were due to the initial transient carried over a range of possible turbulence conditions.

**Table 4-1. Turbulence parameters for the sensitivity study**

Runs	k [m <sup>2</sup> /s <sup>2</sup> ]	epsilon [m <sup>2</sup> /s <sup>3</sup> ]	Corresponding length scale [m]	Corresponding turbulence intensity [%]
Baseline	5.95e-7	4.56e-7	1.7 × 10 <sup>-4</sup>	100
A variation	5.95e-5	1.53e-4	5 × 10 <sup>-4</sup>	1000
B variation	5.95e-5	1.92e-6	4 × 10 <sup>-2</sup>	1000
C variation	5.95e-3	1.53e-1	5 × 10 <sup>-4</sup>	10000
D variation	5.95e-3	1.92e-3	4 × 10 <sup>-2</sup>	10000

The six scenarios with baseline turbulence are plotted again with the data in Table 4-9 (20 mm height). This plot also includes eight scenarios where the turbulence parameters were varied according to the values in Table 4-1. Of particular interest was whether changing the turbulence parameters had an effect on the longer-term entrainment. In Figure 4-9, the long-term entrainment is plotted with the initial pulse ARF. The contribution of the long-term entrainment due to turbulent transport is expressed in red bars as shown in this figure. There were only two cases where this long-term entrainment was found to be significant (above 1% baseline ARF), both related to turbulence case D. The different numbers denote different particle input files, as in the legend title of Figure 4-9. Particle input file 7 uniformly resulted in higher predicted ARF than particle input file 8 for all turbulence assumptions.

These simulations suggest that the turbulence parameters can result in a higher release. The combination of parameters used where the release was significant involved high-turbulence intensity, as well as a large characteristic length-scale. Other more moderate conditions did not exhibit significant entrainment.

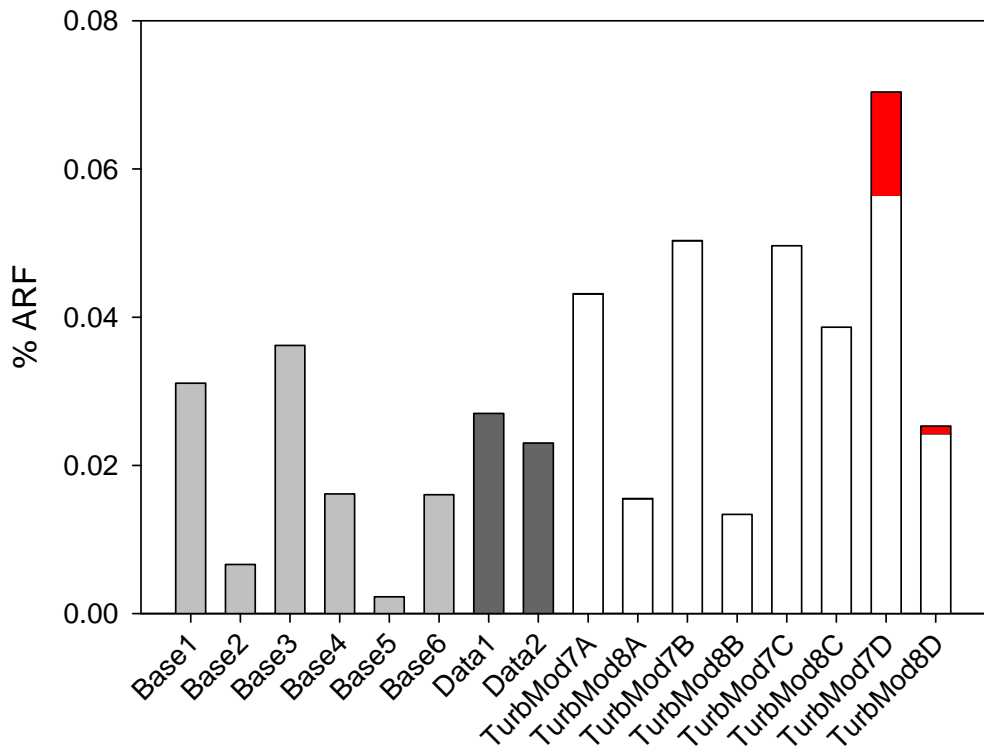


**Figure 4-9. Percentage of ARF for a 20 mm Initial Height for a Variety of Particle Input Files (the simulation number) and Turbulence Assumptions (the simulation letter) Compared to the Data.**

#### 4.1.3 Discussion

The models employed in this exercise gave predicted ARF values that were, on average, reasonably close to those measured experimentally. This could be viewed as a validation of the predictive codes. However, this interpretation is not how the authors believe the results are best interpreted. There were several assumptions made that are believed to have a significant effect

on the quantitative results of these simulations. First, the quantitative-predicted ARF comes primarily from the initial burst in the first few seconds of simulation for most of the cases. Ascribing accuracy to this part of the simulation is not warranted. The method of ignition was not stated in the experiments, and is therefore believed to be most probably based on a match or lighter manually inserted at ignition time. Furthermore, since the liquid was heated to the boiling point prior to ignition, the beaker in the experiments was probably not filled with air down to the liquid level, as it was in our simulation. The initial conditions of the simulation used in the model were convenient, and reflected uncertainties within those reported experimentally. In follow-on work, it may be more practical to try different computational initial conditions to observe how sensitive the predicted ARF is to the initial gas phase fuel in the beaker. Performing new experiments that resolve the temporal contribution to the ARF may also be warranted. The experimental results were integrated over the duration of the test.

Another point of concern is that the liquid drops in the model were not allowed to evaporate. The reason for this assumption is that some minor code modifications are necessary for this capability to exist in the current code. Such modifications are being considered for subsequent development. A viable entrainment mechanism may involve evaporation of the fuel from around the contaminant. The initial formation of a drop may occur before the evaporation of the volatile component, which will then be followed by the transport and escape of the residual (much smaller and more prone to escape) material. It is possible that this mechanism is a dominant mechanism, in which case the negligible mass entrainment after the initial pulse might become more significant as the particle size distribution shifts downward and the density of the contaminant in the particle increases. It would be helpful to revisit these simulations with the model improvements to better reflect the potential for a downward shift in particle size due to evaporation. In this case, a method would need to exist to capture the varying mass of the different particle constituencies at the outflow boundary.

[Mishima 1973] postulates that the deposition on the beaker side-walls and subsequent drying and entrainment might be an active mechanism for contaminant release. These prediction results suggest that the beaker side walls do indeed experience significant deposition of drops. The subsequent mechanistic behavior was not modeled, but remains a viable consideration.

A third point of concern is the fact that these data are being used in the safety analysis space to define a conservative ARF. The Handbook uses bounding values, including data from this test, as a guideline for designing safety systems and risk assessment. The simulations in this exercise suggest a significant relationship between ARF and the initial height of the liquid layer. The best predictions at this point suggest that the initial liquid height was not a particularly conservative selection, as both higher and lower initial levels resulted in increased mean ARF values compared to both the predicted and experimental ARF mean at the conditions of the experiment. Considering this, performing a revised set of experiments at a greater variety of representative conditions would greatly increase the confidence level in the recommended regulatory and design limits. If the model reaches a point at which quantitative confidence can be ascribed to the results, it may obviate the need for further testing.

Even though the modeling methods employed in this effort lack a complete description of the behavior of this complex system, the exercise has uncovered important considerations that should be noted in future studies of these phenomena. Surface boiling and entrainment models are not particularly mature. Although there is not a generalized model for phenomena of this

nature, there are models and data that can be combined to provide reasonable assumptions for simulating the transport of the drops. Simulations suggest that particle-size filtering occurs below the flames that preferentially entrain the smallest particles into the flames and into the plume. This suggests that the film rupture mechanism for particle formation is important, as it produces the smaller drops that are more likely to be entrained. Jet-formed drops may also be significant during initial or transient events if they can evaporate to the point that they become small. This behavior can be explored in future work after implementing a multi-component evaporation model.

#### *4.1.4 Conclusions*

These simulation results suggest that the airborne release of contaminants from a burning fuel was primarily due to the initial flame dynamics during the start of the fuel burn. Subsequent entrainment was subtle by comparison. No data exist to substantiate this finding, but the range of potential turbulent transport under steady conditions is thought to be adequately evaluated. The steady-state entrainment was negligible, except in a few cases where the intensity of the turbulence was augmented. New data in this regard would be helpful.

Varying the initial pool height resulted in scenarios with increased airborne release of contaminant in the models. This was not varied in the experiments, and the data from these experiments are being used as a conservative estimate. It is advisable to conduct additional tests informed by simulations that better capture the conservative conditions for this type of scenario by varying the initial height of the pool. The experiments simulated herein, while helpful, might not be bounding experiments for cases where the fuel height varies.

This comparison effort suggests the need for higher temporal fidelity data sets to better substantiate the mechanistic predictions of contaminant release for boiling pool fires. Data on the turbulence above the boiling pool surface might also be helpful, although results were not particularly sensitive to this parameter.

Some minor model improvements would greatly enhance both the ability to model the physics of this scenario and the confidence in the predicted results. Accurate multi-component particle capabilities might be expected to yield results that show the long-term entrainment to be more significant than it was in these simulations. Resuspension from surface deposits might also be important to the quantitative risk.

## **4.2 Pool Fire**

In addition to the beaker fire experiment shown in Section 4.1, we also simulate the pool fire experiment from the Handbook. Consider the case of a fuel or flammable solvent that is contaminated with radioactive powder or particulate. Spill and fire involving this material in a transportation accident can result in potential radiological releases or consequences to cohorts through the entrainment of the particles, particularly those sizes in the respirable range in the air.

In concert with the beaker fire simulations, we herein simulate a larger-scale scenario with different conditions (i.e., vehicle fire accidents). Combustible pool fires in the atmosphere generally transition from laminar to turbulent as the scale increases past approximately one meter in circular diameter [Drysedale 1998]. Larger-scale fires also become less susceptible to burn rate effects like blow-out and surface heat transfer at the periphery of the pool. This particular fire is also a more realistic condition; unlike the previous effort, the initial fuel temperature is expected to typically be ambient.

This section describes the simulation comparisons of the Fuego to the data of [Mishima 1973a]. In one particular test, a non-volatile contaminant was mixed in a pool of volatile gasoline. Entrainment mechanisms believed potentially active for the test are reviewed, and the methods for modeling the entrainment mechanisms are discussed. Simulations are presented that show the potential for detailed computation of the release in this scenario.

The gasoline pan fire scenario of [Mishima 1973a] involves different physical phenomena (including the effect of cross wind) than the beaker fire scenario as described in Section 4.1. That work involved a pre-heated pool, in which the entrainment was thought to be dominated by the rupture of boiling bubbles emerging from the liquid layer. The TBP was also a potential mitigating factor, creating additional material that can trap the contaminant. The TBP does not boil off and remains mixed with the contaminant at the end of the test. Initially being at ambient temperature, the gasoline fire scenario is thought to be more complex in terms of the contributing physics. None of the recent review articles on contaminant entrainment ([Kogan 2008], [Bagul 2013]) lists a full range of potential contributing mechanisms as such. Rather, they focus on what is thought to be the dominant mechanism (boiling). A careful evaluation of historical information and data provides additional basis for categorization presented herein. Table 4-2 lists four general mechanisms that are considered potentially active for the general problem of a contaminated gasoline fire. It outlines conditions for activity that indicate requirements for this mechanism to be active. The functional sensitivity column lists parameters that are believed to have a functional effect on the quantitative magnitude of the entrainment. We posit that a complete theoretical mechanism for entrainment would include those functional parameters. Note that a strong wind may not be present for a fire in a facility. Thus, higher cross-flow velocity may be only (or increasingly) applicable in the open space environment. The following subsections describe each of the phenomena as shown in this table.

A discussion of the four general mechanisms are considered potentially active for a problem of a contaminated gasoline fire and identified in Table 4-2.

**Table 4-2. Entrainment Mechanisms Believed Potentially Active in Pool Fire**

<b>Mechanism</b>	<b>Conditions for Activity</b>	<b>Parametric Functional Sensitivity</b>	<b>References</b>
Evaporation Induced Entrainment (EIE)	Liquid is actively evaporating	Particle size distribution Density Exposed surface area Rate of evaporation Vapor pressure of the solvent Evaporating species molecular weight	[Mishima 1968]
Surface Agitation by Wind	Existence of a substantial wind and a liquid surface	Wind speed Surface tension viscosity density Fire dimensions Fuel layer depth Geometry present	[Derakhti 2014]
Surface Agitation by Boiling	Pool temperature approaches boiling point of liquid	Rate of boiling Size of bubbles Viscosity Surface tension Density	[Mishima 1973], [Kogan 2008], [Bagul 2013], [Borkowski 1987], [Kataoka 1983]
Residue Entrainment (Resuspension)	Wind , vibration, or other activating factors and no remaining liquid	Wind speed Particle sizes Density Viscosity Particle forces	[Roberts 2003], [Lick 2009], [Sehmel 1984], [Henry 2014]

#### 4.2.1 *Evaporation Induced Entrainment (EIE)*

First, the pool consists of a fuel (gasoline) that will evaporate at ambient conditions. The presence of the fire augments the rate of fuel evaporation. Even though contaminants are not prone to evaporate at the temperatures of the system, they have been observed to escape while the liquid is evaporating in prior testing of this nature [Mishima 1968]. The precise mechanism for this is not perfectly clear, but it is likely due to the liquid evaporating gases that have sufficient energy or force to make the smallest non-volatile particles near the surface of the solvent airborne, as the volatile liquid transitions to a gas. We are calling this mechanism “evaporation-induced entrainment” because it driven by a species that evaporates while evaporation is not anticipated for the particle.

This has been shown in past work to be a fairly subtle effect, and was found to yield ARF between  $10^{-4}$  and  $10^{-7}$  in [Mishima 1968] tests. The results included an average evaporation rate and a total release for heated, simmering, and boiling scenarios. We understand from past experience that radiation detectors can spike based on this mechanism alone—that is, from a spill of contaminated liquid within a facility.

The data from [Mishima 1968] do not describe the full set of parametric criteria in Table 4-2 in that the parametric sensitivity to particle size was not detailed. Data from this test may be adapted in terms of a flux, in which case their data can be considered representative for scenarios with comparable fluids and particles.

#### *4.2.2 Surface Agitation by Wind*

The second mechanism potentially in play for this scenario involves the evolution of material from the fuel surface due to wind-related disturbances and surface instability. Without wind conditions, there will be no surface agitation and this mechanism will not entrain. Under high-speed wind, the liquid will be significantly agitated with waves. The surface may form a frothy layer that includes mixed gas and liquid, and the rupture and agitation of this layer can lead to entrainment. Under a very slight wind, entrainment is not expected, so there is a minimum condition for the onset of entrainment via this mechanism. Wave tips could also form and lead to pinching and particle formation that can entrain contaminant in the air.

A recent computational study gives a fairly detailed review of the literature on this topic. [Derakhti 2014] also states that “liquid–bubble interaction, especially in complex two-phase bubbly flow under breaking waves, is still poorly understood.” They demonstrate some three-dimensional calculations using Navier-Stokes based solvers for predicting the behavior of breaking waves, with a focus on the mechanistic behavior of the waves and the dissipation of energy in the system.

Given the current state of knowledge, it is believed that this mechanism will be difficult to quantify accurately. Some problems would need to reside in the regime where the surface agitation is insufficient to activate this mechanism. In our opinion, this is not an active mechanism because the fire is small and the wind speed is not particularly high (particularly for fires inside in facilities). It could, however, become significant for higher wind speeds and larger pools (in orders of meters). Accurate predictions would require knowledge of the onset conditions, as well as a way to quantify the release past the onset conditions.

This mechanism does not require a fire to be active. The effect of a fire on the entrainment compared to that under non-reacting conditions is not thought to be well understood. It may augment the destruction of a superficial froth layer due to the enhanced evaporation at the top of the fuel layer. Whether or not this increases or decreases the formation of entrained material is not yet known. The presence of a fire also creates a unique flow pattern over the liquid as it burns, which could also play a role in the entrainment. An initial literature review suggests that the descriptions of this mechanism are dominated by non-reacting flows. The majority of the research in this area appears to relate to the behavior of the shore/structure interactions with bodies of water [Derakhti 2014].

#### *4.2.3 Surface Agitation by Boiling*

This mechanism is more heavily studied. It is particularly active for fires in deep pools that can reach near boiling point conditions as well as near burn-out conditions where the liquid layer can heat quickly. It involves the formation of bubbles and the rise and rupture of the bubbles on the surface of the liquid. This mechanism was the primary focus of the fire simulations described in Section 4.1 because the test that was evaluated was designed to exhibit this mechanism as the primary entrainment pathway [Brown 2015]. In that simulation, a particle size distribution was assumed based on data from [Borkowski 1986], and the superficial evolution comes from correlations of [Kataoka 1983]. [Kataoka 1983] provides separate models for the entrainment in

three distinct regions that are separated by a characteristic height. The near surface region entrains the most liquid mass, but the drops are mostly expected to fall back to the surface.

Note that Equations (4-1) to (4-7) described in Section 4.1 do not contain information relating to all the parameters listed in Table 4-2 that are thought to be significant. They are applicable to problems insofar as the materials are similar to those used to fit the parameters for boiling water.

#### 4.2.4 Residue Entrainment

The propensity to entrain the residues after the liquid has been consumed depends heavily on the form of the residue. If the liquid burn-off is complete, the residual material may be simply a derivative of the source material. More complex multi-component mixtures, reactions, and combinations can complicate this. Gasoline, which is mostly residue free during combustion, might leave behind a residue that is more trivial than the clearly complex TBP mixture that was tested and analyzed in Section Table 4-1.

Several methods for simple particle entrainment are deployed. For example, the Shields parameter is a dimensionless relationship between the shear stress and the staying force of the particle due to gravity. This is most commonly used in sediment transport and erosion studies. Using the form presented in [Roberts 2003], the Shields parameter,  $\theta_s$  is:

$$\theta_s = \frac{\tau}{(\rho_s - \rho_w)gd} \quad (4-8)$$

where  $\tau$  is the superficial shear stress,  $\rho_s$  is the density of the solid layer,  $\rho_w$  is the density of the fluid,  $g$  is the acceleration of gravity, and  $d$  is a characteristic length scale (the size of particle).

The Shields parameter is normally plotted versus a dimensionless length scale or the Reynolds number. A curve in such a plot is used to separate regimes of entrainment and non-entrainment. This curve is specific to scenarios, so there would need to be a Shields curve specific to the scenario of interest to know the propensity for entrainment. An erosion rate,  $E$ , is also used in the same community [Lick 2009]:

$$E = A\tau^n \rho_s^m \quad (4-9)$$

where  $E$  is the erosion rate,  $\tau$  is the shear stress, and  $\rho_s$  the density of the solid. The parameters  $A$ ,  $n$ , and  $m$  are fit parameters, and such parameters are specific to the conditions of the problem.

Small particles will be influenced by a parameter that is not present in any of the above mechanisms. They will involve the interfacial forces, which may become dominant for many scenarios where the particles can have an affinity for remaining attached to the surface or other particles. A fairly comprehensive treatment of this topic—one more in the physical regime of the test of interest to this study—is found in [Sehmel 1984]. Such physics have been more recently reviewed by [Henry 2014]. The evolution of particles from rough surfaces in turbulent flows is the topic of that effort, and some recent experimental work to quantify the relevant forces is presented. However, residual entrainment will not be considered in this study due to the

complexity of resuspension, but it will be considered in the future, when appropriate capability is added to the simulation tool.

#### **4.2.5 Methods**

Components of the models described in Table 4-2 are compiled to make simulations of the historical tests feasible. This section describes computational comparisons of model simulations to the experiments described by [Mishima 1973a]. The simulations produce a higher fidelity result than could be obtained experimentally, and therefore constitutes a new interpretation of the experimental effort. Two methods for entrainment are presently considered.

Fuego solves the Navier-Stokes equations for reacting flows. In the case of this study, the TFNS turbulence model is used [Tieszen 2006] with the EDC reaction model [Magnussen 1981]. Particles are simulated with a Lagrangian/Eulerian coupling scheme.

##### **4.2.5.1 Experimental Conditions**

The simulations presented here are based on an experiment conducted by [Mishima 1973a], with specific focus on experiment SA-17a, which studied particle release in a gasoline pool fire conducted inside a wind tunnel with a cross wind of less than four miles per hour (mph). The contaminant, 51.1 grams of depleted uranium dioxide, was distributed by hand into a 15 inch (38.1 cm) diameter stainless steel fuel pan prior to the addition of a gallon of gasoline, which was sprayed onto the surface using a nozzle. The cross wind was sustained for the entire nine-minute burn. High Efficiency Particulate Air (HEPA) filters were placed at the end of the wind tunnel to collect the entrained mass. After the fire died out, the flow was stopped, and the filters were removed for analysis. The initially collected mass was compared to the original contaminant mass to determine the ARF. Fans were re-started and the subsequent mass was measured. The mass initially collected is believed to be the sum of the mass released due to boiling and evaporation-induced entrainment. Subsequent mass may be ascribed to the resuspension mechanism. The wind-induced entrainment mechanism is not believed to be active in this scenario due to the low wind speed of approximately 1.0 m/s (reported less than 4 mph).

##### **4.2.5.2 Input Boundary Conditions**

Of the mechanisms listed in Table 4-2, two were chosen to model: the evaporation-induced entrainment and the surface agitation entrainment by boiling. The evaporation induced entrainment mechanism applies for the majority of the nine minute burn, while the boiling mechanism only takes effect once the fuel reaches its boiling point. Table 4-10 shows cut-away model predictions of exaggerated sized particle parcels colored by size as simulated based on the two mechanisms for the baseline scenarios (B1 and M1). The wind tunnel cross-section is 66 cm (height and width). The left side of the figure indicates that there are different pool heights: the higher one pertaining to a full gallon of gasoline in the steel pan and the lower one representing the same case near burn-out conditions. The particles in the evaporation-induced entrainment mechanism are assumed to be solid  $\text{UO}_2$ , while the particles in the boiling mechanism are assumed to be a mixture of fuel and  $\text{UO}_2$ . The difference in particle sizes for each mechanism will be discussed further as the specifics of each mechanism are disclosed.

Of the two mechanisms not selected, the surface agitation by wind mechanism applies to wind speeds strong enough to create standing waves on the surface of a fluid. Due to the low velocity of about 1 m/s, this mechanism is assumed not to contribute to the overall entrainment. Fuego does not currently have the capability to model the resuspension mechanism to entrain residue particles. As a result, simulations involving these mechanisms are omitted in this simulation. We plan to revisit the phenomena in the coming year (see Section 4.3).

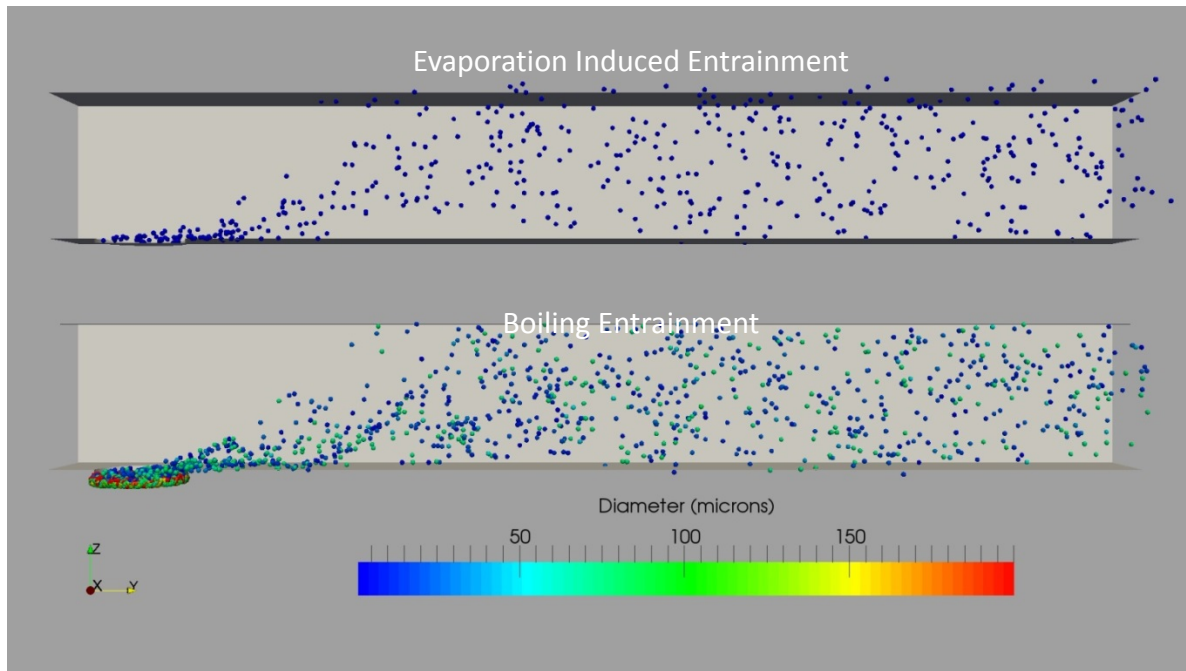


**Figure 4-10. Selected Entrainment Mechanisms.**

#### 4.2.5.2.1 Particle Source Term for EIE

Particles are introduced across the pool surface using a particle mass input rate. The mass input parameters for evaporation-induced entrainment were based on the experimental study of heated aqueous Plutonium Nitrate by [Mishima 1968], as depicted in Table 4-3. By analyzing the contaminant released during the simmering of the solution, the average rate of release was calculated to be  $2.3 \times 10^{-8}$  g/L. This parameter is scaled based on surface area for the pool fire case, giving a mass release rate of  $1.64 \times 10^{-13}$  kg/s. The amount released by this mechanism is very small; presumably only the lightest particles are entrained. Since a size distribution of the source and released particles was not included in [Mishima 1968], three particle sizes were selected for this modeling exercise, 0.2, 0.7, and 2 microns for the simulation. Since they do not rely on the presence of a fire to entrain (simply an evaporating liquid), the particles were injected from the initial starting point of the run.

**Table 4-3. Plutonium Release Rate Data [Mishima 1968]**

Run	Heat time (min)	ARF: wt%	Grams released	Boil-off Rate (ml/min)	Surface Area (m <sup>2</sup> )	Boil Flux L/(s*m <sup>2</sup> )	ARF flux wt%/(s*m <sup>2</sup> )	Release rate (g/L)
1	151	$4.5 \times 10^{-4}$	$3.15 \times 10^{-9}$	0.6	.00115	31.3	$4.3 \times 10^{-5}$	$3.48 \times 10^{-8}$
2	150	$1.3 \times 10^{-4}$	$9.1 \times 10^{-10}$	0.5	.00115	26.1	$1.3 \times 10^{-5}$	$1.21 \times 10^{-8}$

#### 4.2.5.2.2 Particle Source Term for Surface Agitation by Boiling

The pool height at which the gasoline reached its boiling point was taken to be two millimeters, based on preliminary simulations using the code's one-dimensional surface fuel model, which ran a full pan of fuel for the experimentally given nine minutes until burn-out. The experimental report did not give any indication of the duration of boiling [Mishima 1973a]. Because of the nature of the one-dimensional pool model (described in detail in a later section), some uncertainty remains. Boiling time and pool height were varied to account for this uncertainty.

The boiling mass input rate is determined by the superficial liquid velocity,  $j_{fe}$ , which can be calculated by combining Equations (4-1) and (4-3). The equation below was used to calculate the vapor mass release,  $j_g$ ,

$$j_g = \frac{Q}{A_p} = \frac{V_f \rho_f}{\rho_g \cdot A \cdot t} \quad (4-10)$$

where  $V_f$  is the volume of the remaining fluid,  $\rho_f$  is the density of the fluid,  $\rho_g$  is the density of the gas,  $A_p$  is the area of the fluid in the pan, and  $t$  is the total time of the fire while the fluid is boiling. The same particle size distribution method used in Section 4.1 is used in this simulation, including randomly locating the particles sized by a fit to the data.

The mass injected slightly exceeded the approximated total mass remaining in the pool, meaning that some of the mass will fall back to the pool and be released again. The injected mass was found, using Equations (4-1) and (4-3), to be  $8.3 \times 10^{-3}$  kg/s with a mass mean particle diameter of 150  $\mu\text{m}$  and a number mean of 3-4  $\mu\text{m}$ . A parceling method is employed, where a parcel representing multiple particles of the same diameter is injected into the flow instead of individual particles. To achieve the proper boiling particle size distribution, between 2000 and 3000 parcels were injected per time step. The parcels were not injected until three seconds into the run, as the fire first had to reach steady state in order to avoid ignition mechanism effects caused by relighting the pool at the start the simulation.

#### 4.2.5.2.3 Mesh Specifications

Using the experimentally reported dimensions, a wind tunnel mesh was generated (see Figure 4-11). As shown in this figure, the wind tunnel is modeled as a 0.66 m by 0.66 m square cross-section 4.57 m long. Surface 1 is the air inflow boundary condition, with a constant speed of 1 m/s (2.2 mph, assumed based on test report). Surface 2 represents the stainless steel wind tunnel walls, which was modeled with a 1.3 cm conducting wall boundary condition. Surface 4

represents a dirt ring in which the fuel pan sits. This was modeled as a 1D conducting surface 1.3 cm thick. Surface 3 is the outflow boundary condition, close to the experimental filter location. The entrained particles are collected at this surface, representing the collection filters. Since the code does not currently model volumetric receding liquids, a one-dimensional surface pool model was employed on Surface 5, which in the test was a circular pan measuring 0.381 meters in diameter. The gasoline fuel was modeled as pure heptane fuel ( $C_7H_{16}$ ), and the thermodynamics of gas phase heptane were used to simulate the more complex mixture actually used for the experimental test. Finally, Surface 6 represents the exposed stainless steel lip of the pool, which was modeled as a conducting boundary condition.

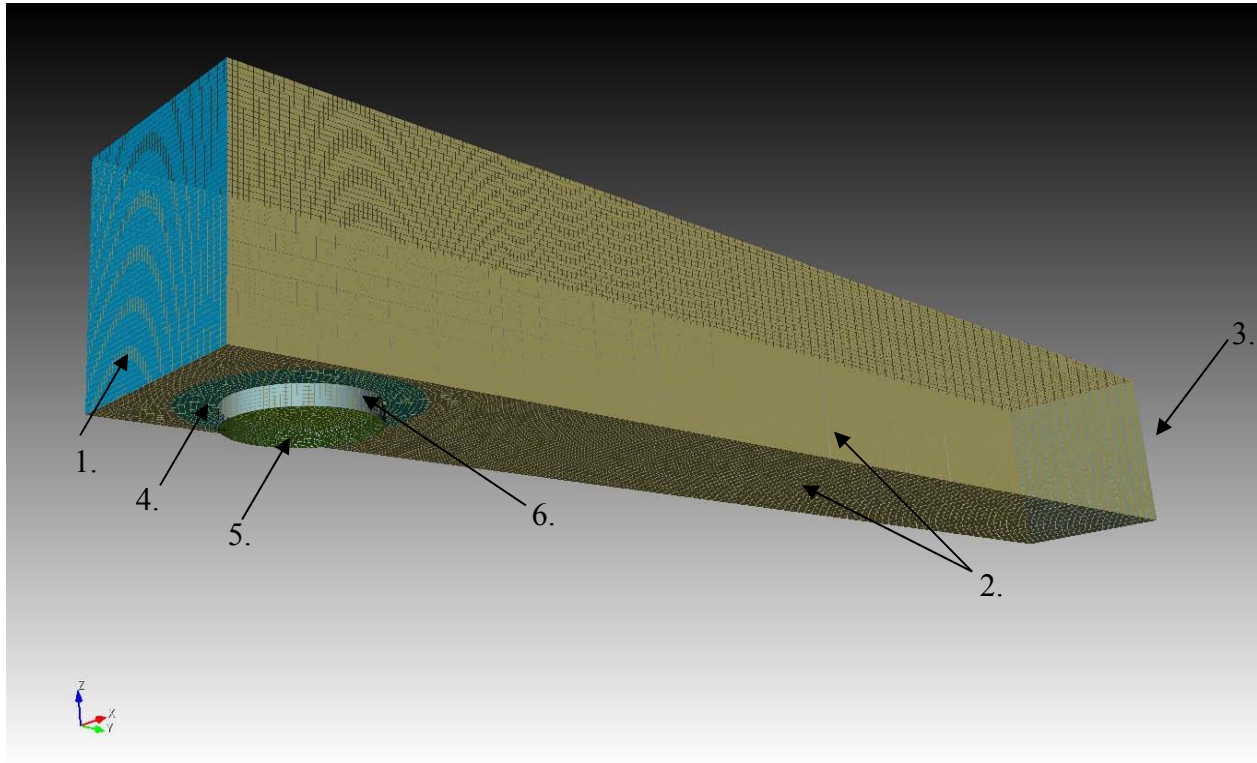


**Figure 4-11. Wind Tunnel Mesh Geometry and Surfaces (# represents a surface number).**

The lip height was 18 mm for the full pan and 51 mm for the near empty case. The full pan mesh is used to simulate the transition from the ignition time to the steady state time, while the near empty pan mesh is used to simulate the behavior near burnout. Multiple mesh refinements were made to determine mesh convergence. The mesh (as seen in the above figure) exhibited adequate mesh convergence, as there were very small variations between the medium mesh and increased refinements. The mesh was relatively uniform, with 12.7 mm spacing in the area of the fuel pan. Further downstream, the mesh was elongated in the flow direction to facilitate faster computation of the results. Mesh resolution was a parameter in this study and used to select the baseline mesh. A coarser mesh was not sufficiently converged with the next higher level of refinement. These results are omitted from this report.

At the end of a simulation, the injected mass is integrated on the outflow boundary, the pool surface, or the pool lip. Because the simulations were not run until all particles exited the domain, some remained entrained or suspended in the air at the end of the calculation. In the case of the simulations modeling the boiling mechanism, the liquid/solid mixture is allowed to deposit on the walls of the wind tunnel. The particles in the boiling case are assumed to be suspended in the entrained fuel droplets, which adhere to the walls, while the solid  $\text{UO}_2$  particles in the evaporation case are presumed not to adhere.

#### 4.2.5.2.4 Turbulence Parameters

To model the turbulence in the system, the TFNS was employed, which is a hybrid LES-RANS model [Tieszen 2006]. Precise turbulent boundary condition parameters could not be gathered from the original experiment. An assumed length scale of 10 cm was chosen, representing a grate on the inlet of the tunnel to protect the blower from foreign objects. A base turbulence intensity of 20% was selected. Because of experimental uncertainty, the turbulence parameters were modified to be significantly higher for one run, increasing the turbulence intensity to 100%, to study the effect on the entrainment. The turbulence parameters used are listed in Table 4-4.

**Table 4-4. Turbulence parameters\***

<b>Turbulence Location</b>	<b>K</b>	<b>Epsilon</b>
Inflow Boundary Surface (1, Fig. 2)	$2.0 \times 10^{-2}$	$4.64 \times 10^{-3}$
Pool Surface (5, Fig. 2), not Boiling	$1.13 \times 10^{-6}$	$1.12 \times 10^{-6}$
Pool Surface, Boiling	$3.11 \times 10^{-4}$	$1.23 \times 10^{-4}$
Inflow Boundary, 100% Turbulence Intensity	$5.0 \times 10^{-1}$	$9.7 \times 10^{-1}$

\*K is the turbulence intensity in  $\text{m}^2/\text{s}^2$ , and Epsilon is the turbulence dissipation rate in  $\text{m}^2/\text{s}^3$

#### 4.2.5.2.5 One-dimensional Pool Model

A simple one-dimensional liquid pool model was employed for these calculations [Brown 2006]. The model conserves mass and energy at the pool surface and emits fuel at a rate governed by the incident radiation and convective flux. Because it is a one-dimensional model, there is no leveling of the fuel, and the model behaves like the fuel was present in prism-shaped volumes at each computational node. Thus, burnout was faster in regions of highest heat flux.

#### 4.2.5.2.6 Particle Injection Method

Particle parcels are inserted into the simulation using an input file which contains parameters for position, initial velocity, temperature, diameter, particles represented by an individual parcel, and the time when they are to be injected. The particles are birthed at a specific height, spread randomly across the pool area. Depending on the mass input rate, individual parcels represent varying amounts of particles. For the EIE mechanism, a fixed particle diameter is given, and solid  $\text{UO}_2$  particles were assumed. A size distribution [Borkowski 1986] is employed for the boiling scenario, and the parcels are assumed to be solid  $\text{UO}_2$  suspended in a droplet of fuel. Quantitative grounds for injecting the particles are outlined in Section 4.2.5.2.1 and 4.2.5.2.2.

#### 4.2.5.2.7 Radiation Boundary Conditions

All radiation boundaries were modeled as having an emissivity of 0.9, and were assumed to be at the temperature of the local gas. Using Kirchoff's law, the emissivity and absorptivity are assumed to be equal.

#### 4.2.5.2.8 Particle Boundary Conditions

For the boiling scenario, all surfaces were assumed to be “stick” boundaries. Any particle that collided with the wall was assumed to stick to the surface without the possibility of re-emerging. This was assumed because the drops were liquid and the surfaces were assumed to be easily wetted. For the entrainment scenario, the boundary conditions were similar; except Surface 2 and Surface 4 were assumed to be ‘rebound’ boundaries where particles could not stick (see Figure 4-11). This was assumed because this model was thought to be the best existing boundary condition for the solid particles.

#### 4.2.6 *Simulation Scenarios*

From the parameters and uncertainties in the above sections, a sensitivity study was conducted. Table 4-5 lists the simulations with the various altered parameters to determine their contribution to the final result. The letter “E” in the run name denotes EIE, while the letter “B” denotes boiling entrainment. The duration parameter is the total time remaining until burnout. Most of the EIE (denoted as letter “E”) simulations run for the full nine minutes. The injection height is the distance above the pool surface where parcels are birthed. The pool boundary cell resolution varied slightly between the two meshes. The cells in the full pool are 6 mm high, while the ones in the empty pool are 8.5 mm high, meaning that the particles were injected in either the first or second cell of the lip, above or in the boundary layer on the pool surface.

**Table 4-5. Entrainment Scenarios\***

Run	Sim. Time (s)	Duration (s)	Fuel Height (m)	Injected Mass (kg/s)	Particle Size (um)	Turbulence	Injection Height (mm)
1E	20	540	$3.3 \times 10^{-2}$	$1.64 \times 10^{-13}$	0.2	Normal	10
2E	20	540	$3.3 \times 10^{-2}$	$1.64 \times 10^{-13}$	0.7	Normal	10
3E	20	540	$3.3 \times 10^{-2}$	$1.64 \times 10^{-13}$	2	Normal	10
4E	20	98	$6.0 \times 10^{-3}$	$1.64 \times 10^{-13}$	0.2	Normal	10
5E	60	540	$3.3 \times 10^{-2}$	$1.64 \times 10^{-13}$	0.2	Normal	10
6E	20	540	$3.3 \times 10^{-2}$	$1.64 \times 10^{-13}$	0.2	High	10
7E	20	540	$3.3 \times 10^{-2}$	$1.64 \times 10^{-13}$	0.2	Normal	5
1B	20	20	0.002	$8.3 \times 10^{-3}$	Distribution	Normal	10
2B	30	30	0.002	$8.3 \times 10^{-3}$	Distribution	Normal	10
3B	20	20	0.002	$8.3 \times 10^{-3}$	Distribution	High	10
4B	20	20	0.001	$4.15 \times 10^{-3}$	Distribution	Normal	10
5B	20	20	0.003	$1.25 \times 10^{-2}$	Distribution	Normal	10
6B	20	20	0.002	$8.3 \times 10^{-3}$	Distribution	Normal	5

\*These simulations were conducted using SIERRA version 4.36.

Table 4-6 and Table 4-7 describe the details of each run in Table 4-5 for the cases with EIE and boiling mechanisms. Runs 1E and 1B were chosen as the baseline scenarios, to which all other variations will be compared. Only one parameter was varied for each individual run numbered 2+ from the baseline case. This was done to study the sensitivity to parameters and to account for some of the experimental uncertainty. Variations 2E and 3E changed the uniform particle size to account for the lack of a specific distribution for this mechanism. Run 4E studied the EIE near the boiling point, with a larger lip and higher pool temperatures, to determine if the evaporation release changed over the duration of the burn. To compare the temporal effects to the baseline, 5E was run for a full minute. As stated in previous sections, the experimental turbulence parameters could not be gathered from the previous work, so the turbulence was increased in 6E. Finally, to determine if particle injection height influenced deposition location, the particle birthing location was reduced from 10 mm to 5 mm above the pool surface.

Similar variations were simulated for the boiling mechanism and compared back to the baseline scenario (Run 1B). Due to the boiling duration and height uncertainty, Run 2B was run for 30 seconds, while Runs 4B and 5B altered the fuel height from 2 mm (in Run 1B) to 1 mm and 3 mm, respectively. The same turbulence uncertainty in the EIE mechanism applies for the boiling case, so Run 3B increased the turbulence to 100% from the original 20% value. Similarly, the particle injection location was moved to 5 mm above the pool in Run 6B.

**Table 4-6. Evaporation Induced Entrainment Simulation Variations**

<b>Run</b>	<b>Detailed Description</b>
1E	Baseline. 20 second simulation, 10 mm particle injection height, 0.2 micron particles, full pan (low lip) mesh, and 33 mm fuel height.
2E	Particle diameter changed to 0.7 microns.
3E	Particle diameter changed to 2.0 microns.
4E	Lower fuel height (Empty mesh) and therefore taller lip.
5E	Simulated for 60 seconds
6E	Turbulence parameter increased to 100%
7E	Particles injected at 5 mm above the bottom of the fuel pan.

**Table 4-7. Boiling Entrainment Simulation Variations**

<b>Run</b>	<b>Detailed Description</b>
1B	Baseline. 20 second simulation, 10 mm particle injection height, particle size distribution, empty pan (high lip) mesh, and 2 mm fuel height.
2B	Simulated for 30 seconds with particle injections from 3 to 20 seconds.
3B	Turbulence parameter increased to 100%
4B	Fuel pool height lowered to 1 mm.
5B	Fuel pool height increased to 3 mm.
6B	Particles injected at 5 mm above the bottom of the fuel pan.

#### 4.2.7 Results

Since the wind tunnel outflow boundary in the experiments was near the experimental sample filter location, the particle mass deposition on this surface (see Figure 4-11, Surface 3) can be expected to relate to the entrained mass collected on the filters in the original report. By

integrating the deposited mass in the simulations, a predicted ARF can be determined by comparison to the original contaminant mass.

Figure 4-12 displays the mass deposition for the evaporation-induced entrainment baseline scenario (Run 1E) as a function of time. After five seconds, the trend is linear, suggesting that the early data could be reasonably extrapolated over the full nine minute duration. Figure 4-13 shows the mass deposition as a function of time for the baseline scenario employing the boiling mechanism (Run 1B). The boiling number deposition is shown in Figure 4-14. The results for the boiling scenario area also steady with time, suggesting the ability to linearly extrapolate deposition trends.

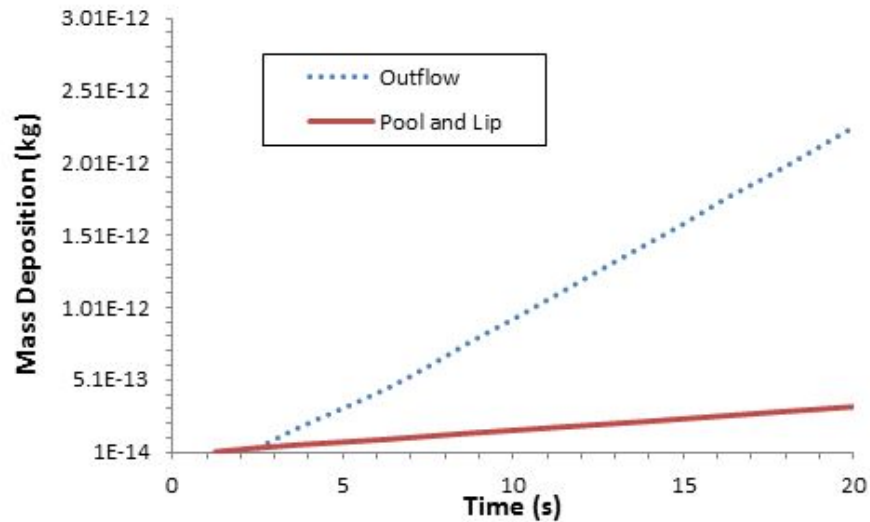


Figure 4-12. Evaporation-Induced Entrainment: Predicted Mass Deposition vs Time for Case 1E.

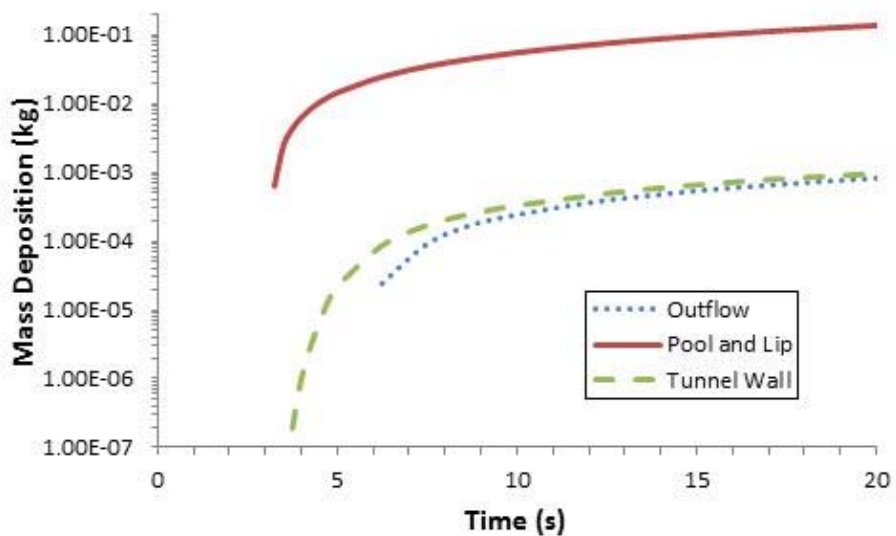
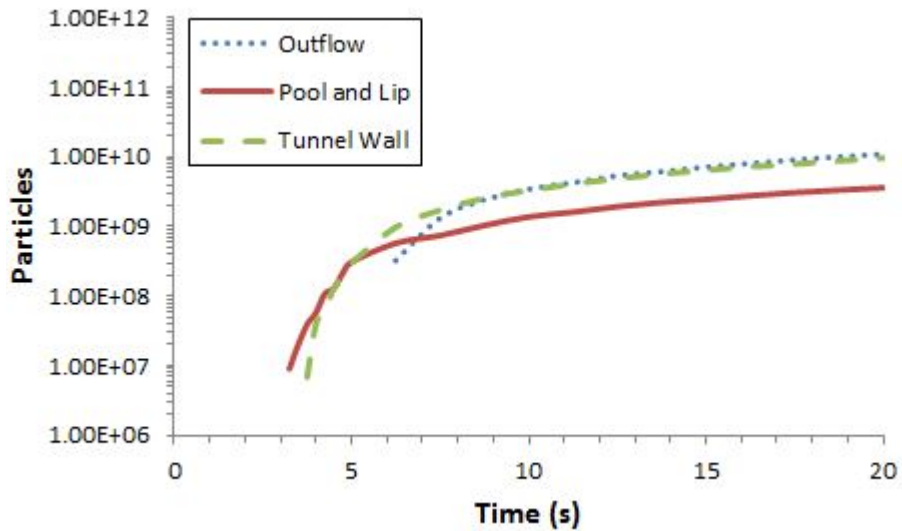


Figure 4-13. Boiling: Predicted Mass Deposition vs. Time for Case 1B.



**Figure 4-14. Boiling: Predicted Number Deposition vs. Time for Case1B.**

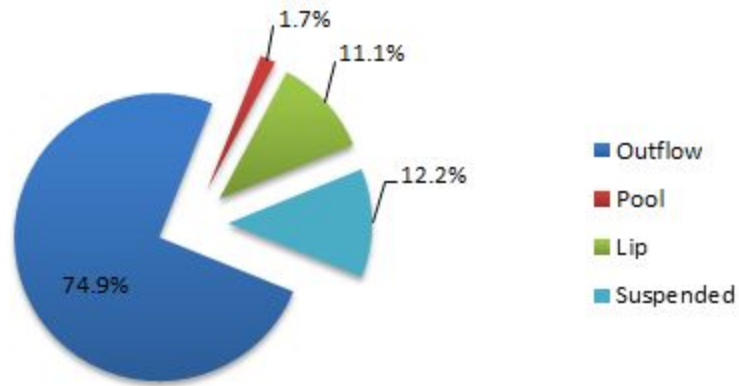
Reported ARF values for the boiling ARF results are only compared to the experimental results because the evaporation ARF results do not significantly contribute to the overall ARF (see Table 4-8). As shown, the predicted boiling ARF dwarfs the predicted evaporation ARF, despite the significantly shorter duration. This suggests the importance of knowing the duration of boiling.

Figure 4-15 and Figure 4-16 are pie charts of the predicted final mass location for the baseline EIE and boiling mechanism simulations, respectively. For the EIE, the majority of the mass is entrained into the flow and exited at the outflow boundary, while a small percentage falls back into the pool. The small particle size in the EIE allows the majority of the particles to follow the flow streamlines. A sizable percentage of the mass remained in suspension at the end of the simulation, meaning that there are particles in the flow which have not had the opportunity to adhere to a surface before the simulation ended. Based on earlier trends, is estimated that 90% of the mass remaining in suspension will exit the outflow boundary and 10% will adhere to the lip or pool surface.

**Table 4-8. Baseline ARF for Evaporation and Boiling**

Mechanism	ARF (%)
Evaporation (EIE)	$1.3 \times 10^{-7}$
Boiling	0.40

In contrast to the EIE scenario, most of the mass falls back into the pool for the boiling scenarios, and a small fraction—usually the smallest particles—exit the outflow. In comparison to the termination of the EIE scenarios, a smaller percentage of mass remains in suspension at the end of the boiling simulation. Trends from the longer simulation case (2B) indicate that 99% of the remaining mass in suspension will fall into the pool or stick to the lip, while the remaining 1% will deposit on either the walls or reach the outflow.



**Figure 4-15. Predicted End of Simulation Mass Fate: Evaporation Case 1E.**

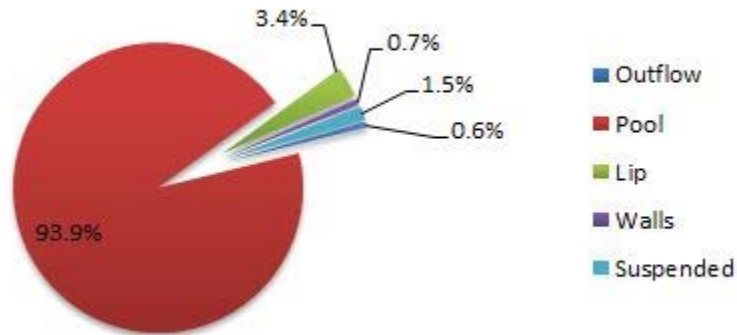


**Figure 4-16. Predicted End of Simulation Mass Fate: Boiling Case 1B.**

A breakdown of the final deposition for the evaporation scenario runs is shown in Figure 4-17. These values were calculated by comparing the deposited mass on varying surfaces to the total injected mass.

In comparison with Run 1E to Run 2E and Run 3E, varying the particle sizes had a very small effect to the overall entrainment, with only a slight increase in the lip deposition and a decrease in final suspended mass for the 2-micron particles. None of the 2-micron particles were deposited the pool surface, believed to be a result of only 40 particles being injected. The lower fuel run, 4E, had only trace amounts of pool deposition. The effect of particle size was relatively small. Comparing Run 4E to Run 1E shows only a slight deviation in the amount deposited. This implies that the deposition does not significantly change as the fuel recesses. Running the simulations for longer, as in Run 5E, confirms that the mass which remains in suspension will generally reach the outflow. Turbulence appears to have the greatest impact to the deposition location, shifting a significant portion of the outflow mass into the pool. This is evaluated by comparing results from Run 1E to Run 6E. In comparison of Run 7E with Run 1E, lowering the injection height in the model reflects the uncertainty in the appropriate height at which to birth particles. This also increased the pool deposition, but to a lesser extent than the turbulence.

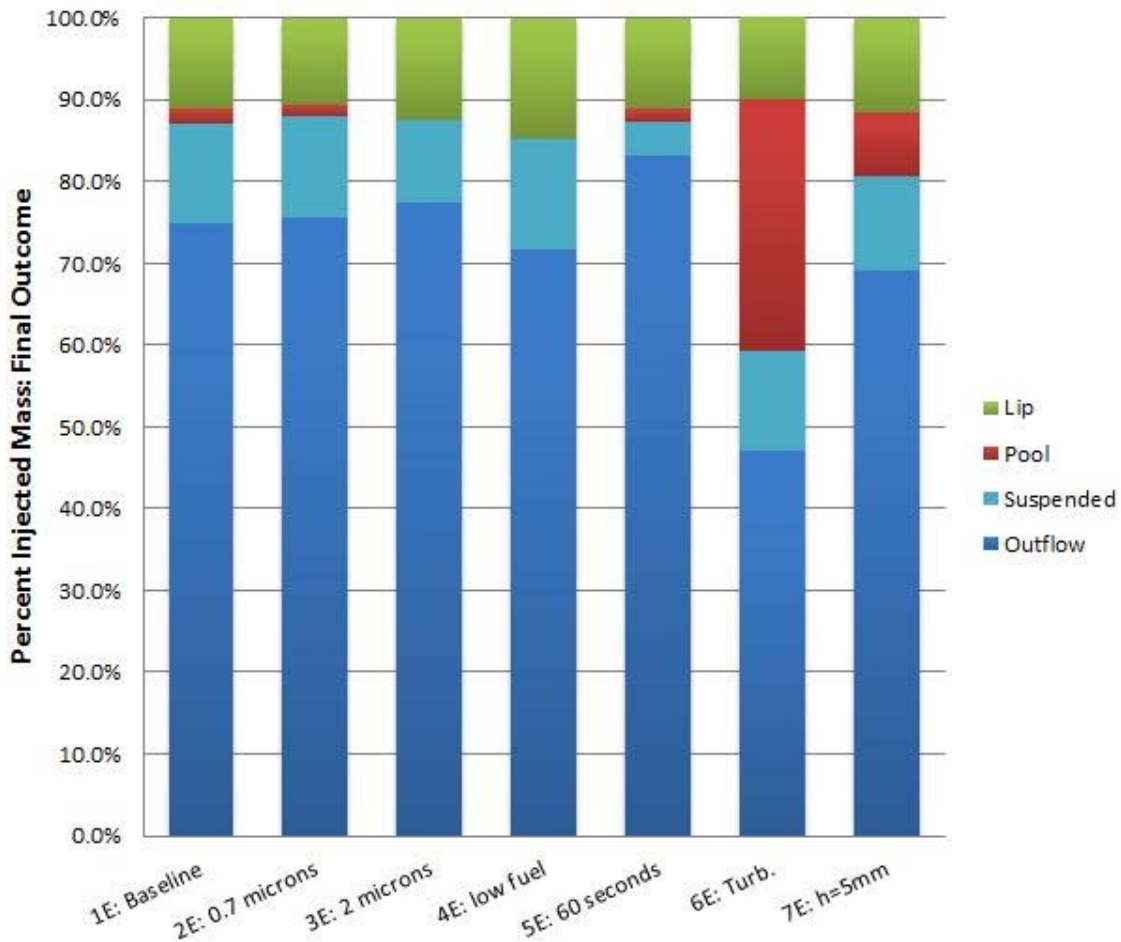


**Figure 4-17. Predicted Evaporation-Induced Entrainment Scenario: Mass Deposition.**

Since the experiment did not provide a boiling onset time, the values for the boiling duration and pool height were determined by preliminary simulations, which burned a gallon of gasoline for the full nine minutes and determined the time at which the fuel reached the boiling temperature. There remains a significant amount of uncertainty in these values. Figure 4-18 displays the final deposition of the injected mass for the boiling case. Note that the vertical axis is truncated; pool deposition dominates this scenario.

Comparing Run 2B to Run 1B confirms that the majority of mass remaining suspended in the flow settles back into the pool. Increasing the turbulence intensity (Run 3B) increases the percentage of mass deposited on the walls and decreases the pool and outflow mass depositions when compared to the baseline. Lowering the fuel height, as in Run 4B, did not significantly alter the deposition percentages, although raising the fuel height has a moderate effect (Run 5B). Comparing Run 6B to Run 1B, birthing particles only 5 mm above the pool surface reduces the deposition percentage on the walls and outflow and increases the amount captured by the pool surface. This is likely due to the increased likelihood of turbulent transport and impact on the walls caused by the close initial proximity.

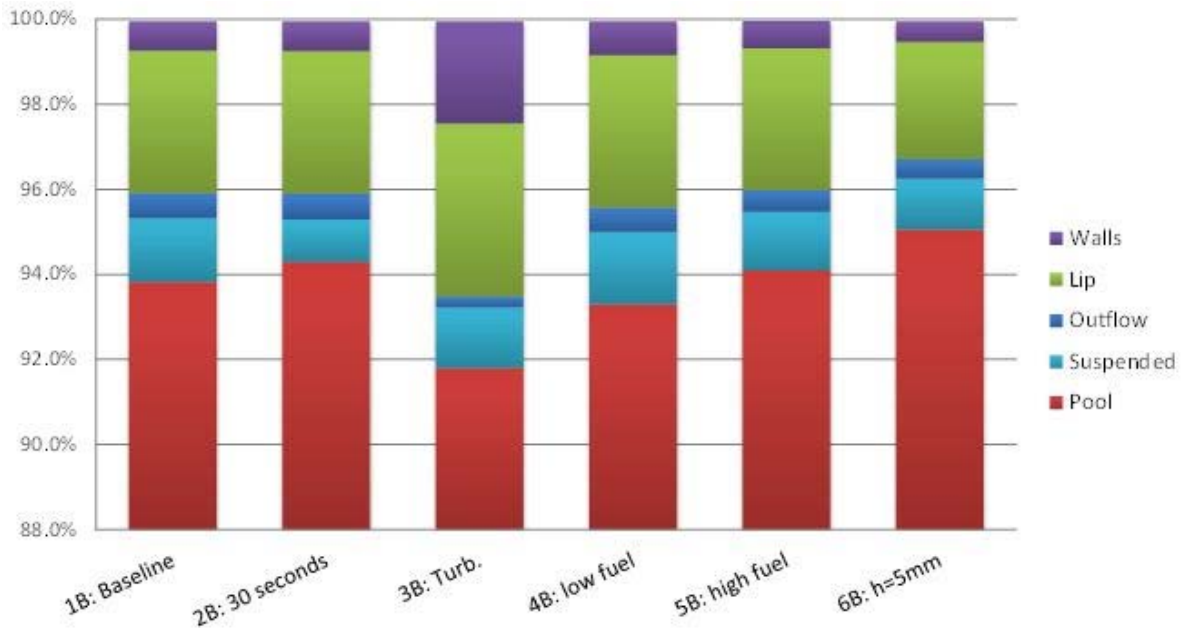


**Figure 4-18. Predicted Boiling Atomization Entrainment Scenario: Mass Deposition.**

Figure 4-19 displays the predicted airborne release fractions compared to the reported value from the physical experiment. The computationally derived results are on the same order of magnitude as the experimental results. Due to uncertainties in the model, the reported ARF is not reproduced. Certain data, like turbulence, inflow velocity, and boiling duration could not be determined from the experimental report, and that uncertainty is transferred to the simulation values.

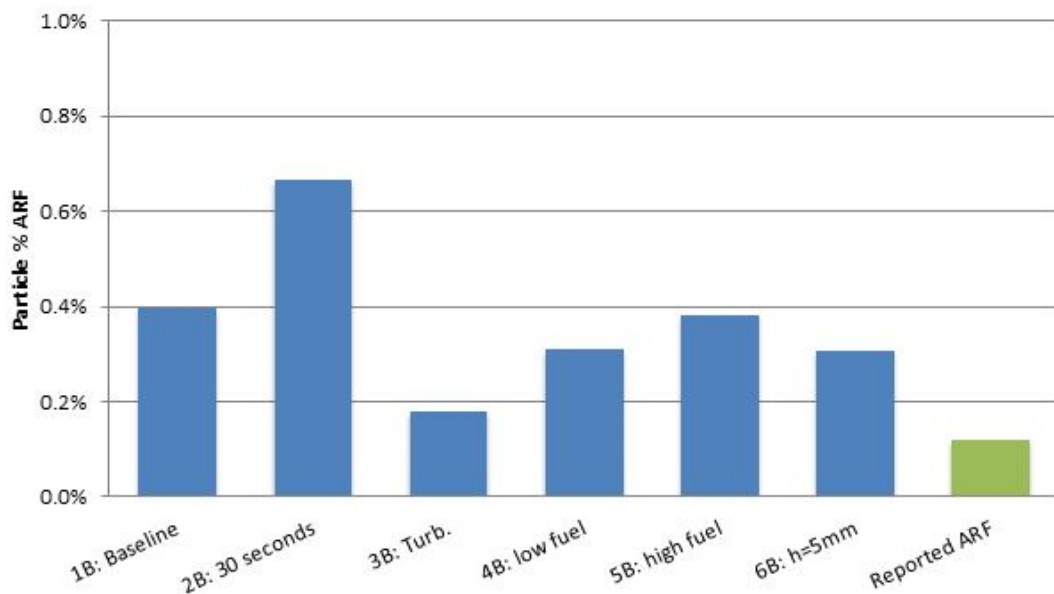


**Figure 4-19. Predicted and Reported Airborne Release Fraction.**

The ARF is calculated by scaling the percent of mass reaching the outflow boundary by a constant mass fraction of contaminant to total initial pool mass. The suspension of the uranium dioxide particles in the gasoline pool is presumed to be uniform (i.e., a homogeneous mixture). However, the large density ratio of contaminant to fuel, 16.1, indicates that the uranium particles would have a propensity settle to the base of the pan. This settling would reduce the ARF in the boiling regime, leaving more mass for resuspension. It is also understood that the concentration of contaminant would increase as the fuel level recedes, but a suitable model for this mechanism could not be established.

#### *4.2.8 Discussions*

The two model features missing from this effort that appear to be among the most critical to accurate predictions are the ability to predict resuspension and the onset and termination of the boiling. After the fire had subsided, we made no comparisons to the data that is likely due exclusively to resuspension. We treated the boiling time as a free parameter and found that a boiling time of about five seconds reproduced the measured ARF data, suggesting that the boiling time was short compared to the total duration of the burn. Our current project will be developing and implementing resuspension models that can be used to re-assess this scenario at a later date. A separate project is currently developing a volumetric model for a burning liquid fuel layer. This effort may produce a model that can be used to quantify boiling times.

Another model feature that may also be critical to accurately assessing these scenarios relates to the distribution and settling of the powder in the liquid. This effort employed an assumption of equal dispersion of contaminant in the fuel. This is not likely to be physical; the location of the solid in the fuel is thought to relate to the likelihood of the ejection of the solid. It is therefore important to have a means to describe the liquid/solid distribution.

In the boiling scenarios, the drops entrained from the surface of boiling liquid were assumed to consist of a mix of the solid contaminant and the liquid. These were not modeled as multi-component drops; rather, they were modeled as non-evaporating particles. The drops were assumed to stick on impact with a surface; however, reality is likely more complex. A particle consisting of mostly fuel might be expected to evaporate quickly at flame temperatures. If such a particle evaporates the liquid completely, it may decrease in size and behave significantly differently in the flow. Due to a lack of multi-component particle capabilities, the possibility for this was not allowed. It is unclear how significant this parameter will be to the outcome of the model predictions.

Turbulence was another parameter that was found to be a significant uncertainty relating to the quantitative accuracy of these predictions. Turbulence remains a challenging phenomenon for flow environments. Predictive accuracy could be enhanced, employing more detailed or higher accuracy models. The main issue with these comparisons, however, was not due to the model inaccuracies; rather, the experiments did not provide a particularly good quantification of the system turbulence.

The impact of a liquid drop on the fuel surface also represents a mechanism whereby entrainment can occur. Such an impact may induce a suspended mixture of water, fuel, and contaminant. This mode of entrainment could be generally described as due to external forces inducing agitation and suspension of the particles, which could be an active mechanism from the time of fire initialization to well after the termination of flaming. This mechanism is unique from both the wind-induced mechanism and the resuspension mechanism, as it involves some external forcing and potentially additional materials.

#### *4.2.9 Conclusions*

The list of mechanisms presented in Table 4-2 provides what is believed to be a unique assembly of the potential entrainment mechanisms for particles entrained from a liquid pool fire. Entrainment by suppression or external forcing activities might also be another mechanism for particle entrainment.

Fuego was used to compare predicted ARF to those measured in a relevant historical experiment. It was found that surface agitation by boiling significantly dominated the entrainment during flaming, as compared to the evaporation-induced entrainment. The duration of the boiling mechanism was found to be the most significant contributor to the amount of entrained mass. Improved modeling of particle entrainment from pool boiling will help quantitative accuracy of this type of modeling.

Future work would include the addition of multicomponent particles where fuel and solids are mixed, allowing the fuel to evaporate while the solid remains at a fixed mass. Resuspension is also an active entrainment mechanism that was not addressed in this effort. Particle dispersal in the liquid layer is also an interesting topic for future assessments. The ability to model resuspension, along with the assumptions of sticky walls, is likely to increase ARF calculated.

### **4.3 Improvement Needs in Fuego**

This section presents the need for certain model improvements to Fuego to more adequately predict the dynamics occurring in fire induced entrainment scenarios. It also highlights some deficiencies in the existing datasets.

#### *4.3.1 SIERRA/Fuego Improvements*

Modeling and simulation needs that were unmet in this effort fit three basic categories. First, models that may exist were unavailable or not deployed in the current code. Second, models do not presently exist, but could be developed. Third, the questionably relevant correlations in lieu of detailed simulations were applied without full justification. The first of these is easily remedied. The other two would require significant effort to improve the simulations.

Table 4-9 lists existing models that could have been leveraged in these analyses. A multi-component particle transport capability did exist, but it was not utilized for several reasons. It might have allowed better prediction of the particle size and motion in the plume. However, the inability to evaporate the components independently of each other, as well as the difficulty in

quantifying the mass fraction in the deposits, led to the currently employed methods. The conjugate heat transport capability for modeling solid temperatures was also not deployed. This would have allowed more accurate predictions of the heat-up of the solid materials in the vicinity of the fire. The reason this capability was not deployed was to simplify scenario set-up. Furthermore, some of the simulations were intended to simulate to the end (i.e., last few percent in time) of the fire experiments and required the assumption that the initial conditions were representative of the mature fire conditions. The complex temperature field of the solid at mature times required the full calculation from start to the near-end point to resolve with accuracy. For convenience, this was assumed to be of low relevancy to the particle and flow dynamics during the actual burn.

**Table 4-9. Existing models capabilities not deployed for these calculations**

<b>Model</b>	<b>Description</b>
Multi-component particle transport	Even though in several cases the particles predicted to evolve were multi-component, they were modeled as single component drops. This is a particular limitation of the SIERRA code suite. Such models may be available in other CFD packages. Fuego can predict multi-component drop behavior, but using this capability would have complicated the data reduction. Further, the evaporation capability does not work correctly for multi-component drops of the nature simulated in this exercise (discussed below in more detail).
Conjugate heat transport	We assumed that the heat-up of solid surfaces around the fire was not a critical aspect to the accurate transport prediction. SIERRA can couple the fluid mechanics predictions to a thermal transport code through coupled calculations. These could be included, but are often omitted in analyses because of the time involved in setting them up.

Table 4-10 lists several models that can be found in the literature or in other codes that would be useful for this application. These capabilities are not currently available in Fuego. The effect of wind and wave-induced entrainment is not thought to be active in the two cases studied, although this has not been verified with any quantitative assessments. Resuspension and wall impact are both difficult physical mechanisms and require added physics that are not presently in the SIERRA particle solvers. Multi-component evaporation is a challenge, since evaporation relates to the local temperature, gas concentrations, and surface area. These are difficult parameters to provide as input to the model, and consequently require further research to accurately assess for scenarios of this nature.

**Table 4-10. Models not existing but needed**

<b>Model</b>	<b>Description</b>
Wind/wave induced entrainment	Mentioned in the introduction to the two simulation analyses, the potential for air flow to induce the suspension of liquid in the air might be important for some scenarios.
Resuspension	Residues and deposited particles may become re-suspended in the air after they form the initial deposit. This propensity is not possible to model without further development activities.
Wall Impact	The outcome of a wall collision can be that the drop/particle sticks, shatters, or rebounds. Existing models can predict this behavior for some liquid drop impacts, but work is needed to be able to model this for the solid particles.
Multi-component evaporation	The ability to describe multi-component evaporation does not presently exist in our tools, and requires a model for available by component surface area to implement.

Table 4-11 lists the correlations that were used specifically to enable predictive calculations of the particle release from the fire environment. The correlations were necessary because the ability to extract this information from first-principles codes is presently lacking. The particle size distribution of [Borkowski 1986] was used because it fit the general description of the

behavior of boiling drops throughout the literature. [Borkowski 1986] took the data from a dataset that used water as the boiling fluid. Fuels and water are not expected to have identical particle distributions because the surface tension, density, boiling temperature, and viscosity are different. A multi-phase code that predicts the interfacial dynamics of a rising drop was considered to quantitatively bridge the gap between water and fuel data. However, the effort was halted before any results were obtained when it became clear that the process was insufficiently agile to meet the programmatic objectives in the time to deliver product simulations. The droplet model in [Kataoka 1983] for the lowest entrainment region was also used to predict the mass evolution of drops from the surface. This model is a dimensionless physical correlation that implicitly models vigorous boiling. It is not clear how accurate this model will be generically, as there is no accommodation for various pool depths or energy input rates. An improved model might include those parameters, as well as a method for determining nucleation and multi-bubble interactions.

**Table 4-11. Correlations that Need Better Justification**

Model	Description
Particle size distribution model from [Borkowski 1986]	The particle size distribution data from this report was obtained using a point-wise extraction. The point-wise extraction was used to create an interpolation table from which the particle distribution was sampled for the fuel fire scenarios. The correlation was based on data from a boiling water scenario.
Mass injection model from [Kataoka 1983]	Reference [Kataoka 1983] provides particle mass evolution data in several regimes at different dimensionless heights above a boiling liquid surface. While the correlations were developed on the basis of a large number of existing datasets, the correlations were derived for air/water and steam/water mixes only.

#### 4.3.2 Dataset improvements

The datasets tested in the previous two sections are incomplete and lack resolution. However, they do represent some of the more relevant datasets for scenarios involving contaminated fuel fires with radioactive particles. The limited number of radioactive particle dispersion tests thus represents some of the most relevant and detailed ones to date. Unfortunately, they still lack completeness. Missing information has already been highlighted, and will be repeated herein. The datasets were not heavily instrumented and the range of parameters varied in the test matrices was limited. There is reason to believe that the conditions that were tested were neither conservative nor representative of many accidents.

The contaminated TBP-kerosene fires in a 50 mL beaker by [Mishima 1973] simulated in Section 4.1 varied two parameters in the tests, neither of which made a significant difference in the ARF. The exhaust flow rate was different by a factor of two for each material, and the type of material was varied as well. There was no discernable effect of the flow rate on the ARF. The iodine was significantly different from all the other materials because it was near its boiling point and hence volatile. The other solids were not volatile, and yielded about the same ARF values. Our simulations varied the turbulence parameters and the initial fuel height. The initial fuel height had the largest effect on the entrainment. Turbulence parameters were also significant to the quantitative results within the range of uncertainty. The initial fuel height can be more largely thought of as a change in geometry or configuration. The ability for a particle to escape was a strong function of the geometry, which was not a parameter of variation in the tests. Table 4-12 lists the parameters that would be important to consider in subsequent fire tests. With the

hindsight from the previous test report and the corresponding simulations, there is good reason to suggest the need for additional data to support a quantitative basis for safety assessments.

**Table 4-12. Recommended Dataset Improvements to the Beaker Fire Test of [Mishima 1973]**

<b>Need</b>	<b>Description</b>
Turbulence Quantification	The tests did not measure or quantify in any way the turbulence induced by the boiling surface. Since this information is not readily available, this would be of interest because this parameter affects the release.
Fuel height in pool	The initial fuel height was a significant parameter in the simulated scenarios. The initial fuel height for the experimental tests appears based on model predictions to be non-conservative.
Geometry	Generally, the geometry around the fire is likely a relevant factor in the ability for particles to entrain. A larger beaker or a different relationship to the ambient flow might result in much higher airborne release factors.
Temporal resolution of release	Release of particles was integrated over time in the tests since a single measurement was taken post-test. The simulations surprisingly indicate that the first few seconds of ignition were the primary factor in the release. This surprising finding should be confirmed experimentally, and would improve confidence in the model results.
Consistent and well described ignition methods	The methods used for ignition were not detailed in the tests. Because the release of contaminants in the model was driven by the dynamics on ignition, this parameter should be more carefully reported.
More details on the fate of the liquid	The tests did not measure the TBP or kerosene airborne fractions. These would be helpful. From reading the test report, one supposes that the TBP mostly remained behind at the bottom of the beaker, whereas the kerosene mostly evaporated. The TBP may be a good surrogate for the contaminant, in which case these tests could be more easily replicated without needing to make experimental accommodations for the more hazardous solid contaminants.

The gasoline fire tests from [Mishima 1973a] were also simulated in Section 4.2. This test did not have any repeats, which means that the aleatoric experimental uncertainties are unknown. These tests were slightly improved in that they had two data collection periods. The early collection was during active flaming and represented the mass extracted through two methods: evaporation-induced entrainment and boiling entrainment. The collection taken after flaming subsided was attributable to re-suspension. It would be helpful to have a collection that was only during the boiling regime, which would greatly improve the ability to distinguish entrainment due to the various mechanisms. Many of the issues in Table 4-12 are also issues relevant to this test. Variations in geometry and turbulence quantification are relevant to this scenario as well. Table 4-13 lists the recommended dataset improvements to the pool fire test as given in Section 4.2.

**Table 4-13. Recommended Dataset Improvements to the Pool Fire Test of [Mishima 1973a]**

<b>Need</b>	<b>Description</b>
Turbulence Quantification	The tests did not measure or quantify the turbulence induced by the boiling surface. This parameter has a strong relationship to the airborne release in the model.
Fuel height in pool	One might consider the fuel height as a parameter.
Geometry	Generally, the geometry around the fire is likely a relevant factor for particles to entrain. A less regular pool shape or objects in the vicinity might significantly affect entrainment because of the effect on turbulence at the pool surface.
Temporal resolution of release	Having two time periods was helpful, but more would be better. It would be convenient to have release corresponding to the boiling times. This would help validate the model finding that the boiling release is dominant.
Boiling time	The most significant parameter for the release may be the duration of time over which the pool is boiling, in which case this should be quantified in future tests.
Better described	For resuspension, it would be nice to have a better indication of the surface finish of the inside of the

boundary conditions	wind tunnel in these tests. It is likely unpainted metal, but could have been painted. As fires are conducted in a facility, there is a deposition pattern composed of soot and heat-treated metal around the fire region. This may be relevant to the resuspension, and hence should have been quantified.
Repeat tests	It would be convenient to have repeat tests to confirm that the single test is not an outlier.
Improved quantification of inflow condition	The duct flow over the fuel pool was only given as a range of velocity. In reality, one expects an incident flow profile, which may or may not be well reproduced by the assumed model boundary conditions.

In summary, the tests simulated herein remain important data because there is a general lack of data of this nature, and because the experiments are highly relevant to conditions of interest. The issues noted here may serve as a guide when designing future experiments. In the interest of improved safety assessments, there is a clear need to add to the supporting data. Having performed simulations of the existing experimental scenarios, there is now adequate new guidance to design appropriate experiments of increased significance. There is also guidance on productive new model developments for the simulation tools.

## 5 EXPLORATORY SIMULATIONS

As described in Chapter 2 of this report, DOE-HDBK-3010 presents the ARF and RF data in various chapters according to the material form. So far, the liquid ARF and RF data have been described in Chapter 4, particularly for the release from a liquid fire. With the work reported in [Gelbard 2013], the simulations on liquid for fire and explosion have been performed. In this chapter, the capability of the SIERRA code suite for material forms such as solid or powder is investigated as the exploratory simulations. Fragmentation of solids (e.g., a uranium oxide pellet) can be difficult to assess in terms of the simulations because it may involve the knowledge of the microstructure of the solids, such as the grain structure and cracking phenomena in a ceramic  $\text{UO}_2$  pellet. It may also relate to the manufacturing sintering process. This may pose a challenge for modeling these phenomena. On the other hand, powder may not be difficult to simulate. Therefore, the focus of the exploratory simulation is on powder behavior in accident conditions.

In this chapter, we propose to examine two specific powder cases to utilize both SIERRA SM code, such as Adagio and Presto, and SIERRA FD code, such as Fuego (see Section 3.1 and Chapter 4 for more details):

- In one powder simulation, we investigate a projectile impacting a can/vessel standing on a surface. This simulation can apply to a can with powder being impacted during an earthquake, an impact (e.g., missile) from an explosion or deflagration, or the impact of a firearm discharge on a container with powder. This can is partially filled with powder. Note that this simulation is arbitrary and is intended to test the SIERRA SM code's particle capability for impact accident scenarios. If this proves to be successful in terms of engineered judgment (such as particle dispersal behavior inside the can upon impact), the concept needs to be validated using experiments.
- For the other powder simulation, we explore a pressurized release experiment similar to those described in Section 4.4 of the Handbook for testing the particle capability in SIERRA FD code, Fuego. As shown in Section 3.1, Fuego currently does not model particle interactions. Therefore, we also model this experiment using MELCOR code (see [Humphries 2015a], [Humphries 2015b] and [Humphries 2015c]), since MELCOR does contain an aerosol physics model.

Note that these exploratory simulations are for assessing the SIERRA codes' applicability for addressing accidents related to powders. Therefore, discussions on qualitative rather than quantitative results are provided.

### 5.1 Impacts to Powder Can

This section describes a simulation using both Adagio and Presto to model a projectile at a constant velocity hitting a can with  $\text{UO}_2$  powder. This impact simulation case could represent an explosion-induced fragment hitting a drum containing radioactively contaminated materials. Once this simulation is proven feasible, other impact cases, such as drop and low velocity impact accidents can be easily simulated by the same or slightly modified input files. The rationale behind performing this simulation is to discover and demonstrate the SIERRA SM code for

simulating dispersal of powders using the smoothed particle hydrodynamics (SPH) element model within the code.

This simulation is based on a projectile, such as bullet hitting a can (i.e., a small food can) on the order of several inches in diameter and height (see Figure 5-1). The can size selected for this simulation has an inner height of 73.025 mm (2.875 in) and an inner diameter of 73.025 mm (2.875 in). A wall thickness of 1 mm is assumed. The projectile, similar to a bullet, has a cylinder attached with a rounded cone: the cylinder has a diameter of 7.9376 mm (0.3125 in) and a length of 19.05 mm (0.75 in), and the rounded cone has the same diameter but with a cone length of 3.81 mm (0.15 in). The powder is filled to about 2/3 of the volume inside the can. There are no corresponding experimental data for this simulation. Two cases with a constant velocity of 20 m/s (787 in/s) and 175 m/s (6890 in/s) were used. Both the projectile and the can are assumed to be steel. The floor, where the can is situated, is modeled as concrete. This floor is modeled with a thickness of 5 mm. The length and width are 10 times the inner radius of the can. Below are the assumptions associated with this simulation effort.

#### Assumption of the Simulation Model:

- Air is not modeled inside the can, which will underestimate inside particle movement. Modeling the air in this impact case may result in premature rupture of the can at the top, which may be unrealistic since air material (above the powder region inside the can) is being treated as a solid material in the SIERRA SM code.
- No lid is modeled in the can. In reality, a can usually contains a lid. This exclusion may underestimate the release of the powder.
- The selection of the impact speed in the simulation may not be representative of the actual accident condition. These speeds are intended to demonstrate the capability of the code.
- Once the particles leave the can due to rupture or can failure, any dispersal of the particles may not be realistic since air is not modeled outside of the can. Thus, one would use the mass flux leaving the can as input for a thermal-hydraulic code, such as MELCOR or Fuego to estimate any further dispersal of the particles.

Two meshes sizes were used in the simulations (see Table 5-1): fine (1 mm mesh for the powder) and coarse (3 mm mesh for the powder). The powder material, which has a density of 10.9 g/cm<sup>3</sup> (corresponding to the density of UO<sub>2</sub>), is being modeled as a solid region in the SM code, but it has been converted into particles (or powder) using the SPH model at time zero when the simulation starts. The maximum particle number conversion per mesh size is set at 5 for the coarse mesh and 2 for the fine mesh. Note that with these conversion factors, the fine mesh case contains about 10 times more particles than that of the coarse mesh case.

**Table 5-1. Mesh Size for Fine and Coarse Cases**

Volume/Block Name (material)	Number of Elements Modeled	
	Coarse Mesh	Fine Mesh
Projectile (steel)	328	1456
Vessel (Can), shell (steel)	3120	27608
Powder (UO <sub>2</sub> )	8960*	244412**
Floor (concrete)	29768	29768

\*Conversion to powder using a maximum multiplier of 5

\*\*Conversion to powder using a maximum multiplier of 2

The input deck for this simulation incorporated many models from the previous explosion simulation effort [Gelbard 2013]. The powder material is based on the equation of state (EOS) material model Mie-Grunesien (see Section 5.1.1). This model has been used successfully to model the liquid explosion, where the liquid drops is modeled using the Mie-Grunesien material model within an SPH element model [Gelbard 2013]. As stated in Chapter 3, Adagio is the primary code used to execute the SIERRA SM calculation. However, the Mie-Grunesien material model, having export restrictions, required using Presto (itar version) executable within the SIERRA SM code (see Section 5.1.2 for details). To avoid having to use export-controlled Presto, simulations have been made to switch the material model from Mie-Grunesien to the Soil and Crushable Foam material model in simulations that do not involve explosions. The Mie-Grunesien EOS model is particularly suited for modeling very high strain rate shock regime, whereas the Soil and Crushable Foam material model comprises compressible materials loaded at lower strain rates. The following two sub-sections describe these two models in more detail.

SIERRA/SM includes a capability to remove elements from a simulation once one or more user-defined criteria have been satisfied. This element removal capability can be used to approximately model material rupture/failure. In the simulations described here, elements comprising the can were removed from the simulation when the von Mises effective stress at the mid-plane in the element reached or exceeded the critical stress of  $10^5$  psi (690 MPa). This criterion allowed the projectile to rupture the can if it generated high enough stresses at the point of impact.

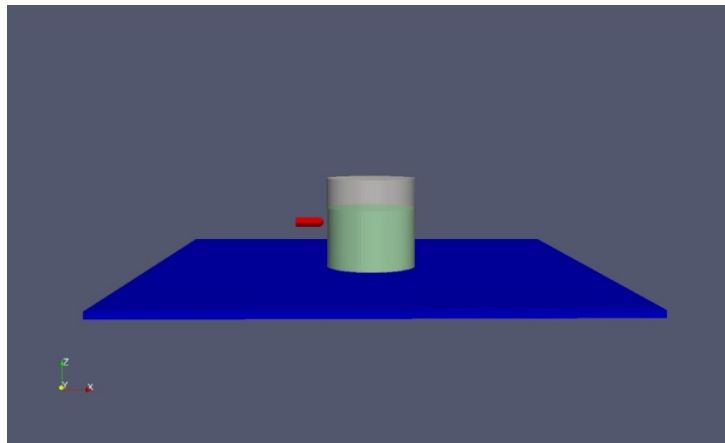


**Figure 5-1. Geometry of a Projectile Impact to a Powder Can.**

### 5.1.1 Mie-Grunesien EOS Model

The use of this EOS model was adapted from the work done on simulating the liquid explosion using Presto [Gelbard 2013]. The description of the model is given in SAND2015-4022 [SNL 2015b]. This EOS material model can work with SPH elements, but this element model experiences numerical (un-physical) failure in tension for all materials. Thus, the SPH element should be used with caution. The theory behind this Mie-Grunesien model is described in SAND2009-3801P [Sweogle 2009]. A brief description of this model and its input requirements are provided below.

Essentially, this model describes the non-linear pressure-volume (i.e., pressure-density) response of solids or fluids in terms of a reference pressure-volume curve. Since this model is used for modeling shocks, it can be described in terms of the Hugoniot principle [Sweogle 2009]:

$$p = p_H + \rho \cdot \Gamma \cdot (E - E_H) \quad (5-1)$$

Where  $p$  is the mean pressure,  $E$  is specific internal energy,  $p_H$  and  $E_H$  are the pressure and energy along the principal Hugoniot,  $\rho$  is the density, and  $\Gamma$  is the Gruneisen parameter. In this equation,  $\rho\Gamma$  is taken to be constant and equated to  $\rho_0\Gamma_0$ , their ambient values (or input values).  $p_H$  can be given as:

$$p_H = \frac{\rho_0 c_0^2 \eta}{(1-S\eta)^2} \quad (5-2)$$

Where  $c_0$  is the ambient speed of sound (an input value), which is related to the shock velocity ( $u_s$ ) and the particle velocity ( $u$ ) as  $u_s = c_0 + S \cdot u$ . For many materials, both  $c_0$  and  $S$  are tabulated. For water, the value of  $c_0$  is much greater than that of air (at least four times higher). In solids, the values are much larger than that of water.  $\eta$  can be defined in term of the volumetric strain, assuming that the strain ( $\epsilon$ ) is proportional to the density change ( $\rho_0/\rho$ ) as  $1 - \frac{1}{\epsilon+1}$ .  $E_H$  in Equation (5-1) is given by:

$$E_H = \frac{p_H \eta}{2\rho_0} \quad (5-3)$$

In this Mie-Gruneisen model, Equation (5-1) is written as:

$$p = f_1 + f_2 E \quad (5-4)$$

where  $f_1$  and  $f_2$  are functions of density, and are given by:

$$f_1 = p_H \left(1 - \frac{\Gamma_0 \eta}{2}\right) \quad (5-5)$$

$$f_2 = \rho_0 \Gamma_0 \quad (5-6)$$

Other properties given for this model include bulk modulus ( $k$ ) and shear modulus ( $\mu$ ) which are given as:

$$k = \rho c_b^2 \quad (5-7)$$

$$\mu = \frac{3(1-2\nu)}{2(1+\nu)} k \quad (5-8)$$

where  $\nu$  is the Poisson's ratio, and  $c_b$  is the bulk speed of sound.

Note that the plasticity is based on the von Mises yield criterion, so the stress deviators ( $s_{ij}$ ) are limited by

$$\frac{1}{2} s_{ij} s_{ij} \leq \frac{y_0^2}{3} \quad (5-9)$$

where  $y_0$  is a constant yield strength, which is zero for the hydrodynamic or fluid case in which all stress deviators are zero.

For more details about this model, the reader is encouraged to consult SAND2009-3801P [Swegle 2009]. The original input data were obtained from existing simulation [Gelbard 2013]. In [Gelbard 2013], the simulation for liquid water properties ( $S=1.921$ ,  $\nu=0.5$ ,  $\Gamma_0=1$ ) were used. It may not be representative for modeling a powder in a can without any liquid. Therefore, a verification simulation using the sand and air properties ( $S=2.2$ ,  $\Gamma_0=1$ ,  $\nu=0.35$ ) is used [Wardlaw 1996]. Note that even though we are modeling  $UO_2$  powder inside the can, loose sand can be used to represent this powder. Additionally, the reason to use air speed of sound for the verification test is that sand's sound speed is much larger than that of water, which may not be appropriated [Antoun 2012]. The summary of the parameters used in this model is shown in Table 5-2.

**Table 5-2. Mie-Gruneisen Model Parameters Used in Simulations**

Parameter	[Gelbard 2013]/water (Original)	Air/Sand (Improved)
$\rho_0$	$UO_2$	$UO_2$
$\nu$	0.5	0.35
$S$	1.921	2.2
$\Gamma_0$	1	1
$y_0$	0.0	0.0
$c_0$	water	air
Pressure cutoff	-1 psi (6895 Pa)	-1 psi (6895 Pa)

### 5.1.2 Soil-Crushable Foam Material Model

The details of this material model are given in SAND2015-2199 [SNL 2015a]. This model is a plasticity model, which is intended to model the lower strain limits for compressible materials. The inputs for this model include:

- Density
- Bulk modulus
- Poisson's ratio
- Yield stress function
- Pressure cutoff
- Pressure-volume function

Both bulk modulus and Poisson's ratio are sufficient to provide other properties, such as shear modulus and Young's modulus. The pressure function is a function of the volumetric strain, which can be related to the density change. The pressure cutoff is defined as the tensile-failure pressure of the material. The yield stress function requires three constants of a polynomial as input so that the yield stress is a function of the compression pressure.

This model has been used in simulating the fuel dispersal in high-speed aircraft impact into a soil material [Tieszen 1996]. This fuel dispersal simulation has defined the soil properties based on the experimental results. Attempts have been made to utilize the soil properties from the fuel dispersal simulation as described in Table 13 and Table 14 of SAND96-0105 [Tieszen 1996] to be considered the UO<sub>2</sub> powders as soil. As shown in Section 5.1.3, the use of this property caused unexpected results. Therefore, an attempt is made to use the Mie-Gruneisen EOS model input for this model.

### 5.1.3 Discussions and Results

Two projectile speeds were simulated: 20 m/s and 175 m/s. Initially, the coarse mesh and the Mie-Gruneisen EOS material model (see Section 5.1.1) were used for the simulation. Because the Mie-Gruneisen model is export controlled, the Presto executable was used. This limits the information that can be discussed for the models in this code. Therefore, we attempted to use a different non-exported controlled material model available in Adagio (see Section 3.1 more details).

As shown in Section 5.1.2, the Soil-Crushable Foam material model reasonably approximates solid particles in the can, such as dry sand with a soil composition. Attempts have been made to use the combination of UO<sub>2</sub> density and the properties of sands and soil; however, this did not give results close to the Mie-Gruneisen model. When the properties provided in Table 13 and Table 14 of SAND96-0105 [Tieszen 1996] were attempted, the results at the beginning of the simulations seemed reasonable, but then particles began to fly out from the bottom center of the can, which then caused the can to explode. This is due to the small value of the bulk modulus reported in Table 13 of SAND96-0105, which does not match the slope of the pressure function provided in Table 14 of SAND96-0105. Additional attempts were made to change the slope of the pressure function required by the model and to increase the bulk modulus to be a reasonable

value while not introducing instability. However, this was unsuccessful. Therefore, attempts have been made to transfer the properties of Mie-Gruneisen model as described in Section 5.1.2 to the Soil-Crushable Foam model (see Section 5.1.2). This was more successful; therefore, we utilized both models for the impacts to powder can simulations. Table 5-2 shows the cases that were simulated. Both coarse and fine meshes are described in Table 5-1. The input parameters for both Mie-Gruneisen EOS and Soil-Crushable Foam material models are given in Section 5.1.1 and Section 5.1.2, respectively. The simulation configuration is given in Figure 5-1.

**Table 5-3. Simulation Cases for Impacts to Powder Can**

<b>Case</b>	<b>Parameters</b>
1 <sup>P</sup>	Coarse mesh, Mie-Gruneisen EOS material model, water properties and UO <sub>2</sub> density at the impact speed of 20 meters per second
2 <sup>P</sup>	Same as Case 1, except the impact speed is at 175 meters per second
3 <sup>P</sup>	Coarse mesh, Mie-Gruneisen EOS material model, sand/air properties and UO <sub>2</sub> density at the impact speed of 20 meters per second
4 <sup>A</sup>	Same as Case 3, except using Soil and Crushable Foam material model
5 <sup>A</sup>	Same as Case 4, except using fine mesh

<sup>P</sup> PRESTO\_ITAR is used for this simulation (version 4.36.1)

<sup>A</sup> Adagio is used for this simulation (version 4.36.1).

As shown in Table 5-3, four out five cases were done with an impact speed of 20 m/s. For Case 1, as shown in Figure 5-2 to Figure 5-5, the projectile in-elastically rebounds back upon hitting the can, which punctures a hole in the can in the area of the impact. As shown in these figures, the particles inside the can near the area of the impact displace vertically toward the ceiling of the can, while some particles escape through the hole. The simulation stops at 0.03 s (see Figure 5-5). If the simulation continues, the particles inside the can above the elevation of the hole would be free to leak out under the influence of gravity. Thus the impact location is important for the amount of the particle release. If the object impacts the can near the bottom, it may result additional release because of the penetration's position, assuming that the impact is sufficient to puncture the hole on the can. Additionally, if the lid is modeled in this simulation, the impact force that results from the particles hitting the lid (the ceiling of the can in this case), may be sufficient to force the lid off. This could result in the additional release of particles.

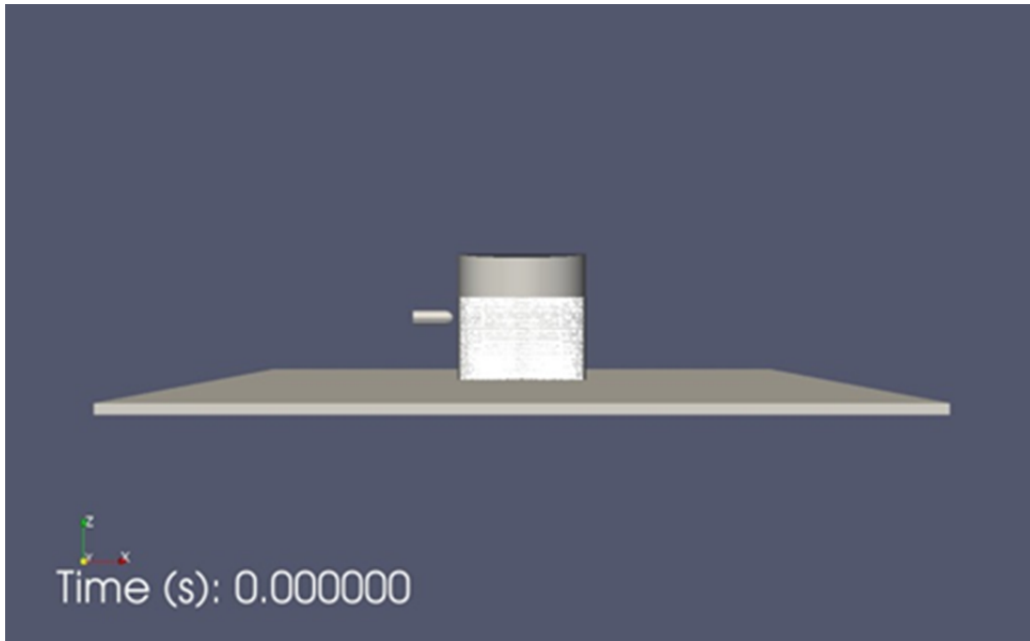


**Figure 5-2. Simulations of Case 1 at Time Zero.**

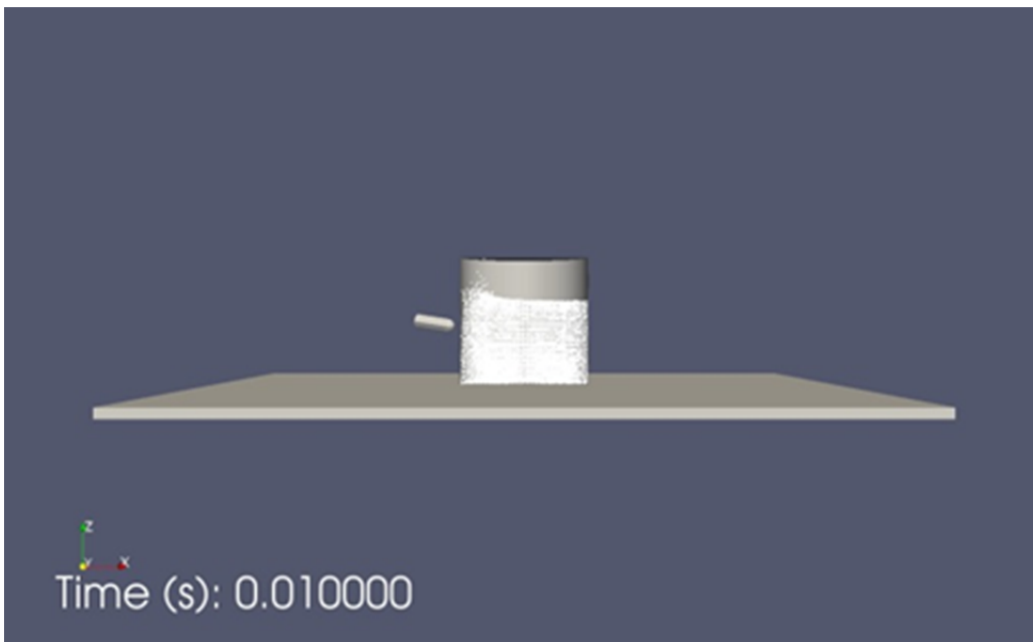


**Figure 5-3. Simulations of Case 1 at 0.01 s. (coarse mesh, Mie-Gruneisen EOS material model, water properties and UO<sub>2</sub> density at the impact speed of 20 meters per second.)**

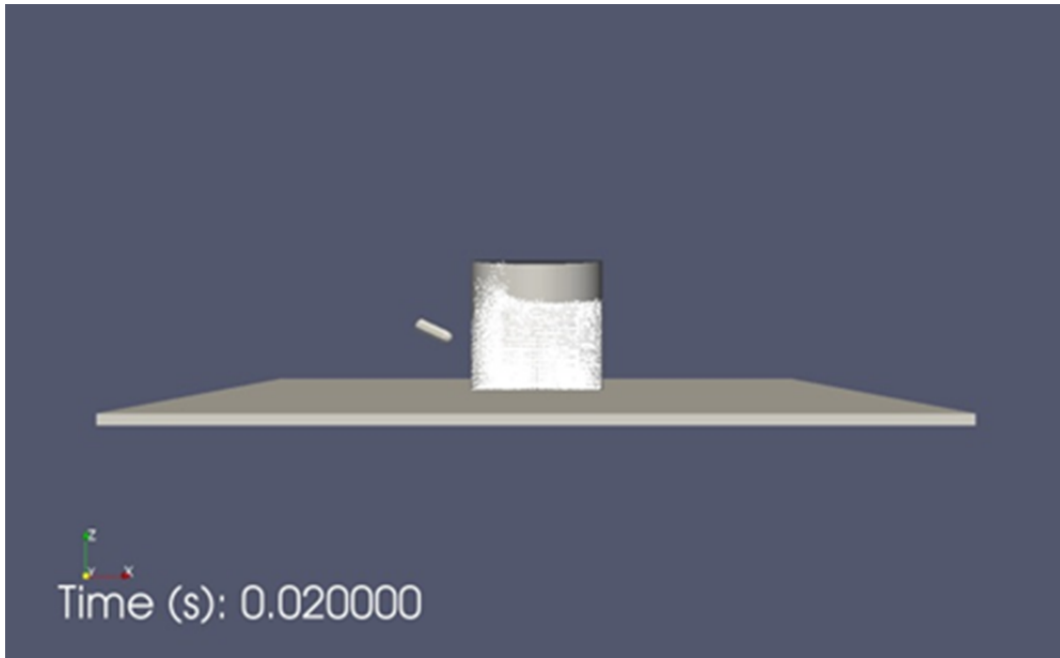


**Figure 5-4. Simulations of Case 1 at 0.02 s. (coarse mesh, Mie-Gruneisen EOS material model, water properties and UO<sub>2</sub> density at the impact speed of 20 meters per second)**

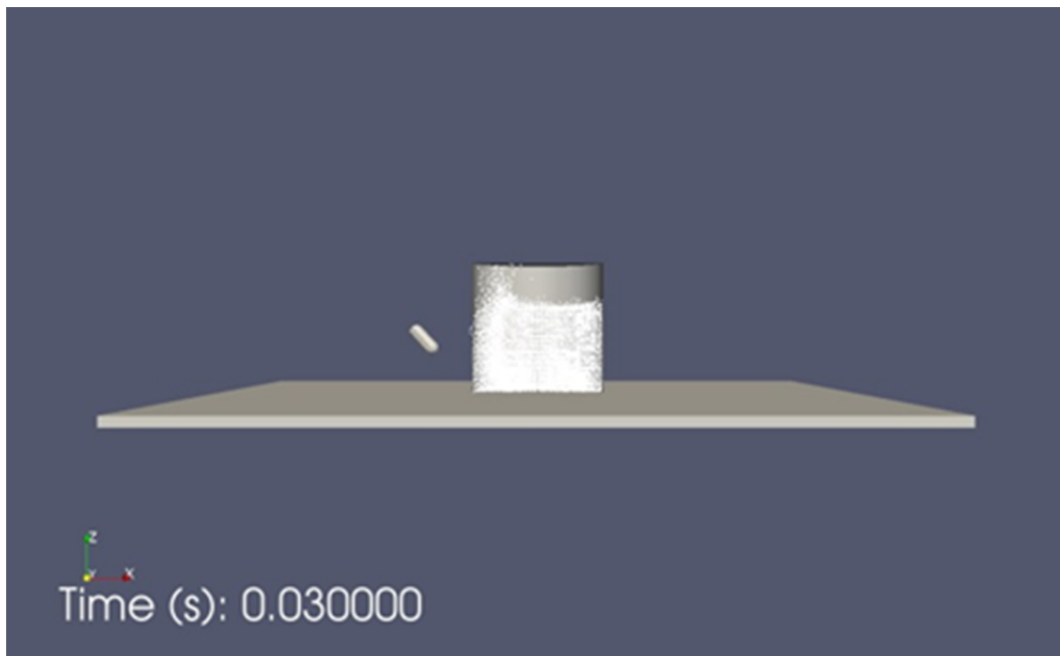


**Figure 5-5. Simulations of Case 1 at 0.03 s. (Coarse mesh, Mie-Gruneisen EOS material model, water properties and UO<sub>2</sub> density at the impact speed of 20 meters per second)**

For Case 2, the configuration of the simulation is provided in Figure 5-6 because the increased impact velocity of 175 m/s will cause the can to fly upwards. This simulation was run to 0.15 s to observe any secondary impact or release. Figure 5-7 to Figure 5-13 shows the sequences of the simulations out to about 0.15 s. As shown in these figures, particles continue to be released

through the penetration as the can and the projectile are lifted. The release can be observed for the entire 0.1 s of run time from 0.05 s. However, there is additional release near the can surface between the bottom and the wall near the top. This release is due to the stress failure at that location (based on the von Mises failure criterion mentioned earlier), allowing the particles to escape. In this simulation, a small portion of particles escape through the impact hole and the cracks near the bottom of the can. Thus, this amount represents the DR times ARF as described in the FFF in Section 2.1. Note that RF is not included here because the particles are on the order of 100s of microns in diameter, rather than few microns.

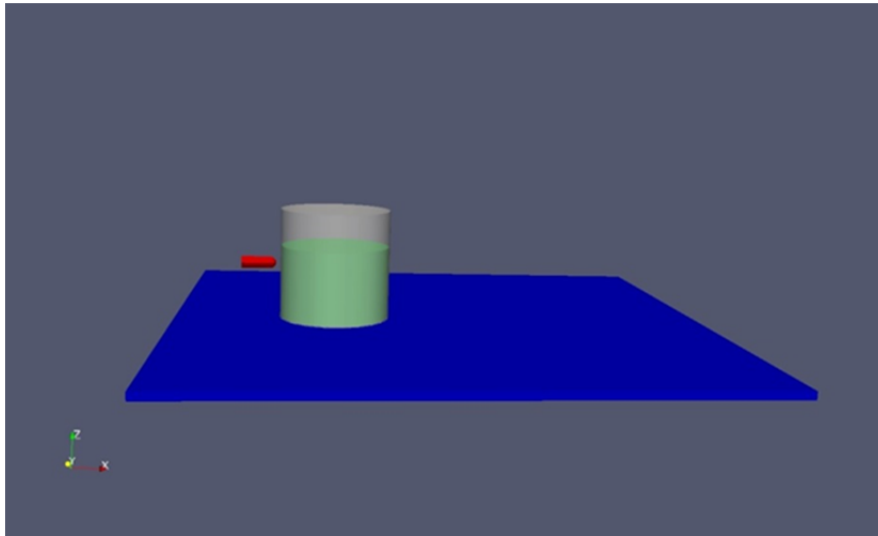


**Figure 5-6. Initial Configuration of Case 2 (same as Case 1, except the impact speed is at 175 meters per second).**

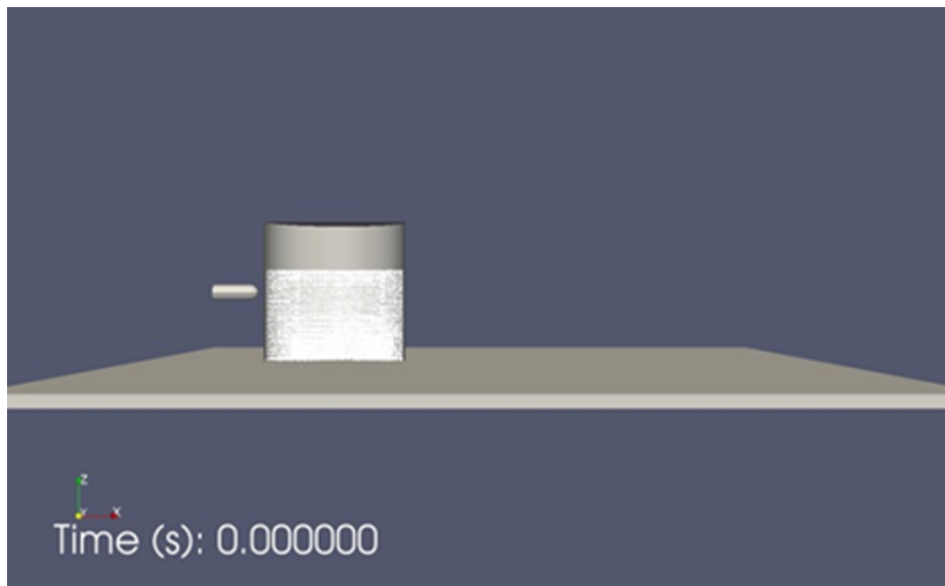


**Figure 5-7. Simulation of Case 2 at Time Zero (same as Case 1, except the impact speed is at 174 meters per second).**

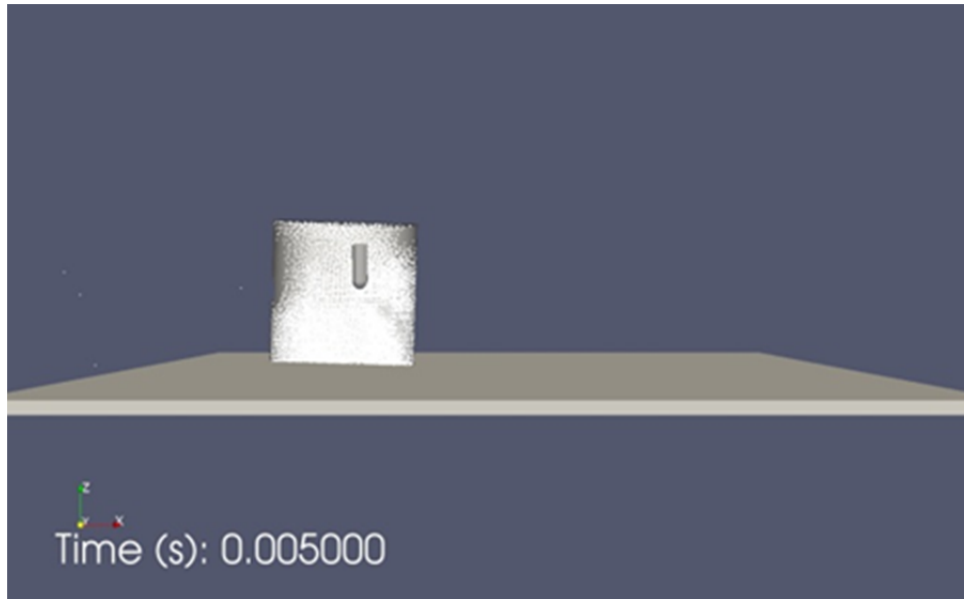


**Figure 5-8. Simulation of Case 2 at 0.005 s (same as Case 1, except the impact speed is at 175 meters per second).**

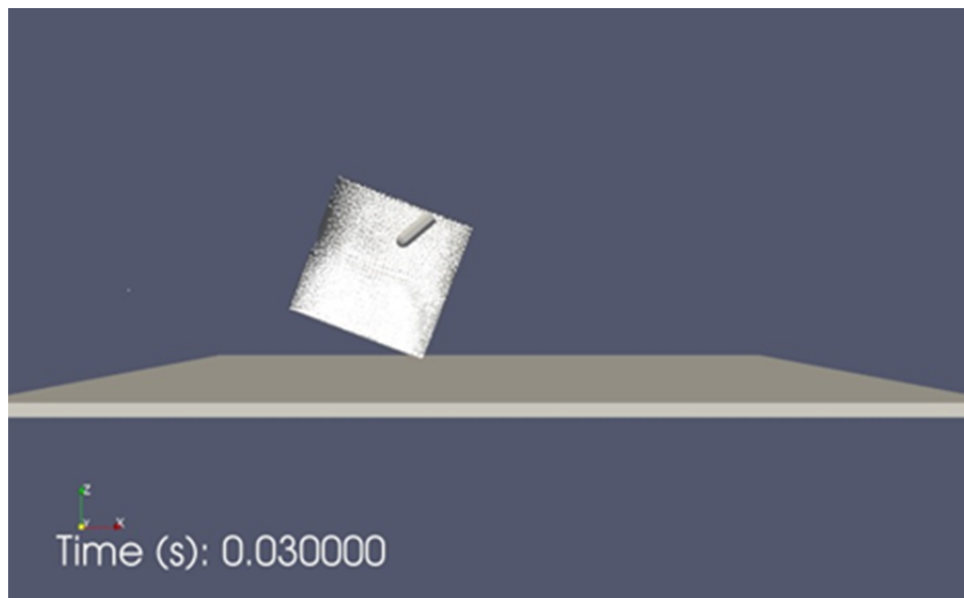


**Figure 5-9. Simulation of Case 2 at 0.03 s (same as Case 1, except the impact speed is at 175 meters per second).**

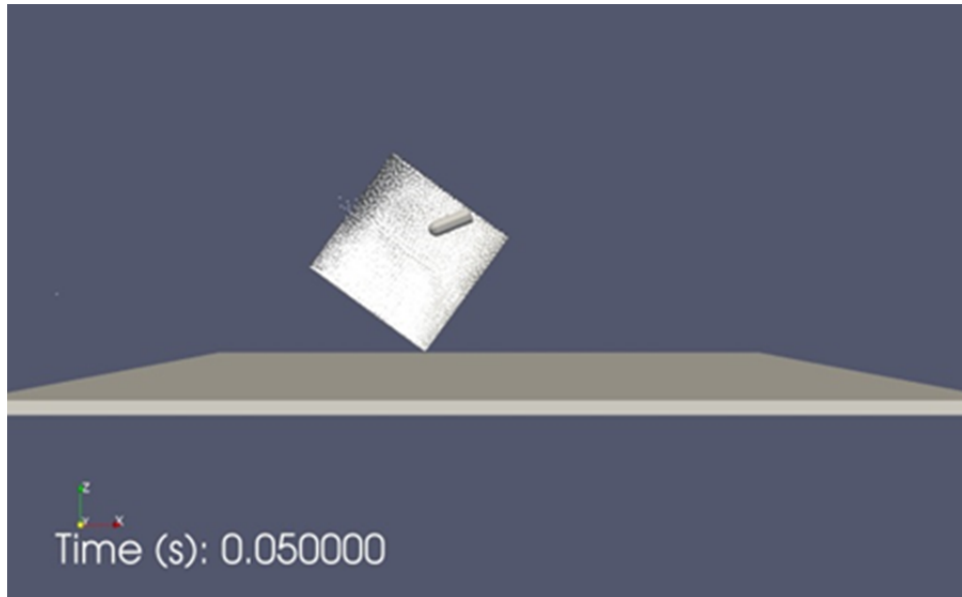


**Figure 5-10. Simulation of Case 2 at 0.05 s (same as Case 1, except the impact speed is at 175 meters per second).**

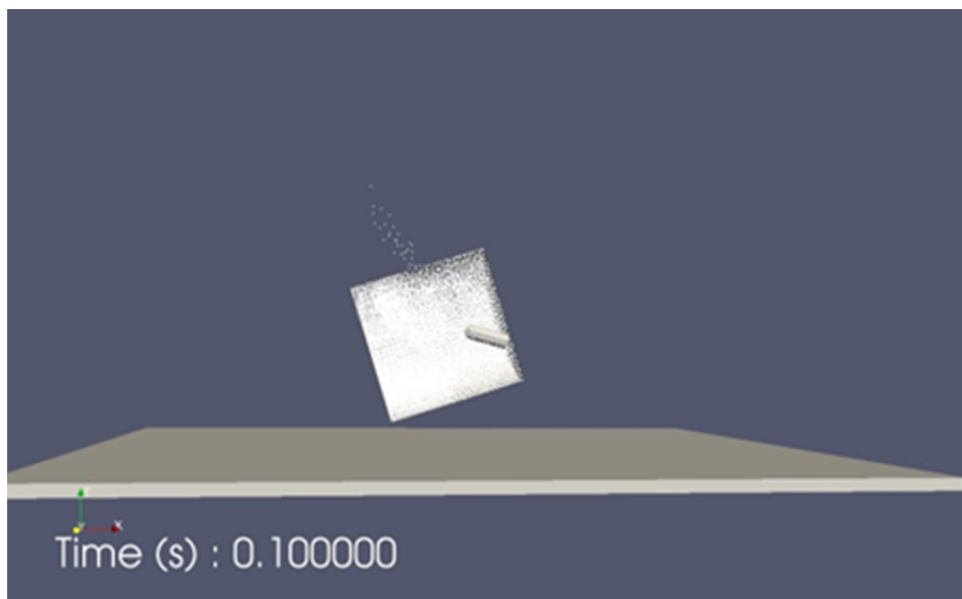


**Figure 5-11. Simulation of Case 2 at 0.1 s (same as Case 1, except the impact speed is at 175 meters per second).**

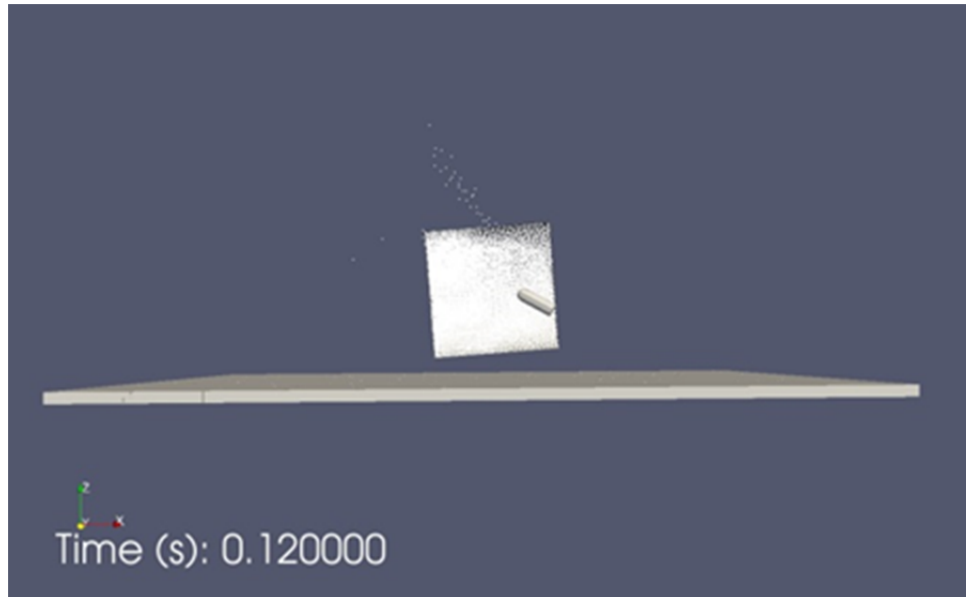


**Figure 5-12. Simulation of Case 2 at 0.12 s (same as Case 1, except the impact speed is at 175 meters per second).**

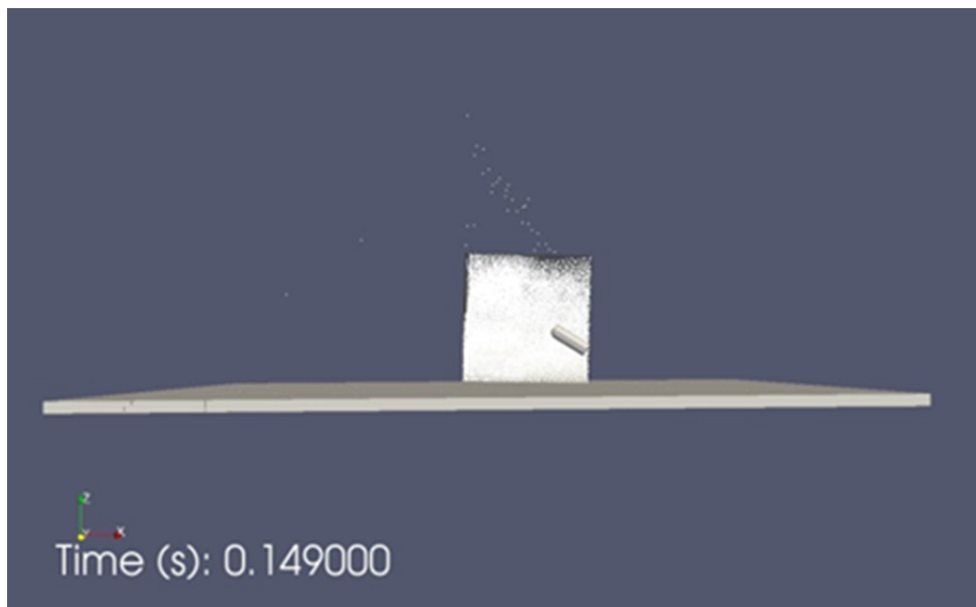


**Figure 5-13. Simulation of Case 2 at ~0.15 s (same as Case 1, except the impact speed is at 175 meters per second).**

Both Case 1 and Case 2 use a Mie-Gruneisen material model with the water properties. Case 3 is the same as Case 1, but this simulation uses the sand/air properties instead of the water properties. As shown Figure 5-14 to Figure 5-17, the Case 3 simulation ran to 0.1 s to detect any secondary failure of the can and particle release. As shown in these figures, the movement of projectile and particles after impact is different from that of Case 1 for the time to 0.03 s (see

Figure 5-5). This may be due the difference in the properties selected. Since Case 3 ran much longer than Case 1, the results are sufficiently long to indicate longer-term failure of the can near the bottom rim due to the Von mises failure. At about 0.4 s, particle leakage through the bottom rim near the floor is noticeable. After that, additional leakage is also noted. It is not certain that the leakage is realistic or an instability of the code.

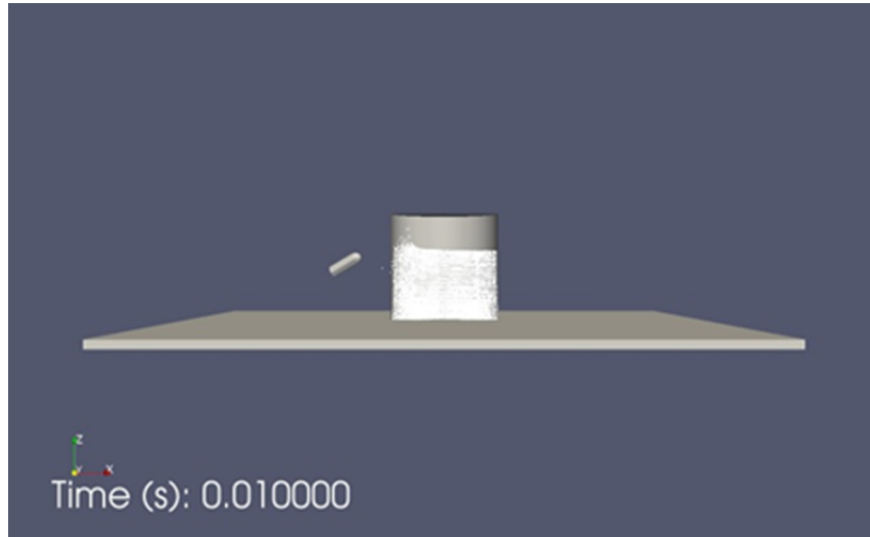


**Figure 5-14. Simulations for Case 3 at 0.01 s (coarse mesh, Mie-Gruneisen EOS material model, sand/air properties and UO2 density at the impact speed of 20 meters per second).**

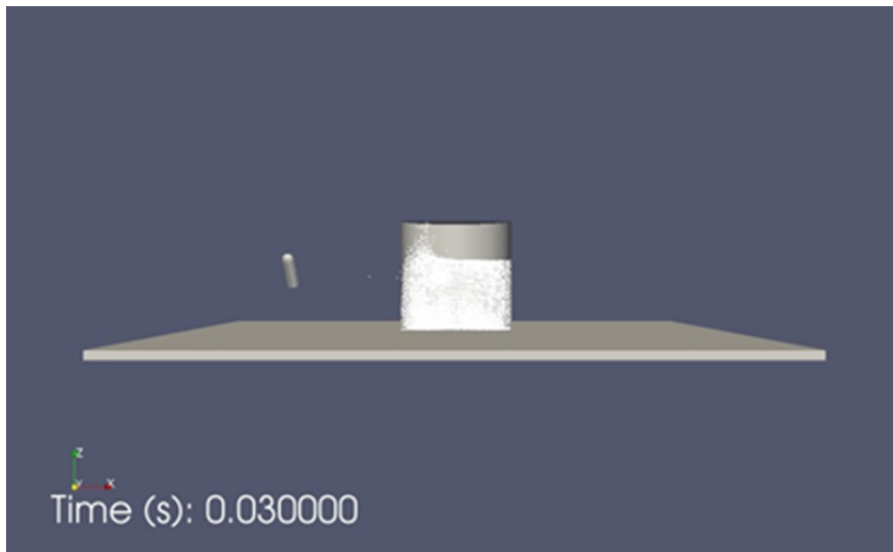


**Figure 5-15. Simulations for Case 3 (coarse mesh, Mie-Gruneisen EOS material model, sand/air properties and UO2 density at the impact speed of 20 meters per second).**

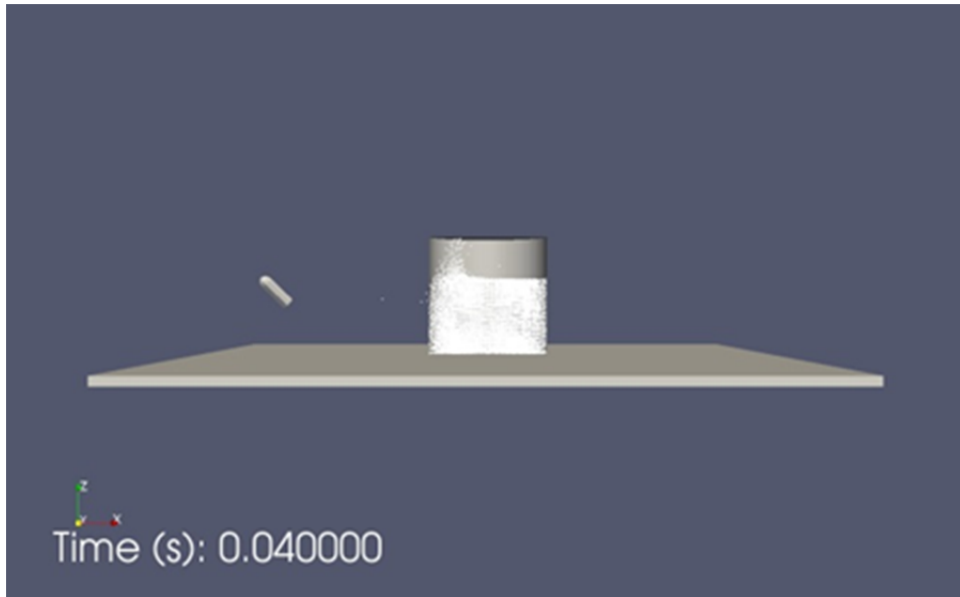


**Figure 5-16. Simulations for Case 3 at 0.04 s (coarse mesh, Mie-Gruneisen EOS material model, sand/air properties and UO2 density at the impact speed of 20 meters per second).**

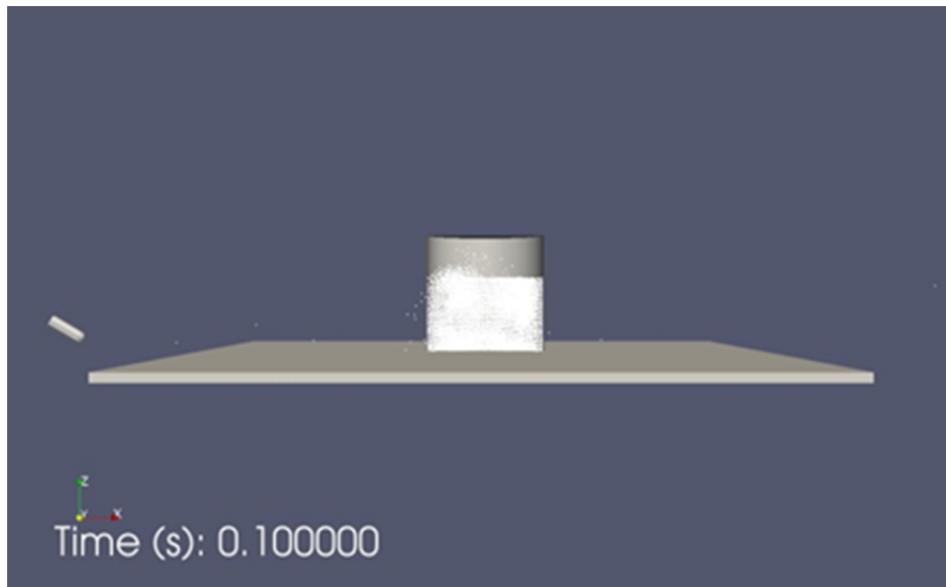


**Figure 5-17. Simulations for Case 3 at 0.1 s (coarse mesh, Mie-Gruneisen EOS material model, sand/air properties and UO2 density at the impact speed of 20 meters per second).**

So far, we have discussed the results using the Mie-Gruneisen material model in Presto for these simulations. As previously described, we plan for Adagio to be adequately used for all powder simulations involving accident scenarios other than those involving explosion events. Therefore, the remaining two cases, namely Case 4 and Case 5, use the Soil-Crushable Foam material model with Adagio (see Table 5-2). The objective of these two cases is to determine if this

material model can be used to simulate the powder dispersion in impact accident scenarios, similar to that of the Mie-Gruneisen material model.

In Case 4, which is similar to Case 3 with the Soil-Crushable Foam material model, the simulation results are shown in Figure 5-18 to Figure 5-21. The results for Case 4 are similar to the results for Case 3, except they do not have any stress failure resulting from the initial impact by the projectile to the can. In addition, the movement of the particles, especially inside the can near the impact area (such as how the particles fly up in the space above the particle bed), is different than that of Case 3.

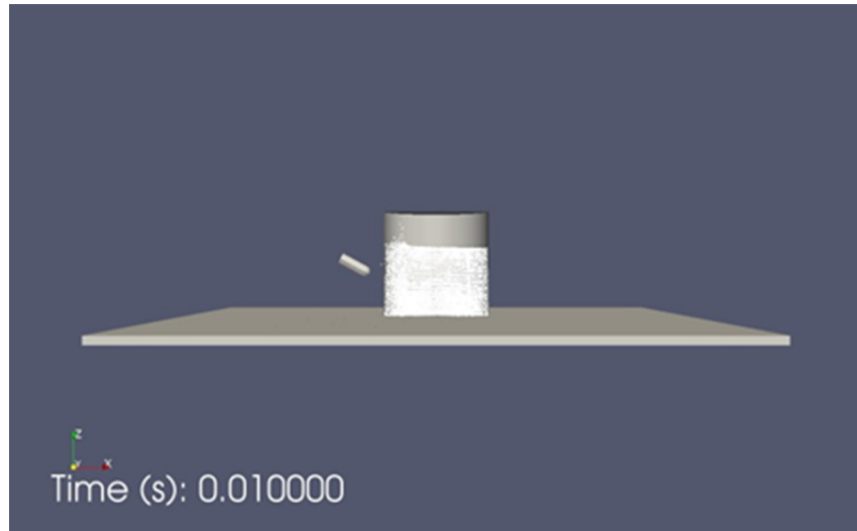


**Figure 5-18. Simulations for Case 4 at 0.01 s (same as Case 3, except using soil and crushable foam material model).**

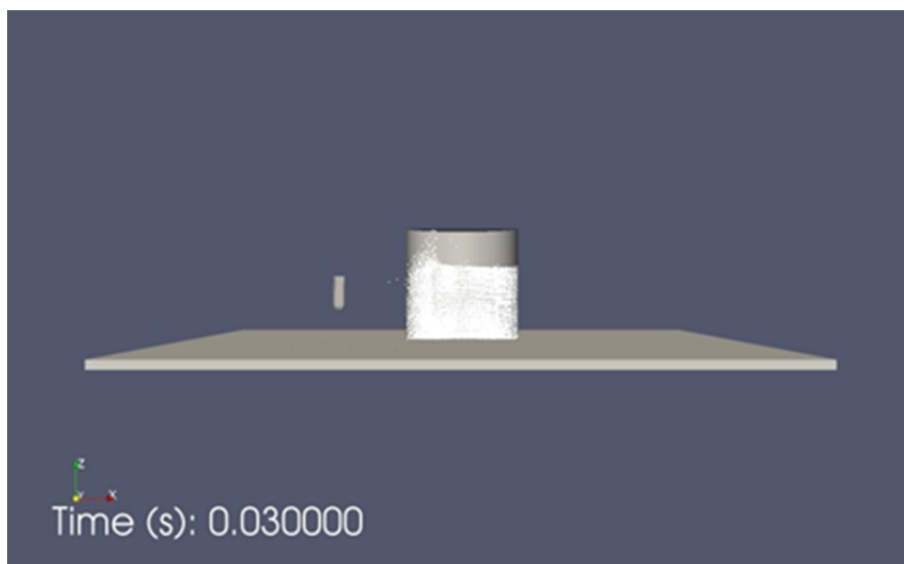


**Figure 5-19. Simulations for Case 4 at 0.03 s (same as Case 3, except using soil and crushable foam material model).**

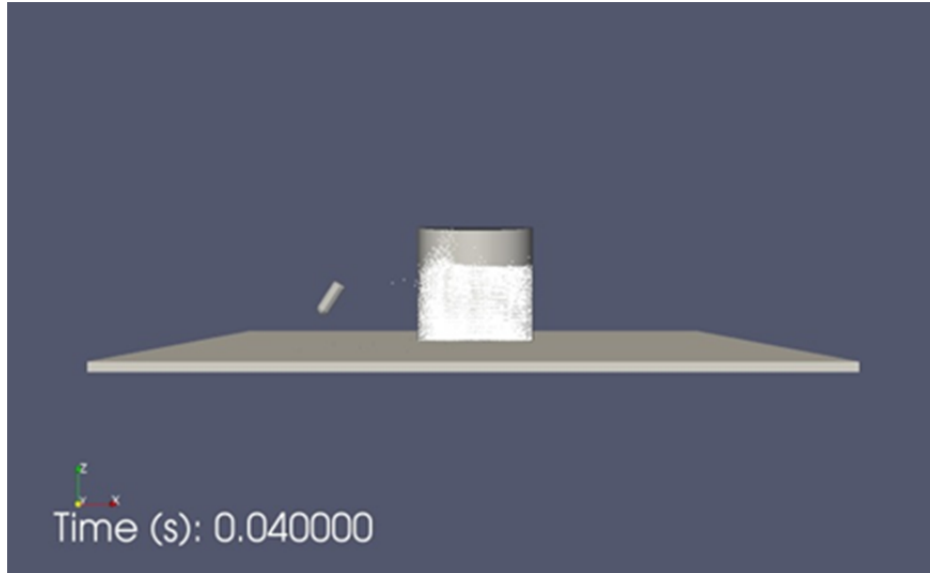


**Figure 5-20. Simulations for Case 4 at 0.04 s (same as Case 3, except using soil and crushable foam material model).**

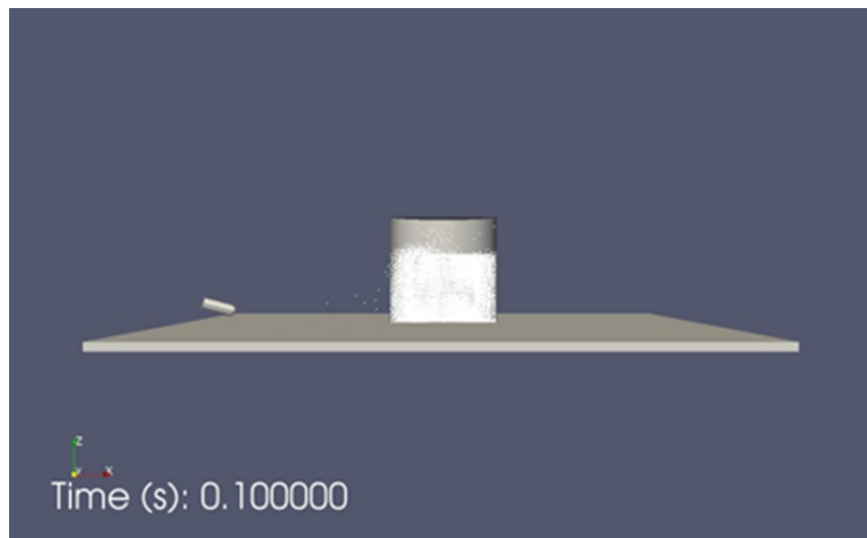


**Figure 5-21. Simulations for Case 4 at 0.1 s (same as Case 3, except using soil and crushable foam material model).**

Case 5 is the same as Case 4 but with a finer mesh (see Table 5-1). Case 5 was only run out to 0.01 s because of the significant increase in computation time as a result of the larger number of nodes. This case was made to determine if the fine mesh would have significantly different results than the coarse mesh model. As shown in Figure 5-22 and Figure 5-23, the projectile does rebound upon impacting the can similar to that of Case 4. However, the particle behavior inside the can is different than that of Case 4 for the time period of comparison. It may be caused by the

number of particles modeled is about 10 times more than that of Case 4 (see Table 5-1 for details of the mesh difference between the coarse and fine mesh models).

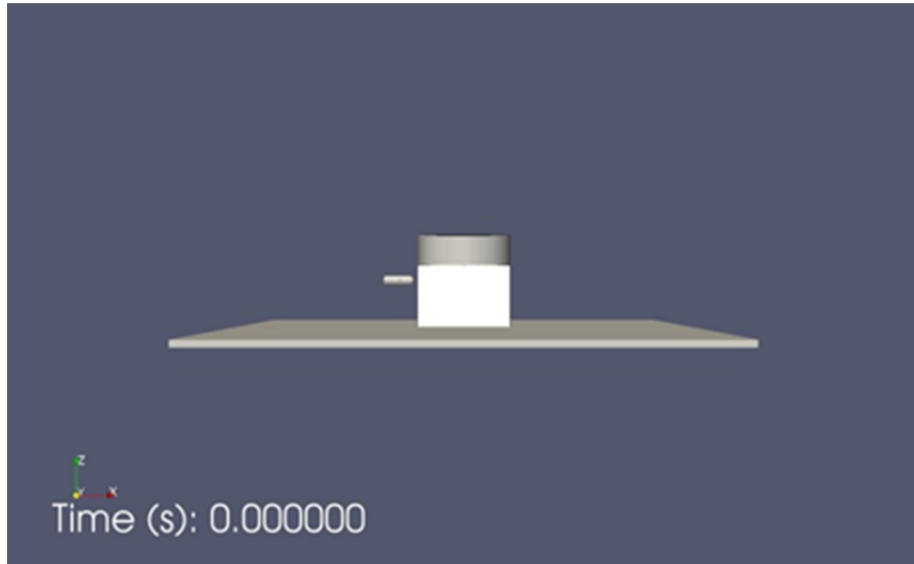


**Figure 5-22. Simulations for Case 5 (same as Case 4, except using fine mesh).**

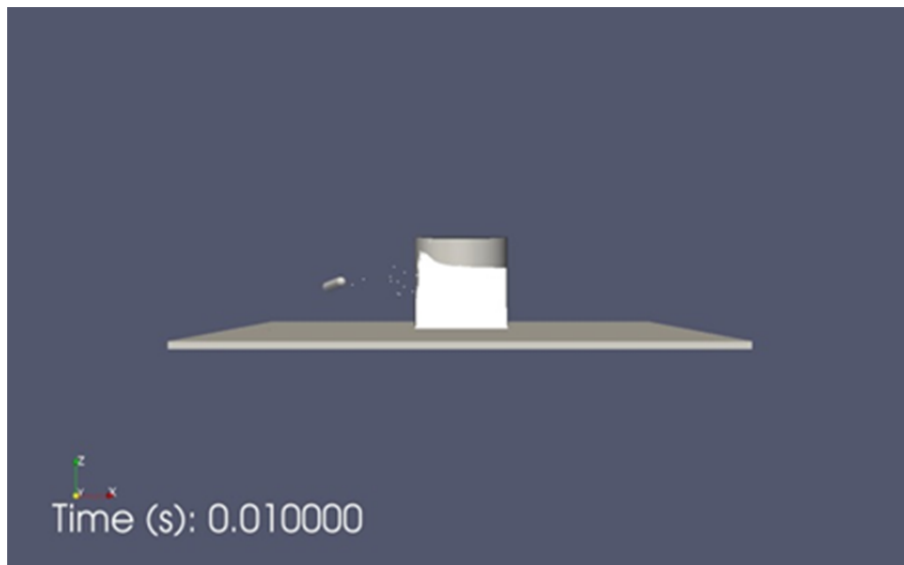


**Figure 5-23. Simulations for Case 5 (same as Case 4, except using fine mesh).**

This exploratory simulation has shown that SIERRA SM code can be used to simulate the impact scenarios with powders in a container. Since the simulation conditions were arbitrarily selected and there are no known experimental data, the simulation results are for demonstration purposes only. The observations of the powder dispersal inside provide a measure of the particle interactions. In addition, the use of the fine and coarse meshes for a same impact velocity case demonstrates the stability of the model. In terms of material models used, the Soil and Crushable

Foam material model seems to be more appropriate than the Mie-Gruneisen EOS model for modeling impact case without any shock involved. The former material model is stable in comparison to the latter model for this type of simulations. The simulation model described in this section may also be applied to drop scenarios and other mechanical insult cases.

## 5.2 Pressurized Powder Release

This section describes simulations of experiments investigating the generation of airborne aerosols by pressurized release of powders conducted at Pacific Northwest Laboratory (PNL) [Sutter 1983]. The experiment consists of two parts: (1) release equipment, called Pressurized Airborne Release Equipment (PARE), which generates airborne particles, and (2) enclosure, called Pressurized Airborne Release Tank (PART), which provides containment for the particles to settle and collect. Figure 5-24 shows the make-up of the PARE. Here, the powder chamber is located at the center on the floor of PART. PARE has a volume of about 800 cm<sup>3</sup> and can hold up to 524 cm<sup>3</sup> of powder. The powder is pressurized by air injected below the chamber and is released upon the failure of the rupture disks. The two-rupture disk system allows an accurate pressure release measurement. An air volume between two rupture disks allows a precise release pressure. When the condition is right, the evacuation of the air in this volume allows the rupture of both disks, even though the top rupture disk may fail a second later than the bottom rupture disk. A number of cases were conducted using PARE, with the ejection pressure being one of the main variables. The PARE is housed inside PART, which is shown schematically in Figure 5-25. In addition, aerosol measuring equipment such as the high volume filter and impactors are located on the walls of the PART. The impactors are located at the mid-point of the PART height. The PART is constructed from stainless steel, which is approximately 3 m high and 2.9 m in diameter: a total of 20 m<sup>3</sup> in volume, the equivalent of a small room.

This powder release experiment setup includes various powder sources, such as TiO<sub>2</sub> and depleted uranium oxide (DUO), in the amounts of 100 g and 350 g. Although liquid release was also conducted in the PARE, no further discussion on the liquid release experiment is made in this section.

Sutter [Sutter, 1983] provided a number of results:

- Both the pressurization and initial aerosol size were significant variables, even though the initial size is about 1.7 μm in diameter.
- The average mass airborne from the PARE experiments increased as a function of pressure for both TiO<sub>2</sub> and DUO. Except for the case of 1000 psig, the airborne fraction is lower than that of 500 psig. The explanation is the powder impacted on the ceiling where a portion was retained. These include those on the wall as well. Therefore, less is available to become airborne.
- Because the focus of the experiment was to identify the maximum airborne release. The 1000 psig case was not pursued. Ceiling impaction was a factor for lower pressures.
- During a 250 psig run, 10 grams became airborne, but only 288 g were recovered from the PART. 50 g of 350 g source was unaccounted for.

SIERRA FD code, Fuego, was used to simulate this experiment. Fuego currently does not model particle interactions. MELCOR, a system level code with aerosol physics models, is used to augment results from Fuego.

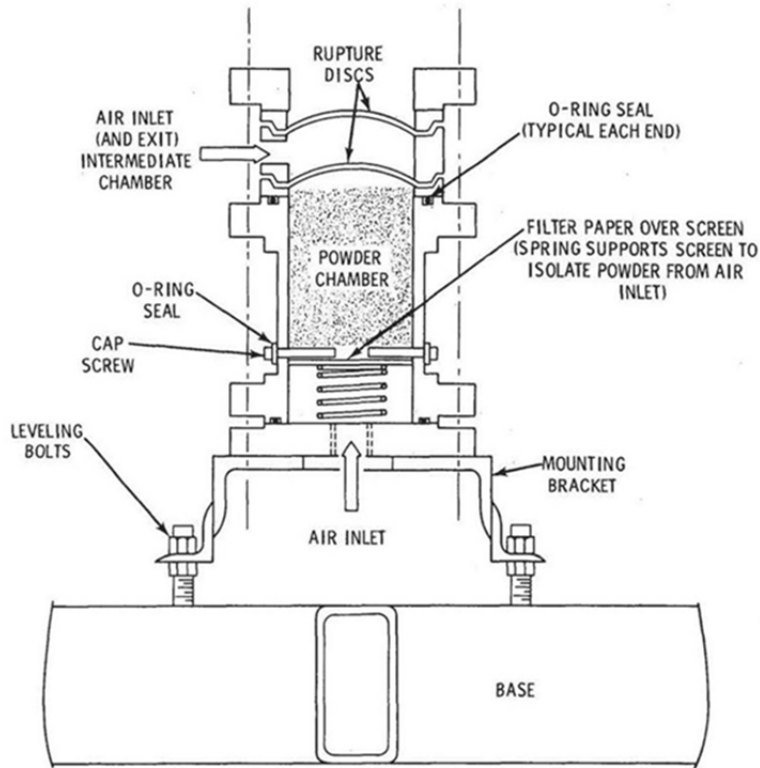


Figure 5-24. Layout of PARE [Sutter, 1983].

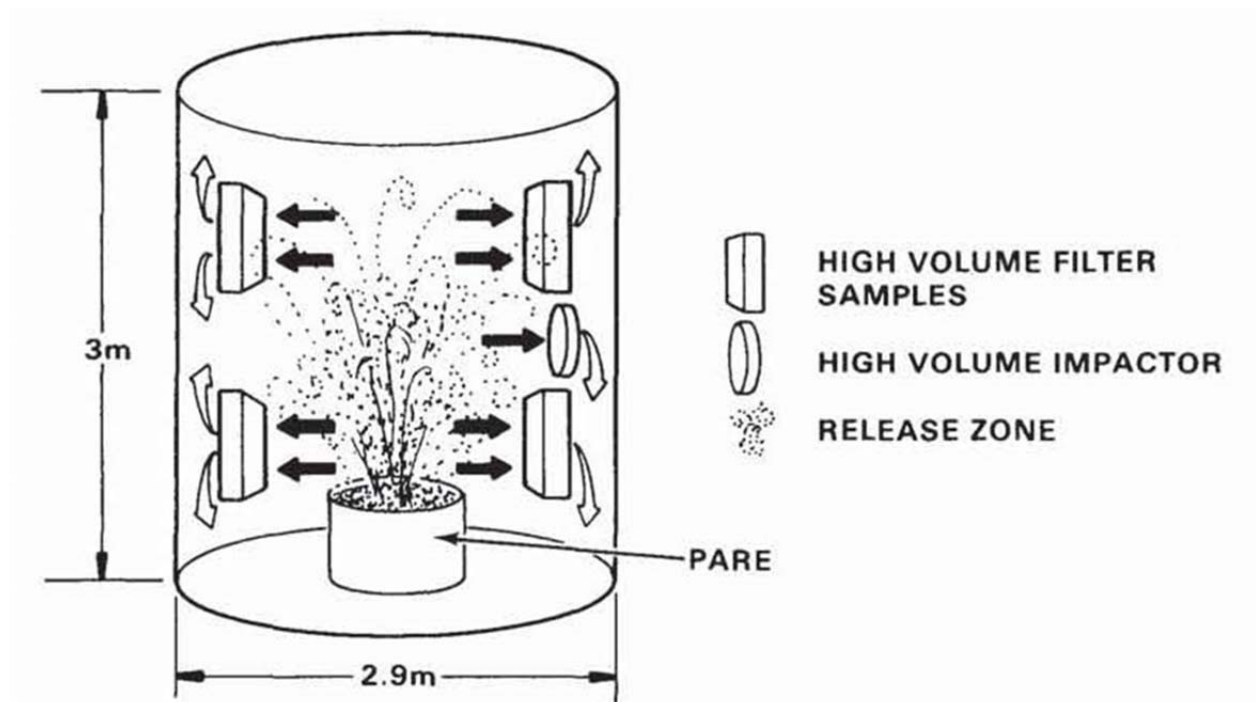


Figure 5-25. Schematic of PART [Sutter, 1983].

### 5.2.1 MELCOR Simulations

The MELCOR code is used to validate the aerosol physics model in the MAREOS code, which is an aerosol physics model within MELCOR [Humphries 2015b]. The exploratory MELCOR simulations are conducted for the geometry specified in the experiment for TiO<sub>2</sub> with 100 g initially at pressure release of 50 and 250 psig. The MELCOR 2.1 (revision 7128) code is used for these simulations: [Humphries 2015a], [Humphries 2015b], and [Humphries 2015c]. Two configurations are modeled: the PART volume is modeled as a single volume and a two-volume where the entire PART volume is divided into two equal top and bottom volumes. These two cases were examined to assess the effect of concentration on the aerosol model (MAEROS) in MELCOR [Humphries 2015b]. Table 5-4 shows the input parameters in the MELCOR model. All 100 g is assigned to the first bin of the 10 sections model. Below are the major assumptions in this simulation.

#### Assumptions for Simulation Model:

- One- and Two-volume MELCOR models for the PART volume are simulated. It may still underestimate the suspended particles in comparison to the experiment because MELCOR uses concentrations to estimate aerosol physics. The smaller volume would enhance more particle interactions. Thus, a multi-volume MELCOR model may be warranted.
- No air exchange is modeled in this simulation. In the experiment, 80 times of the PART volumes of air were exchanged during the 30 minutes of the test for the aerosol measurement. This exclusion may contribute the difference in MELCOR results in comparison to the experiment.
- Since MELCOR does not model accurately any impingement phenomena, this simulation may underestimate the deposition of the aerosols, particularly for higher pressures cases.

For the single PART volume case at 50 psig, MELCOR predicts about 69% of the powder in the atmosphere and 31% deposited at the end of a 30-minute run. Figure 5-26 to and Figure 5-27 show the aerosol histogram results for this case. As shown in this figure, the color legend aligns with the aerosol class designation in MELCOR. TiO<sub>2</sub> is being modeled in the ‘Ce’ class and is white. The locations in the histogram are for the aerosol bins in the suspended aerosols and the deposition locations such as walls and floors. As shown in this figure, all 100 g of the aerosol is at the PARE volume at time zero. At 100 s, much of the aerosol is suspended in the PART volume. At the end of 30 minutes, this figure shows that some depositions (~1 g) are on the floor and wall of the PARE volume and a lot deposited (~2 g) on the PART floor. The remainder of the aerosol is still airborne. Most of the aerosol size is within the first three bins (1 to 2.5 μm) (see Figure 5-27).

**Table 5-4. Input Parameters for the MELCOR 2.1 Models [Sutter 1983]**

Parameter	Value
PART volume	
1-volume case	20 m <sup>3</sup>
2-volume case	
PART-Top	10 m <sup>3</sup>

PART-Bottom	10 m <sup>3</sup>
PARE volume	8.62×10 <sup>-4</sup> m <sup>3</sup>
PART condition	
Pressure	1.01×10 <sup>5</sup> Pa
Temperature	289.65K*
PARE temperature	
50 psi (3.45×10 <sup>5</sup> Pa)case	980 K**
250 psi (1.72×10 <sup>6</sup> Pa)case	4900 K**
Aerosol	
No of sections	10 (default)
Mass	100 g (assigned to Section 1)
Density	4230 kg/m <sup>3</sup>
Minimum and maximum size range	10 <sup>-6</sup> m to 10 <sup>-4</sup> m

\*Since there was no specific temperature provided. However, the experiment provided a temperature range of 14 to 19 °C or 23 °C for early runs. Therefore, it is assumed a uniform temperature of 16.5°C (289.65 K).

\*\*The adjustment of the initial temperature to ensure that the air expansion from PARE into PART would not result significant cool down. Therefore, it is assumed an ideal gas to estimate the temperature.

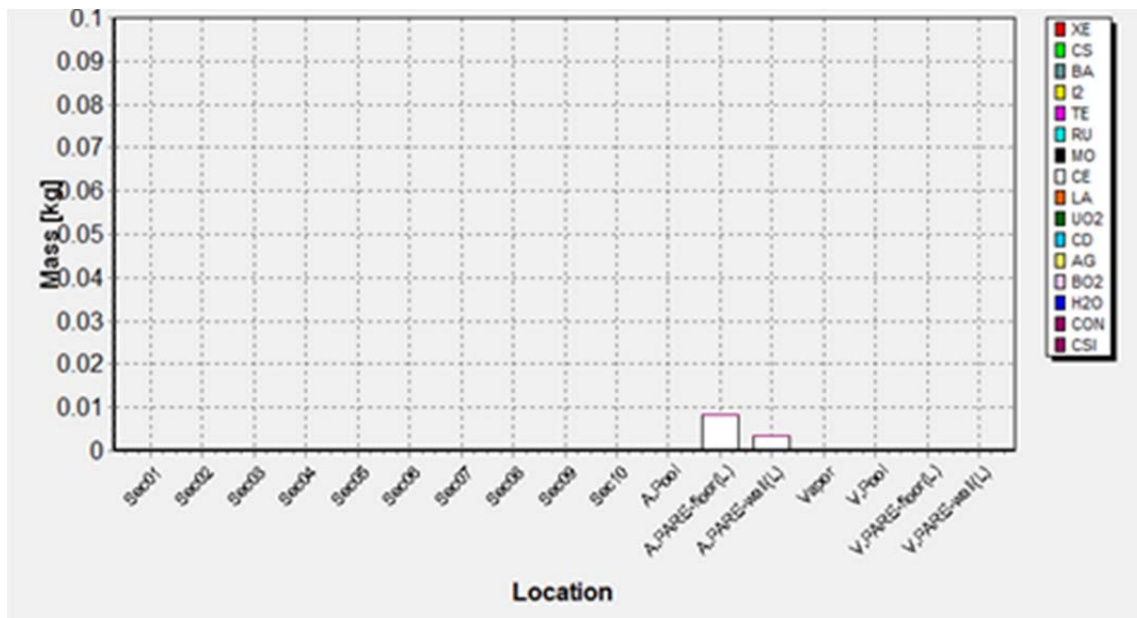
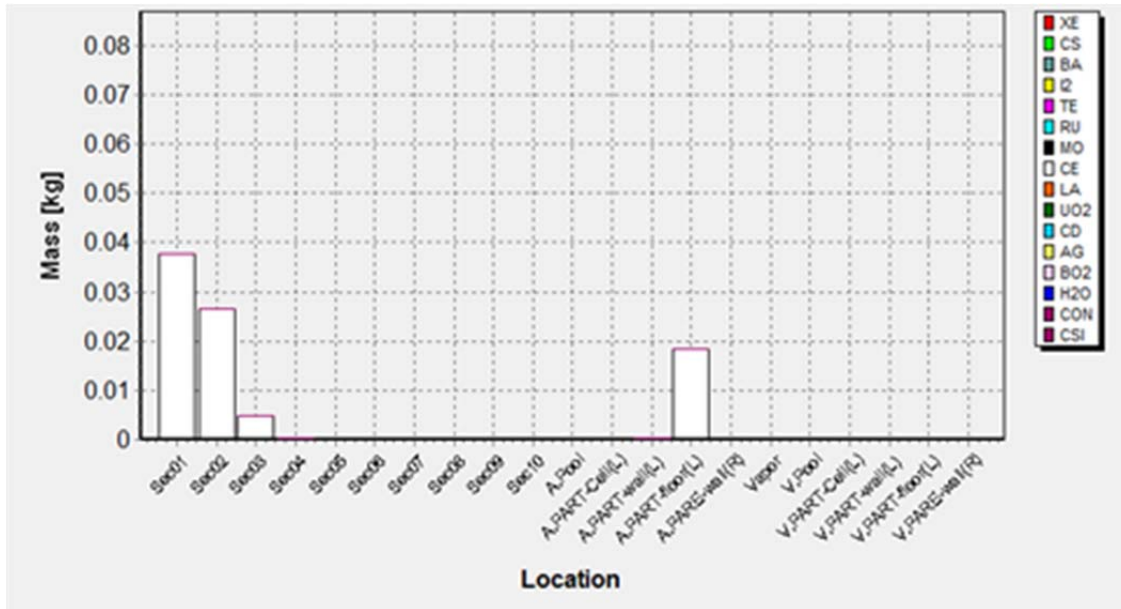


Figure 5-26. Aerosol Histogram Results in PARE Volume for a Single PART Volume at 50 psig Case at 30 Minutes.



**Figure 5-27. Aerosol Histogram Results in PART Volume for a Single PART Volume at 50 psig Case at 30 Minutes.**

The preliminary results indicate that MELCOR predicts a much larger suspension of aerosol than the actual experiment (in which 4-5% remained airborne). The average size particle is about 10  $\mu\text{m}$  in the experiment compared to MELCOR, which predicted a 2.5  $\mu\text{m}$  maximum.

Since the MELCOR aerosol physics model is based on concentration, two PART volumes (equal volumes) are simulated. Figure 5-28 and Figure 5-29 show the histogram results of the 30 minute aerosol locations for this case at the end of 30 minutes. As shown in these figures much of the aerosols (~40 g) in the PARE volume are located on the wall and floor at 100 s and beyond this time. When comparing to the single volume case (see Figure 5-27), the amount deposited is double that for the two volume case. In terms of the PART aerosol behavior, much of the aerosols are located in the bottom PART volume rather than the top PART volume (no top PART volume results are shown because the amount is less than 1 g). As shown in Figure 5-29, significant aerosol remains suspended at 100 s in the bottom PART volume, and a very small amount is deposited. At the end of 30 minutes, approximately 23 g is located on the PART wall while approximately 36 g or 36% is suspended. Similar to the single PART volume case, only airborne aerosols are within the first three bins. In comparison to the experiment, this airborne fraction is still larger than the 4-5% value from the experiment. It is expected that if additional volumes are modeled, the results will be improved because the concentration in the smaller volume is larger, which can allow increased aerosol interaction to occur.

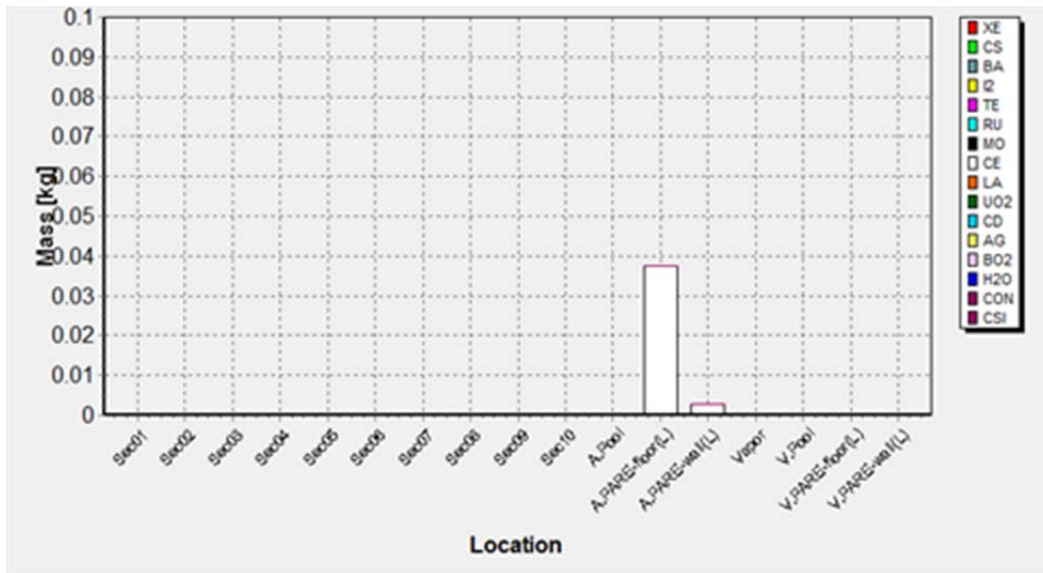


Figure 5-28. Aerosol Histogram Results in PARE Volume for a 2 PART-Volume at 50 psig Case at 30 Minutes.

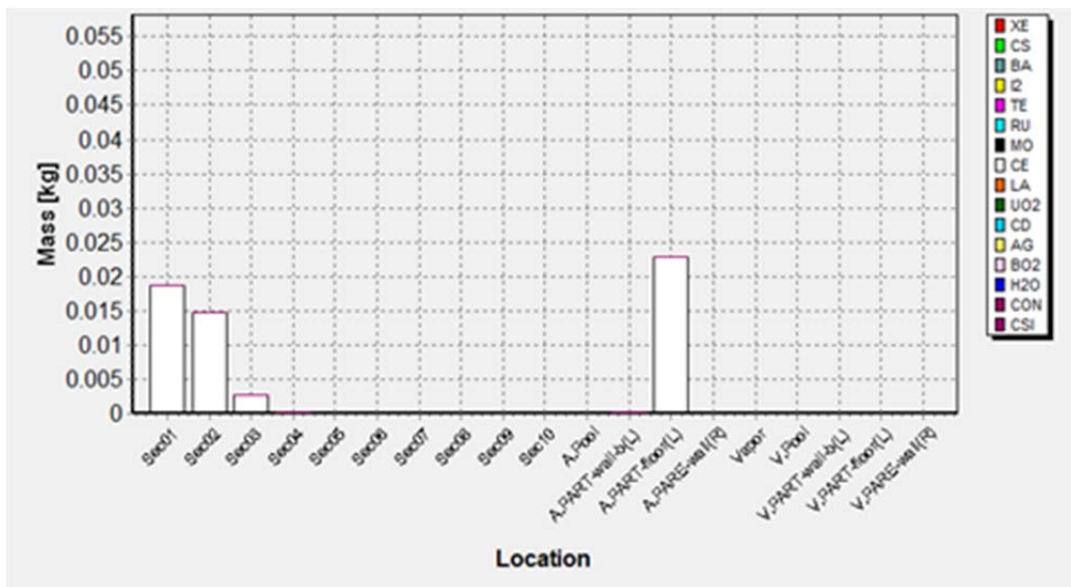
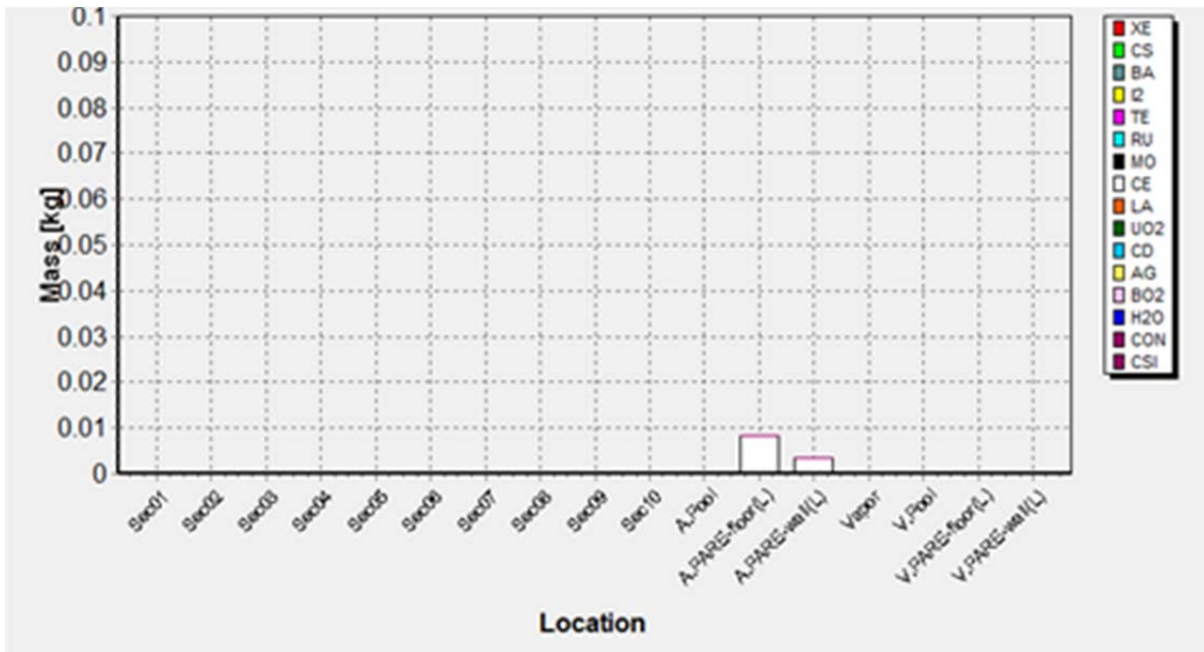


Figure 5-29. Aerosol Histogram Results in Bottom PART Volume for a 2-PART Volumes at 50 psig Case at 30 Minutes.

In addition to the 50 psig case, two cases of the single and 2 PART-volume cases are conducted at 250 psig. The temperature of PARE (see Table 5-4) is very quickly in equilibrium with the ambient temperature of 289 K. Figure 5-30 and Figure 5-31 show the aerosol results for this case at 30 minutes. For this case about 11 g aerosol is deposited on the floor of the PARE, about 70 g is suspended, and 19 g is deposited on the PART floor. In comparison, the experiment measured

17 to 20 g suspended. MELCOR predicts 2.5 times larger deposition in this case. Similar to the 50 psig case, MELCOR predicts that most of the suspended aerosol is within the first three bins (2.5  $\mu\text{m}$  max.), compared to the experimental measurements of 6 to 17  $\mu\text{m}$ . Figure 5-32 and Figure 5-33 show the aerosol results for this 2 PART-volume case at 30 minutes. As shown here, only about 50 g aerosol remains suspended. At only about two times higher, this result is closer to the experiment result.

At the pressures reported in the pressurized release cases in [Sutter 1983], the outdoor experiment indicated that the plume height for 50 psig release is 4.5 m. The PART height is only 3 m, so the plume rise from PARE into PART will definitely hit the ceiling [Sutter 1983]. For a 1000 psig outdoor experiment, the plume height is 10.7 m [Sutter 1983]. Therefore, the 250 psig plume height is between 4.5 m and 10.7 m. Ceiling impingement and wall and floor impingement are all possible. Because MELCOR does not model the turbulent mixing, ceiling impingement, and initial plume rise of the release, some underestimations by MELCOR are possible.



**Figure 5-30. Aerosol Histogram Results in PARE Volume for a Single PART Volume at 250 psig Case at 30 Minutes.**

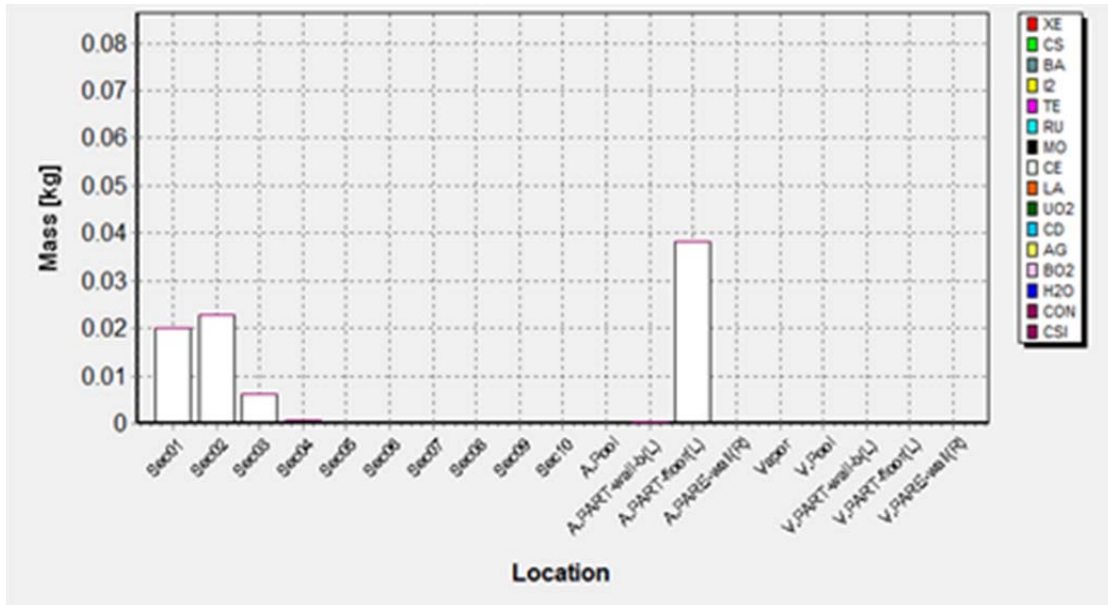


Figure 5-31. Aerosol Histogram Results in PART Volume for a Single PART Volume at 250 psig Case at 30 Minutes.

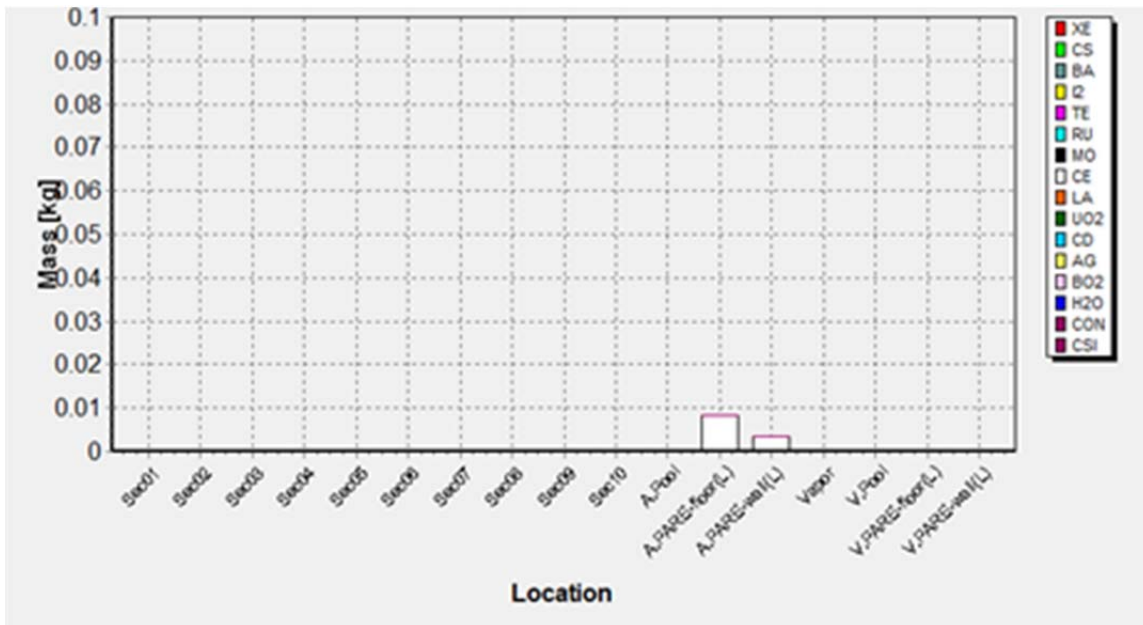
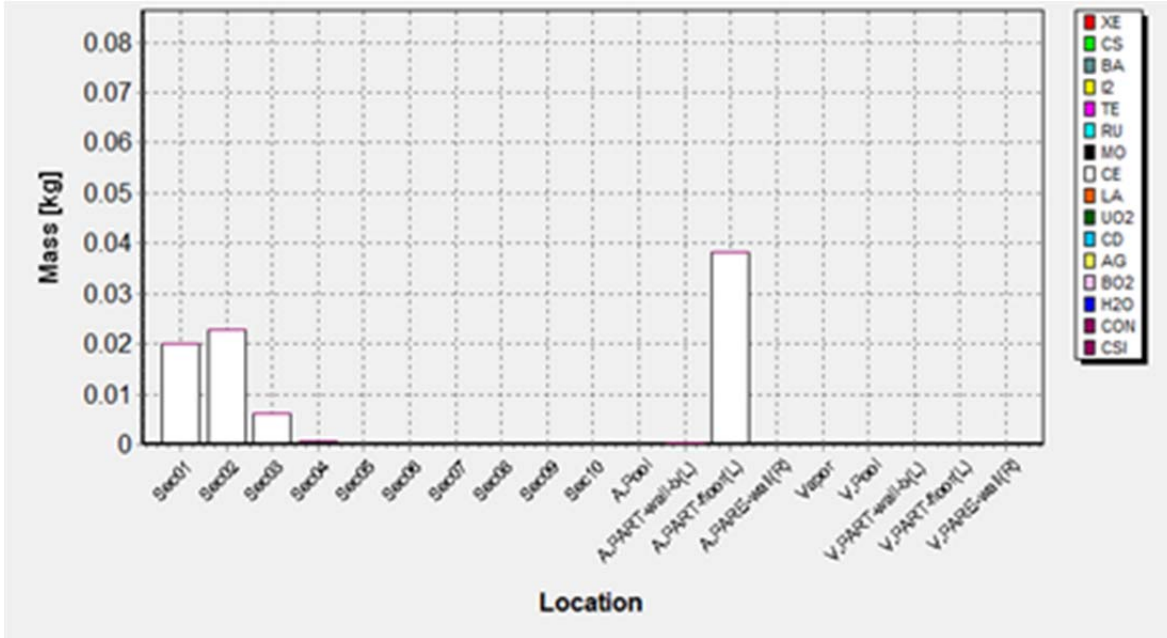


Figure 5-32. Aerosol Histogram Results in PARE Volume for a 2 PART-Volume at 250 psig Case at 30 Minutes.



**Figure 5-33. Aerosol Histogram Results in the Bottom PART Volume for a 2 PART-Volume at 250 psig Case at 30 Minutes.**

### 5.2.2 Fuego Simulations

As indicated in Section 3.1, the SIERRA FD code Fuego can be used to model particle dispersion, even though this code is primarily used for fire analysis (see Chapter 4). The suspension of the particles in space follows the following momentum exchange equation between the fluid (in this case air) and particle:

$$F_{\text{drag}} = -6 \pi \mu_f \text{Re}_p f_D v_f \quad (5-10)$$

Where  $f_D$  is the drag coefficient, which is a function of the Reynolds number ( $\text{Re}_p$ ) of the particle:

$$f_D = \begin{cases} 1 + \text{Re}_p^{2/3} \\ 0.0177 \text{Re}_p \end{cases} \quad (5-11)$$

As described previously, Fuego currently does not model particle interactions, which implies that no agglomeration is possible. Therefore, this simulation of the pressurized powder release can only be used to determine if the particles in the PARE will be imparted to the walls and ceiling of the PART. These determinations may help to explain extensive deposition rather than re-suspension during the time of measurement.

To model this experiment, the locations of the particles (particle bed) in the PARE chamber needs to be specified. For this exploratory simulation, 100,000 particles were assumed to be sufficient to represent the release of the 100 g of  $\text{TiO}_2$  in the experiment.

Initial particle data can be specified in an input file. A program has been written to output the initial particle data. The cylindrical shape of the PARE was assumed. Because we are modeling the particle bed, the insertion time is set at time zero and the temperature is set at the initial temperature of the problem. The program then positions the particles starting from the base of the geometry selected and filled to top of the geometry, according to the number of particles to be simulated. A particle distribution was assumed. The maximum diameter is  $1 \times 10^{-5}$  m and minimum diameter is  $1.7 \times 10^{-6}$  m. Thus, the average diameter is  $6 \times 10^{-6}$  m. Because Fuego allows the user to specify the number of particles in each parcel (or bin), each of the 100,000 particles represents a parcel. Thus each, parcel is assumed to have 1000 particles and a total of  $1 \times 10^8$  particles are simulated. To model 100 g of  $\text{TiO}_2$  at its density of 4.23 g/cc, the number of particles required is about  $10^{11}$  particles, assuming that about half of the PARE volume is air. Thus, this simulation is only studying a very small fraction of the available powder. Below are the major assumptions associated with this simulation.

Assumptions for Simulation Model:

- Only 100,000 particles were modeled in the simulation. This is only a fraction of the particles in the experiment, which overestimate the suspended particles.
- No wall deposition is modeled. This would underestimate the wall depositions, which will better match the experiment and its reported significant deposition, particularly for the high pressure tests.

Two cases were simulated: 50 psig and 250 psig. SIERRA 3.46 version was used in these simulations. Preliminary simulations showed that the 250 psig case may not be appropriate for Fuego. Fuego is a low-Mach number code, and this pressure creates velocities that exceed that limit. At 250 psig, the fluid that expands from PARE into PART attains an unrealistically high velocity of  $> 1000$  m/s. Additional studies will be carried out next year to revisit the higher pressure case (i.e.,  $\geq 250$  psig cases). The use of both Adagio and Fuego may be necessary. Therefore, only the discussions on the 50 psig case are described in this report.

A mesh has been generated for the simulation to simulate both PARE and PART volumes (see Figure 5-34). As shown here, the mesh is fine at the center of the PART volume and increases with mesh size to reflect the number of the particles located as a function of time. The PARE volume is modeled at the bottom center of this figure. Unlike the MELCOR model, this simulation was created to study the particle dispersal. Wall deposition is not simulated since no material adhered to the surfaces of the wall, floor and ceiling of the PART. Only 60 s of 1800 s of the problem are simulated for this exploratory exercise to identify when the particles reach the ceiling and wall of the PART. As shown in Figure 5-35, the simulation of the particles disperses into the PART from the PARE. At about 24 s, the particles have reached the ceiling. If surfaces are allowed to stick, particles are then deposited upon impaction. Currently, a rebound wall boundary condition is set, so this deposition is not allowed. Note that the particles have not reached the cylindrical side wall of PART at 60 s.

As shown in this exploratory exercise, particles from this 50 psig case do reach surfaces of the PART, which means that the higher pressure cases ( $>50$  psig) from [Sutter 1983] will definitely hit PART's surfaces. This is consistent with the observations in the experiment. Therefore, a

better representative model of the experiment is needed to capture particle impingement onto surfaces.

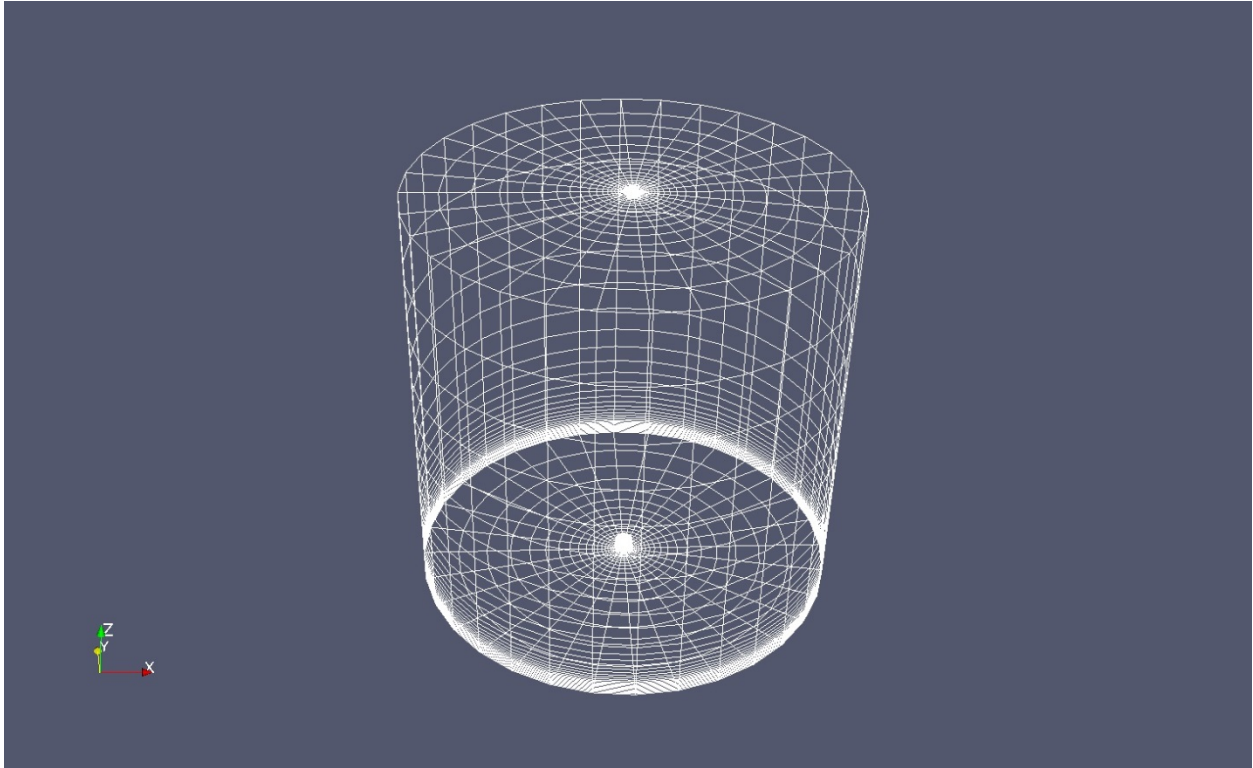


**Figure 5-34. Fuego Mesh Used.**



**Figure 5-35. Fuego Simulation Results for the 50 psig Pressurized Powder Release Test.**

## 6 SUMMARY AND CONCLUSION

This report discusses an NSRD project on substantiating the DOE-HDBK-3010 using SNL SIERRA code suite, such as the SM code Adagio or Presto and the FD code Fuego. Two specific fire experiments in Chapter 3 of the Handbook were simulated to demonstrate Fuego capability: a Beaker fire experiment (described in Section 3.3.1 of the Handbook) and a gasoline pool fire (described in Section 3.3.6 of the Handbook).

For the beaker fire, there were 25 ml of kerosene with 30% TBP and contaminants in a beaker and a chimney apparatus to ensure no cross-flow. A Fuego model was developed for droplet entrainment during the boiling for the release of the contaminants. An initial droplet size distribution was employed to model droplet breakup during rising bubbles. The simulations include a number of parameter variations, including the initial liquid height and turbulence induced at the boiling surface. The sensitivity to the initial fuel height is significant, since results indicated that this parameter is closely related to the airborne release. The aerosol release for a 20 mm initial liquid height shows reasonable agreement with the data. Beaker wall deposition is also observed in the simulations. Since Fuego does not currently have such a model, no resuspension is used. This beaker simulation study identified two major findings:

- Liquid height may have an effect on the release of contaminant, a parameter not considered in the experiments.
- The effect of flow turbulence was not particularly significant.
- Much of the airborne release was predicted to occur at the beginning of the simulations during the ignition.

In addition to the beaker fire, a gasoline pool fire with 50 g of  $UO_2$  powder was simulated using Fuego. For this experiment, a steel pan was located inside a wind tunnel, in which gasoline contaminated with  $UO_2$  was allowed to entrain. In this simulation series, a number of entrainment phenomena were considered in the model such as EIE and agitation by boiling (similar to that in the beaker fire). Although wind can be important for resuspension, this aspect of these tests was not simulated because Fuego currently does not model resuspension. In subsequent work, we plan to implement and test resuspension. As demonstrated in this simulation, the deposited mass on the walls of the wind tunnel is small compared to the outflow of the airborne materials. The magnitude of the EIE is very small in comparison to the boiling. All cases were found to have higher ARF values than that of the experiments, but this was driven by the assumed boiling time. Better assessments of the boiling time are needed.

The major conclusions for this pool fire simulation series are listed below.

- The entrainment mechanism of surface agitation by boiling significantly dominated the entrainment during flaming.
- Turbulence boundary conditions were not reported, and a practical range of assumptions results in significant uncertainty in the ARF for the above entrainment mechanisms.
- The boiling mechanism was found to be the significant contributor to the amount of entrained mass. Modeling of particle entrainment from pool boiling will improve the modeling accuracy.

In addition to these fire simulations, exploratory simulations were also conducted to identify if SIERRA codes can be used to model solid entrainment.

For a projectile impacting a can filled with  $\text{UO}_2$  powder, the simulations for the powders included the use of the Mie-Gruneisen EOS Model and the Soil-Crushable Foam material model. Two simulation impact speeds of 20 m/s and 175 m/s were conducted. A coarse and a fine mesh model were also used for the simulation. A total of five cases were simulated. In general, a 20 m/s impact velocity of the projectile would puncture a hole to the can, which leads to powder escaping. At this velocity, the can remains stationary while the projectile rebounds. On the other hand, when the impact speed increases to 175 m/s, the projectile penetrates the can and becomes lodged inside while the can flies upward. During can lofting, particles escape through the opening. Eventually, the can falls back and hits the floor again. During this time, additional release near the bottom of the can was observed in the simulation. This release may not be realistic. Therefore, additional 20 m/s impact velocity cases were simulated to observe this secondary release. Only cases with the Mie-Gruneisen EOS material model were observed to have this behavior. The use of the Soil-Crushable Foam material model did not exhibit the secondary release. Perhaps the Mie-Gruneisen EOS material model may not be appropriate for this low impact speed scenarios; it may instead be appropriate for explosion simulations or high-impact velocity simulations where shocks are developed. Further analysis of this behavior for the Mie-Gruneisen EOS model may be needed. On the other hand, the Soil-Crushable Foam material model is useful for modeling the impact type of an accident.

The major conclusions for this projectile impact case are listed below.

- SIERRA SM code can be used to simulate solid entrainment by the use of a SPH model.
- The use of Mie-Gruneisen EOS material model should be limited for shock related impact type of accidents.
- The use of a Soil-Crushable Foam material model is useful for modeling impact accidents.
- The use of coarse and fine mesh models for the same simulation model suggests that the model may behave well.
- Problems with a longer duration are needed to observe unrealistic model results.

The other powder simulations involved the pressurized release from a container to a containment type volume (see Section 5.2). Here, because of known limitations of Fuego particle interactions, the MELCOR code was also used. Although MELCOR is a system-level code, it contains an aerosol physics model. Because the MELCOR aerosol physics model is based on concentrations of the airborne aerosol, multiple volumes were required. A single volume model and a two-volume model have been developed. We found that the results can be a function of the number of volumes modeled. Two pressure cases were simulated (50 psig and 250 psig). A better modeling method is needed to include this exchange.

A preliminary Fuego model was developed to simulate the 50 psig case of the experiment. Although the surfaces for the model are assumed to be re-bound rather than stick, the 60-s run

showed the impingement of the particles on the ceiling. This result is consistent with the experimental results.

The major conclusions for the pressurized powder release simulations are listed below.

- Although MELCOR is a system-level code with a concentration based on an aerosol physics model, it can be used to simulate this type of experiment.
- Fuego, on the other hand, has been used to model fires as described in Chapter 4. This FD code can be extended to model pressurized powder release case.
- Fuego may not be appropriate for modeling higher pressure conditions since it is designed for low-Mach flow.
- Although Fuego currently does not have a particle interaction model, it can be used to identify the particle impingement to walls and ceilings.

Note that these exploratory simulations are intended to demonstrate the code's capability. At this stage, the simulations are not intended to be compared to experimental results. Further analyses of scenarios using MELCOR and Fuego for pressured powder release are to be continued in subsequent work.

Intentionally Left Blank

## 7 RECOMMENDATIONS FOR FUTURE WORK

Although a number of model improvement needs are described in Section 4.3 of this report, two near-term Fuego improvement needs are described below for the fire simulations described in Chapter 4 (see Table 7-1). As shown in this table, the multicomponent particle capability would allow the modeling of separate liquid combustible and solid contaminants in a contaminated fuel mixture. This would be used for beaker and pool fire simulations described in Chapter 4, and will permit a more accurate ARF prediction for contaminants in the fire. The resuspension of particles from surfaces is an active entrainment mechanism. Resuspension would allow more accurate ARF during a strong cross-flow condition, which is likely to be present during accident conditions.

**Table 7-1. Fuego Improvement Proposed for Next Year**

<b>SIERRA FD code (Fuego) Recommendation</b>	<b>Potential Benefit</b>
Multicomponent particle capability	This capability is particularly useful when fuel and solids (contaminants) are mixed, allowing fuel to evaporate while solids remain during the fire
Resuspension of particle capability	This capability is important for resuspension of deposited materials from the walls or burn residues resuspended under wind conditions

In addition to the fire simulations, a number of exploratory simulations were conducted as a part of this current research. Table 7-2 lists the recommendations for modeling mechanical insult accidents using SIERRA SM code. Note that no additional simulation would be carried out next year.

**Table 7-2. Recommendation for Modeling Mechanical Insult Accident Using SIERRA SM Code**

<b>Model and Simulation Improvement</b>	<b>Potential Benefit</b>
Mie-Gruneisen EOS Material Model	This model should be used with caution, particularly with the SPH capability for modeling particle dispersal. It should only be applied to explosion simulations and high-velocity impact cases where shocks can be developed. In addition, this model is only available in Presto (itar version) of the SIERRA SM code. Discussions of the model and results are limited.
Soil-Crushable Foam Material Model	This material model should be suitable for modeling low-velocity impact cases as described in Section 5.1. It tends to be stable in comparison to the Mie-Gruneisen EOS model above for the same simulation model. Unlike the Mie-Grunesien EOS model, this material model can be obtained from Adagio, which may not be restricted in terms of export controls.

Coupling to Fuego	Once the particles leave the can for the impact simulations in structural code such as Adagio described in Section 5.1, any tracking of the particles may not be accurate due to lack of aerodynamic models in Adagio. Therefore, it is important to couple Fuego in this case.
Temperature consideration	The effect of temperature should be included to properly account for the energy transfer from mechanical (kinetic) to heat during the impact.
Wall/shell resolution	Quantitative accuracy may require that the wall resolution be refined to model material failure properly.

For the pressurized powder release simulations, there are number of recommendations as shown in Table 7-3.

**Table 7-3. Recommendations on Modeling Pressurized Powder release Simulations for Next Year**

<b>Model Improvement</b>	<b>Potential Benefit</b>
Multi-volume MELCOR model	This multi-volume MELCOR model may improve results with the experiment since the aerosol physics model depends on concentration.
Flow of Air exchange during experiment needed to be included in MELCOR model	During the aerosol measurement, air inside the PART volume was exchanged 80 times. This exchange may improve MELCOR model results with experimental data.
Refined Fuego model	Proper modeling of the experiments is needed, including those described in the MELCOR model improvement above. This would improve the particle deposition results on the walls and ceiling of PART.
Fuego/MELCOR Coupling	Since Fuego currently does not model particle interactions, the Fuego results, particularly for the wall and ceiling deposition, can be used in conjunction with MELCOR results to compare with the experimental data. This coupling would improve the calculation results to experiments.
Adagio/Fuego/MELCOR Coupling	As described in this research, Fuego can only model pressurized powder release with a 50 psig pressure. To model higher pressure cases, the use of the SPH particle model in Adagio may be required. The results of Adagio are then used by Fuego to predict impingement. Finally, the results are used in MELCOR to determine the final results to compare with the experiments.

## 8 REFERENCES

- [Antoun 2012] Antoun, T., Herbold, E., and Johnson, S., **Dynamic Behavior of Sand: Annual Report FY 11**, LLNL-TR-539077, Lawrence Livermore National Laboratory, Livermore, CA, March 19, 2012.
- [Bagul 2013] Bagul, R.K., D. S. Pilkhwal, P.K. Vijayan, and J.B. Joshi, "Entrainment phenomenon in gas-liquid two-phase flow: A review," *Sadhana*, 38(6), pp. 1173-1217, (2013).
- [Borkowski 1986] Borkowski, R., Bunz, H., and Schoeck, W., **Resuspension of Fission Products during Severe Accidents in Light-Water Reactors**, KfK3987, EUR 10391, May (1986).
- [Brown 2006] Brown, A.L., Vembe, B.E., "Evaluation of a Model for the Evaporation of Fuel from a Liquid Pool in a CFD Fire Code," Proceedings of the ASME International Mechanical Engineering Congress & Exposition, November 5-10, 2006, Chicago, IL, USA, IMECE2006-15147.
- [Brown 2015] Brown, A.L., and Louie, D. L. Y., "Contaminant Entrainment in a Liquid Fuel Fire," Proceedings of the 1st Thermal and Fluid Engineering Summer Conference, TFESC, New York City, USA, August 9-12, 2015. SAND2015-1360C.
- [Brown 2015a] Brown, A.L., Zepper, E., Louie, D. L. Y., and Restrepo, L., "Contaminant Entrainment from a Gasoline Fuel Fire," SAND2015-7185C, Paper 134IE-0033, Fall 2015 meeting of the Western States Section of the Combustion Institute in Provo, UT, USA, October 5-6, 2015
- [Cosandey 2001] Cosandey, J.O., von Rohr, P.R., "Entrainment of Soluble and Non-soluble Tracers from a Boiling Water Surface," *Nuclear Engineering and Design*, 208, pp. 87-97, (2001).
- [Cosandey 2003] Cosandey, J.O., Günther, A., von Rohr, P.R., "Transport of Salts and Micron-Sized Particles Entrained from a Boiling Water Pool," *Experimental Thermal and Fluid Science*, 27, pp. 877-889, (2003).
- [Derakhti 2014] Derakhti, M., and Kirby, J.T., "Bubble Entrainment and Liquid-Bubble Interaction under Unsteady Breaking Waves," *J. Fluid Mech.* 761, 464-506, 2014.
- [DOE 1994] Department of Energy, **Airborne Release Fractions/Rates and Respirable Fractions for Non-Reactor Nuclear Facilities**, Volume 1 and 2, DOE-HDBK-3010-94, U.S. Department of Energy, Washington, DC, December 1994, Reaffirmed 2013.
- [Drysdale 1998] Drysdale, **An Introduction to Fire Dynamics**, Second Edition, John Wiley & Sons, Inc., 1998.
- [Duchemin 2002] Duchemin, L., Popinet, S., Josserand, C., Zaleski, S., "Jet Formation in Bubbles Bursting at a Free Surface," *Physics of Fluids*, 14(9), pp. 3000-3008, (2002).
- [Gelbard 2013] Gelbard, F., Brown, A., Louie, D., Feng, C. and Bixler, N., "A Basic Principles Approach for Determining Radionuclide Releases from Accidental Explosions in Reprocessing Facilities," Proceeding to the 2013 ANS Winter Meeting and Nuclear Technology Expo, Washington DC., November 10-14, 2013.

- [Henry 2014] Henry, C., Minier, J.-P., “Progress in particle resuspension from rough surfaces by turbulent flows,” *Progress in Energy and Combustion Science*, 45, pp. 1-53, (2014).
- [Humphries 2015a] Humphries, L.L., Cole, K.K., Louie, D.L., Figueroa, V.G. and Young, M.F., **MELCOR Computer Code Manuals- Vol.1: MELCOR Primer and Users Guide, Version 2.1 6840 2015**, SAND2015-6691 R, Sandia National Laboratories, Albuquerque, NM, August 2015.
- [Humphries 2015b] Humphries, L.L., Cole, K.K., Louie, D.L., Figueroa, V.G. and Young, M.F., **MELCOR Computer Code Manuals- Vol.2: MELCOR Reference Manual, Version 2.1 6840 2015**, SAND2015-6691 R, Sandia National Laboratories, Albuquerque, NM, August 2015.
- [Humphries 2015c] Humphries, L.L., Louie, D.L.Y., Figueroa, V.G., Young, M.F., Weber, S., Ross, K., Phillips, J. and Jun, R.J., **MELCOR Computer Code Manuals- Vol.3: MELCOR Assessment Problems, Version 2.1 6850 2015**, SAND2015-6693 R, Sandia National Laboratories, Albuquerque, NM, August 2015.
- [Kataoka 1983] Kataoka, I., and Ishii, M., **Mechanistic Modeling and Correlations for Pool-Entrainment Phenomenon**, NUREG/CR-3304, ANL-83-37, April (1983).
- [Koch 2000] Koch, M.K., Vobnacke, A., Starflinger, J., Schütz, W., Unger, H., “Radionuclide re-entrainment at bubbling water pool surfaces,” *J. Aerosol Sci.*, 31(9), pp. 1015-1028, (2000).
- [Kogan 2008] Kogan, V., Schumacher, P.M., “Plutonium release fractions from accidental fires,” *Nuclear Technology*, 61, pp. 190-202, (2008).
- [Lick 2009] Lick, W.J., **Sediment and contaminant transport in surface waters**, Taylor & Francis, 2009.
- [Louie 2015] Louie, D. L.Y., Brown, A.L. and Restrepo, L., “Computer Capability to Substantiate DOE-HDBK-3010 Data,” *Proceeding of the 2015 Annual ANS Meeting*, San Antonio, TX, June 7-11, 2015.
- [Magnussen 1981] Magnussen, B.F., “On the Structure of Turbulence and a Generalized Eddy Dissipation Concept for Chemical Reactions in Turbulent Flow,” *9th AIAA Sc. Meeting*, St. Louis, (1981).
- [Minana 2012] Minana, M., Turgeon, J., Lujan, C., Pilch, M., and Hackney, P., **Sandia National Laboratories Advanced Simulation and Computing (ASC) Software Quality Plan – ASC Software Quality Engineering Practices, Version 3.1**, SAND2008-5517, Sandia National Laboratories, Albuquerque, NM, March 2012.
- [Mishima 1968] Mishima, J., Schwendiman, L.C., and Radasch, C.A., **Plutonium Release Studies IV. Fractional Release from Heating Plutonium Nitrate Solutions in a Flowing Air Stream**, BNWL-931, UC-41 Health & Safety, November 1968.
- [Mishima 1973] Mishima, J., and Schwendiman, L.C., **The Fractional Airborne Release of Dissolved Radioactive Materials During the Combustion of 30 Percent Normal Tributyl Phosphate in a Kerosine-Type Diluent**, BNWL-B274, June 1973.

- [Mishima 1973a] Mishima, J., Schwendiman, L.C., **Some Experimental Measurements of Airborne Uranium (Representing Plutonium) in Transportation Accidents**, BNWL-1732, August, 1973.
- [Roberts 2003] Roberts, J.D., Jepsen, R.A., and James, S.C., “Measurements of Sediment Erosion and Transport with the Adjustable Shear Stress Erosion and Transport Flume,” *Journal of Hydraulic Engineering*, Vol. 129, No. 11, 2003.
- [Sehmel 1984] Sehmel, G.A., “Deposition and Resuspension,” Chapter 12 in “*Atmospheric Science and Power Production*,” Randerson, D., editor, DOE/TIC-27601, 1984.
- [Shaw 2015] Shaw, R.P., Agelastos, A.M., and Miller, J.D., **Guide to Using Sierra**, SAND2015-1642, Sandia National Laboratories, Albuquerque, NM, March 9, 2015.
- [SNL 2015] <http://compsim.sandia.gov/compsim/Docs/Sierra/4.36/GeneralRelease>
- [SNL 2015a] SNL, **SIERRA/SolidMechanics 4.36 User’s Guide**, SAND2015-2199, Sandia National Laboratories, Albuquerque, NM, March 26, 2015.
- [SNL 2015b] SNL, **SIERRA/SolidMechanics 4.36 User’s Guide: Addendum for Shock Capabilities**, SAND2015-4022, Sandia National Laboratories, NM, May 22, 2015.
- [SNL 2015c] SNL, **SIERRA/SD – Theory Manual**, SAND2011-8272, Sandia National Laboratories, NM, April 21, 2015.
- [Spiel 1997] Spiel, D.E., “More on the Births of Jet Drops from Bubbles Bursting on Seawater Surfaces,” *Journal of Geophysical Research*, 102(C3), pp. 5815-1521, (1997).
- [Spiel 1997a] Spiel, D.E., “On the Births of Film Drops from Bubbles Bursting on Seawater Surfaces,” *Journal of Geophysical Research*, 103(C11), pp. 24907-24918, (1997).
- [Sutter 1983] Sutter, S.L., **Aerosols Generated by Releases of Pressurized Powders and Solutions in static Air**, PNL-4566, NUREG/CR-3092, Pacific Northwest Laboratory, Richland, WA, May 1983.
- [Swegle 2009] Swegle, J.W., **PRESTO Theory Documentation: Energy-Dependent Materials Version 1.0**, SAND2009-3801P, Sandia National Laboratories, Albuquerque, NM, June 2009.
- [Tieszen 1996] Tieszen, S.R., and Attaway, S.W., **Fuel Dispersion in High-Speed Aircraft/Soil Impact Scenarios**, SAND96-0105, Sandia National Laboratories, Albuquerque, NM, January 1996.
- [Wardlaw 1996] Wardlaw, Jr., A.B., McKeown, R., and Chen, H., Implementation and Application of the P- $\alpha$  Equation of State in the DYSMAS Code, NSWCDD/TR-95/107, Naval Surface Warfare Center, Dahlgren, VA, May 1996.
- [Zhang 2012] Zhang, J., Chen, J.J.J., Zhou, N., “Characteristics of Jet Droplet Produced by Bubble Bursting on the Free Liquid Surface,” *Chemical Engineering Science*, 68, pp. 151-156, (2012).

Intentionally Left Blank

## APPENDIX A

### Summary Table for Handbook Data

This appendix provides a summary table for the Handbook, including a number of columns: Column 1 identifies the chapter or section number; Column 2 identifies the category, such as liquid, solid, etc.; Columns 3 and 4 tabulate the bounding values; Column 5 describes any initial size distribution provided; and Column 6 provides comments. Note that Column 1 intends to provide the information of interests from those chapters/sections from the Handbook. It is not necessarily a complete list, since Chapter 2 of the Handbook deals with gaseous forms, which are often assumed to be released during an accident. Thus, it may not have an interest in this current research in terms of ARF and RF. Note: this summary table is an “in-progress” table, which means that it would be updated as more substantiating studies are done to the data in the Handbook.

Chapter /section	Category	ARF	RF	Initial Size Distribution	Comments
3.0	<b>LIQUID</b>				This chapter divides into types of liquids, which includes aqueous solutions, organic, and combustible solvents.
3.2	<i>Aqueous solution</i>			Droplet distribution during bubbling is provided	This section describes models related to evaporation and boiling. Formulations on entrainment of liquid droplets from the surface of a bubbling or boiling pool are provided. Phenomena associated with these entrainments are described. (see Chapter 4 of this report for more details about describing the use of these models in the simulations)
3.2.1	<u>Thermal Stress</u>				
	(a) Heating of aqueous solution in flowing air without surface rupture bubbles	3.00E-05	1		
	(b) Boiling (bubbles continuously breaking the surface of the bulk liquid with < 30% of volume of the liquid as bubbles)	2.00E-03	1		
3.2.2	<u>Explosion Stress</u>				
	Venting of pressurized liquids				
	(a) Venting below liquid level	1.00E-04	1	< 10 μm	
	(b) Venting above liquid level				
	[1] low pressure (< 0.35 MPa)	5.00E-05	0.8		
	[2] high pressure (>0.35 MPa)				
	(aqueous solution)	2.00E-03	1		~1 g/cc solution density
	(conc. Heavy metal solution)	1.00E-03	0.4		≥1.2 g/cc solution density
	[3] superheated liquid				
	(≤ 50°C superheat)	1.00E-02	0.6		
	(50 to 100°C superheat)	1.00E-01	0.7		
	(> 100°C superheat)	0.33*(MF) <sup>0.91</sup>	0.3		MF = mole fraction of pressurized gas/water vapor flashed
3.2.3	<u>Free-Fall Spill</u>				

Chapter /section	Category	ARF	RF	Initial Size Distribution	Comments
	3-m distance				
	(a) aqueous solution				
	[1] aqueous solution	2.00E-04	0.5		~ 1g/cc solution density
	[2] conc. Heavy metal solution	2.00E-05	1		≥ 1.2 g/cc solution density
	(b) slurries < 40% solids	5.00E-05	0.8		
	(c) viscous solution, viscosity > 8 centipoise	7.00E-06	0.8		
	> 3-m				Both ARF and RF should be larger than the 3-m fall, and the empirical correlations for ARF and drop size presented in Ballinger et.al (Jan 1988)
3.2.4	<u>Aerodynamic Entrainment and Resuspension</u>				Use of these values for < 100 hours would not introduce serious error due to the severe depletion of the source.
	(a) indoor surfaces (SS, concrete) up to normal facility ventilation flow; outdoors, pool for low wind speeds	4.00E-07	1		
	(b) indoor, covered with debris or under static condition	4.00E-08	1		
	(c) outdoors, large pools wind speed ≤ 30 mph	4.00E-06	1		
	(d) outdoors, absorbed on soil, no lengthy pooling wind speed ≤ 50 mph	9.00E-05	1		
3.3	<i>Organic Combustible Liquids</i>				No experimental data on the behavior of organic, combustible liquids in response to explosive release, venting of pressurized liquid, free-fall spills or aerodynamic entrainment were found. We are examining some of the experiments referenced in this section for this year in the area of fire in Section 3.3.1 and Section 3.3.6 of the Handbook (see Chapter 4 of this report)
	<u>Thermal Stress</u>				
	(a) volatiles (i.e., I2)	1	1		
	(b) Quiescent burning, small surface pool, or on larger pool	1.00E-02	1		
	(c) vigorous burning large pools	3.00E-02	1		This includes solvent layer burning over limited aqueous layer with sufficient turbulence to disrupt bulk of aqueous layer
	(d) Same as (C) to complete dryness	1.00E-01	1		
	(e) air-dried salts under gasoline fire	5.00E-03	1		Includes aqueous solution, on a porous or cracks, depression
	(f) same as (e) above, except on metal surface	2.00E-01	1		May not include porous, cracks or depression
4.0	<b>SOLIDS</b>				This chapter of the Handbook describes the data related to metals (primarily the release

Chapter /section	Category	ARF	RF	Initial Size Distribution	Comments
					from energetic hydride reactions, nonmetallic (such as ceramics) or composite solids, and powders.
	<i>Metal</i>				
4.2.1	<u>Thermal Stress</u>				
	(a) Plutonium				
	[1] oxidation (corrosion) at room temperatures				These values intended for < 100 hours
	(unalloyed Pu)	$2 \times 10^{-6} \mu\text{g Pu/cm}^2\text{-hr (dry air)}$	0.7		
		$7 \times 10^{-3} \mu\text{g Pu/cm}^2\text{-hr (100\% RH)}$	0.7		
	(delta-phase metal)	$7 \times 10^{-8} \mu\text{g Pu/cm}^2\text{-hr (dry air)}$	0.7		
		$6 \times 10^{-4} \mu\text{g Pu/cm}^2\text{-hr (100\% RH)}$	0.7		
	[2] oxidation at elevated temperatures	3.00E-05	0.04		
	[3] self-sustained oxidation	5.00E-04	0.5		Includes molten metal with oxide coat, self-induced convection
	[4] disturbed molten metal surfaces	1.00E-02	1		Such as flowing metal, actions resulting in continual surface renewal, high turbulence at surface. Impacted by high air velocity or free-fall, 95% confidence on these values. It is not applicable to oxidation of trace hydride, metal, powder contamination
	[5] oxidation of small metal drops	1	0.5		hundreds of $\mu\text{m}$ size, passing through air or explosive reaction of entire metal mass
	(b) Uranium				
	[1] complete oxidation of metal mass	1.00E-03	1		For thermal condition > 500 °C and for upward flow velocity of 0- 2 m/s. It is for airborne particles < 10 $\mu\text{m}$ . A 95% confidence level is for flow velocities < 100 cm/s.
	[2] free-fall of molten metal drops	1.00E-02	1		This is based on an arbitrary increase of 95% confidence to the experiment data.
	[3] explosive dispersal of molten uranium	1	1		If the uranium is molten and subdivided in very small drops and ejected at sonic velocities (very fine particles and aggregates $\leq 10 \mu\text{m}$ )
4.2.2	<u>Explosive Stress</u>				No recommended value is given. It refers to the surface contamination section of the handbook. For shock effects, it refers to the size of the TNT equivalent for respirable release. 20% of the metal should be used as respirable fraction. Consult national laboratories for analyses.
4.2.3	<u>Free-Fall and Impaction Stress</u>				No significant release as indicated. Refer to the surface contamination section of the handbook.
4.2.4	<u>Aerodynamic Entrainment and Resuspension</u>				Identical correlations as described in the Thermal Stress type (a)[1] above.
4.3	<i>NONMETALLIC OR COMPOSITE</i>				

Chapter /section	Category	ARF	RF	Initial Size Distribution	Comments
	<i>SOLIDS</i>				
4.3.1	<u>Thermal Stress</u>				
	(a) vitrified waste				No significant release by industrial-type fire.
	(b) aggregate (e.g., concrete and cement)				
	[1] tritium release from concrete				
	(if present and 200 °C)	5.00E-01	1		
	(if present and 600 °C)	1	1		
	[2] suspendible powder	6.00E-03	0.01		
	[3] spent commercial nuclear fuel				These materials were discussed in general for accident conditions related to severe accidents in commercial reactors. Thus release related to thermal stress is related to the release described in Section 4.4.1 of the Handbook
4.3.2	<u>Explosive Stress</u>				No recommended value is given. It refers to the surface contamination section of the handbook. For shock effects, it refers to the size of the TNT equivalent for respirable release. 20% of the metal should be used as respirable fraction. Consult national laboratories for analyses.
4.3.3	<u>Free-Fall and Impaction Stress</u>	see comment	see comment	A distribution related to the UO <sub>2</sub> pellet impacts is provided	A correlation for a combined value of ARF*RF is given as A*P*g*h, where A is an empirical correlation of 2E-11 cm <sup>3</sup> per g-cm <sup>2</sup> /s <sup>2</sup> , P specimen density, g/cm <sup>3</sup> , g is gravity at sea level, and h is fall height in cm.
4.3.4	<u>Aerodynamic Entrainment and Resuspension</u>				No significant release. See contamination section of this handbook.
4.4	<i>Powders</i>				For high energy stresses, the bounding values of 10 μm AED and RF =0.1 should be assumed.
4.4.1	<u>Thermal Stress</u>				Based on the thermal condition of < 1000 °C
	(a) non-reactive compounds	6.00E-03	1.00E-02		Entrainment of pre-formed particles by the flow upwards of heated surface.
	(b) reactive compounds except PuF <sub>4</sub>	1.00E-02	1.00E-03		Particles formed by reaction given by the experiments
	(c) PuF <sub>4</sub>	1.00E-03	1.00E-03		Particles formed by reaction given by the experiments
4.4.2	<u>Explosive Stress</u>				
	(a) shock effect				No data
	(b) blast effect				Detonations and deflagrations
	[1] above the surfaces	see comment	see comment		No detailed information is provided for detonation. For large deflagration, use ARF of 1 and RF for the original powder size that is < 10 μm. It is for a container failure pressure of ~ < 0.17 MPa.
	[2] accelerated airflow parallel to surface	5.00E-03	0.3		This represents a condition of the powders shield from the effects of a detonation or strong deflagration by standard containers.

Chapter /section	Category	ARF	RF	Initial Size Distribution	Comments
	(c) venting of pressurized powders for deflagration > 25% confined volume				This also includes the condition of a deflagration and pressurized release. We are examining the pressurized release of powder experiment this year (see Section 5.2 of this report)
	[1] $\leq 0.17$ MPa	5.00E-03	0.4		
	[2] 0.18 to 3.5 MPa	1.00E-01	0.7		
4.4.3	<u>Free-Fall/Impaction Stress</u>				We are examining a projectile hitting a can filled with powder (see Section 5.1 of this report). There is no experimental data for this simulation.
	(a) fall height < 3 m	2.00E-03	0.3		
	(b) fall height > 3 m	See comment. The calculated value must exceed those in (a)	See comment. The calculated value must exceed those in (a). The RF is limited in the total RF in the original powder.	see comment	Using PSPILL code to model powder spills - varying Mo (mass of powder spilled, kg). Air density and viscosity assumes to be 1.18 kg/m <sup>3</sup> and 1.85e-5 Pa-sec, respectively. The correlation is given as: $ARF = 2 * 0.1064 * (M_o^{0.125}) / (H^{2.37} / \rho^{1.02})$ , where H = spill height, and $\rho$ = bulk density of powder. $AMMD = 12.1 - 329 * \rho + 7530 * F$ , where F is the airborne fraction (ARF). Note this equation only has a 46% correlation coefficient due to the variability in the data.
	(c) suspended solid dispersed into flowing air	$ARF = 0.0134 v_{wind} + 0.00543$ , where $v_{wind}$ is the wind speed (m/s)	The RF is limited in the total RF in the original powder.		For enhanced air velocities normal to direction of powder flow.
	(d) suspension of bulk powder in confinement	1.00E-03	0.1		Due to vibration of substrate from shock-impact to powder confinement (e.g., glovebox or can) due falling debris or external energy (i.e., seismic vibration)
	(e) suspension of bulk powder by debris impact and air turbulence from falling object	1.00E-02	0.2		No confinement is involved.
4.4.4	<u>Aerodynamic entrainment and resuspension</u>				Use of values given for short time frame (< 100 hours)
	(a) homogeneous bed of powder exposed to ambient condition	ARR = 4E-5/hr	1		Normal process facility ventilation flow, nominal atmospheric wind speed < 2 m/s, gusts up to 20 m/s, following the event.
	(b) homogenous bed of powder buried under structural debris exposed to ambient condition	ARR = 4E-6/hr	1		Including static conditions within structure following the event.
	(c) entrainment of powders from road surface by passage of vehicular traffic	1.00E-02	1		ARF is per passage
5.0	<b><i>SURFACE CONTAMINATION</i></b>				
5.2	<i>Contaminated, combustible solids</i>				
5.2.1	<u>Thermal Stress</u>				

Chapter /section	Category	ARF	RF	Initial Size Distribution	Comments
	(a) packaged mixed waste	8.00E-05	1		For contaminated combustible materials heated/burned in packages with largely non-contaminated surfaces
	(b) uncontained cellulosic or largely cellulosic mixed waste	1.00E-02	1		For burning of unpackaged, loosely strewn cellulosic materials
	(c) uncontained plastics				
	[1] except polystyrene	5.00E-02	1		
	[2] polystyrene	1.00E-02	1		
	(d) dispersed ash dropped into air stream or forced draft air				These values are not typically applied to burning masses of combustible material in large fires. These apply to extremely severe conditions where loosely contaminated combustible material is driven airborne as part of an updraft fireball.
	[1] loose powder	4.00E-01	1		
	[2] air-dried solution or adherent contamination	8.00E-02	1		
5.2.2	<u>Explosive Stress</u>				
	(a) shock effect				No data. Assume to be venting of pressurized gases over material.
	(b) blast effect				No data. Assume to be venting of pressurized gases over material.
	(c) venting of pressurized gases over contaminated combustible waste	1.00E-03	1		
5.2.3	<u>Free-Fall and Impaction Stress</u>				
	(a) materials with high surface area to mass ratios	0	0		No significant suspension is expected for freefall spill from working heights (~1 to 1.5 m)
	(b) combustible material is unpackaged/lightly packaged and strongly impacts the floor	1.00E-03	1		Or is impacted by falling debris. The values are based on reasoned judgment
	(c) combustible material is packaged in a relatively robust container that is opened or fails due to impact with the floor or impaction by falling objects	1.00E-03	0.1		
5.2.4	<u>Aerodynamic Entrainment and Resuspensions</u>				Note that no applicable data found. Reasoned judgment is used. For < 100 hours)
	(a) indoor or outdoor exposed to ambient conditions	ARR = 4E-5/hr	1		Normal process facility ventilation flow, nominal atmospheric wind speed < 2 m/s, gusts up to 20 m/s, following the event.
	(b) buried under debris exposed to ambient condition	ARR = 4E-6/hr	1		
5.3	<i>Contaminated, noncombustible materials</i>				
5.3.1	<u>Thermal Stress</u>	6.00E-03	0.01		Reasoned judgment applies
5.3.2	<u>Explosive Stress</u>				

Chapter /section	Category	ARF	RF	Initial Size Distribution	Comments
	(a) shock effects				No recommended value is given. It refers to the surface contamination section of the handbook. For shock effects, it refers to the size of the TNT equivalent for respirable release.
	(b) blast effects				bounded by venting of pressurized gases in (c) below
	(c) venting of pressurized gases				These apply only to loose surface contamination on the solid, not the solid as a whole. It includes corroded solids.
	[1] accelerated gas flows in area without significant pressurization	5.00E-03	0.3		
	[2] venting of pressurized volumes				
	(> 0.17 MPa)	5.00E-03	0.4		
	(< 0.17 MPa)	1.00E-01	0.7		
5.3.3	<u>Free-Fall and Impaction Stress</u>				
	(a) free-fall				Most materials will not experience free-fall spill. It is bounded by impact, shock vibration (b) below
	(b) impact, shock-vibration				
	[1] under brittle fracture	see comment	see comment		A correlation for a combined value of ARF*RF is given as $A * P * g * h$ , where A is an empirical correlation of $2E-11 \text{ cm}^3$ per $\text{g-cm}^2/\text{s}^2$ , P specimen density, $\text{g/cm}^3$ , g is gravity at sea level, and h is fall height in cm.
	[2] materials that do not undergo brittle fracture	1.00E-03	1		
5.3.4	<u>Aerodynamic Entrainment and Resuspensions</u>				It is bounded by powders estimates
	(a) indoor or outdoor exposed to ambient conditions	ARR = 4E-5/hr	1		Normal process facility ventilation flow, nominal atmospheric wind speed < 2 m/s, gusts up to 20 m/s, following the event.
	(b) buried under debris exposed to ambient condition	ARR = 4E-6/hr	1		
5.4	<u>HEPA Filters</u>				
5.4.1	<u>Thermal Stress</u>	1.00E-04	1		extrapolation of maximum experimental of release of particles accumulated by the passage heated air through HEPA filters
5.4.2	<u>Explosive Stress</u>				
	(a) shock effects	2.00E-05	1		Based on experimentally measured release of accumulated particles from HEPA filters, localized failure from a momentary high pressure pulse.
	(b) blast effects	1.00E-02	1		High velocity air flow through up to filter break pressure
	(c) venting of pressurized gases	1.00E-02	1		
5.4.3	<u>Free-Fall and Impaction Stress</u>				No applicable experimental data for airborne release during free-fall of HEPA filters were uncovered
	(a) HEPA filter upon impact with hard unyielding surface				Bounded by conservative extrapolation of maximum releases measured for contained and uncontained HEP filters.
	[1] enclosed (e.g., packages, filter or plena housing)	5.00E-04	1		

Chapter /section	Category	ARF	RF	Initial Size Distribution	Comments
	[2] unenclosed	1.00E-02	1		
5.4.4	<u>Aerodynamic Entrainment and Resuspensions</u>				No significant release by nominal air velocities
6.0	<b>INADVERTENT NUCLEAR CRITICALITY</b>				
	<i>Solution</i>	see comment	none		The criticality is generically considered terminated by the evaporation of 100 liters of water or some lesser amount. The airborne source term is given by $(MAR_{c1} * DR_{c1} * ARF_{c1}) + (MAR_{s1} + DR_{s1} + ARF_{s1})$ , where $MAR_{c1}$ = inventory of gas and volatile, $DR_{c1}$ = damage ratio for gases and volatiles generated in criticality, 1.0, $ARF_{c1}$ = 1 for noble gas, $MAR_{s1}$ = inventory of non-volatile fission products generated, $DR_{s1}$ = damage ratio radionuclides in solution, 1.0, and $ARF_{s1}$ = 5E-4 for non-volatiles, 1E-3 for ruthenium in fuel reprocessing solutions.
	<i>Fully Moderated/Reflected Solids</i>	see comment	none		This includes reflected bulk metal and metal pieces or solid fines such as powders that are moderated or reflected. It assumes no severe molten eruption, reactions and vaporization. Airborne source term = $MAR_{c2} * DR_{c2} * ARF_{c2}$ , where $MAR_{c2}$ = inventory of fissionable material and radionuclides from criticality, $DR_{c2}$ = damage ratio, metal pieces = 0.1, fines or powder = 1.0, and $ARF_{c2}$ = non-volatile can be neglected, 5E-1 for noble gases, and 5E-2 for iodine.
	<i>Bare, Dry solids</i>	see comment	none		No moderation, rather reflection. Airborne source term = $MAR_{c3} * DR_{c3} * ARF_{c3}$ , where $MAR_{c3}$ = inventory of radionuclides from fission, $DR_{c3}$ = damage ratio, metal pieces = 0.1, fines or powder = 0.1, and $ARF_{c3}$ = 5E-1 for noble gas, 5E-2 for iodine.
	<i>Large Storage Arrays</i>				No data available

## Distribution

### External Distribution

- 2 U.S. Department of Energy  
Office of Nuclear Safety - Nuclear Safety R&D Program  
Attn: Alan Levin, NSR&D Program Manager  
1000 Independence Avenue, SW  
Germantown, MD 20585
  
- 2 U.S. Department of Energy  
Office of Nuclear Safety Basis and Facility Design (AU-31)  
Attn: Patrick Frias, NSR&D Project Manager  
19901 Germantown Road (AU-31)  
Germantown, MD 20874
  
- 1 U.S. Department of Energy  
Office of Nuclear Safety Basis and Facility Design (AU-31)  
Attn: Garrett Smith, Director, Office of Nuclear Safety Basis and Facility Design  
19901 Germantown Road (AU-31)  
Germantown, MD 20874
  
- 1 U.S. Department of Energy  
Office of Nuclear Energy  
Attn: James C. Bresee  
Mail Stop NE-52  
19901 Germantown Road  
Germantown, MD 20874
  
- 2 U.S. Nuclear Regulatory Commission  
Office of Nuclear Material Safety and Safeguards  
Attn: Yawar Faraz (1) and Wendy Reed (1), Division of Spent Fuel Management/LTSF  
Mail Stop 4 B34  
Washington DC, 20555-0001
  
- 1 U.S. Nuclear Regulatory Commission  
Office of Nuclear Regulatory Research, Environmental Transport Branch  
Attn: Mark Fuhrmann  
Mail Stop 10 A12  
Washington, DC 20555-0001
  
- 1 Louis F. Restrepo  
Atkins Nuclear Solution US  
2500 Louisiana Blvd NE, Suite 310  
Albuquerque, NM 87110

1 Jose R.O. Munoz  
DOE-NNSA, Sandia Field Office  
P.O. Box 5400  
Albuquerque, NM 87185-5400

Internal Distribution

1	MS0481	John S. Bowers	2225
1	MS0721	Susan Y. Pickering	6200
1	MS0736	Richard O Griffith	6230
1	MS0744	Patrick D. Mattie	6233
1	MS0748	Nathan E. Bixler	6232
1	MS0748	Randall O. Gauntt	6232
1	MS0748	David L.Y. Louie	6232
1	MS1135	Alexander Brown	1532
1	MS1135	Randall D. Watkins	1532
1	MS1141	Michael R. Greutman	1383
1	MS0899	Technical Library	9536 (electronic copy)

Intentionally Left Blank

